NOVA SCHOOL OF SCIENCE & TECHNOLOGY

DEPARTMENT OF CHEMISTRY

MARIANA ISABEL BARATA MOÇO

Bachelor's degree in Biology

DERIVATION OF KIDNEY ORGANOIDS FROM HUMAN INDUCED PLURIPOTENT STEM CELLS UNDER 3D CONDITIONS

MASTER IN BIOTECHNOLOGY

NOVA University of Lisbon
December, 2021

NOVA SCHOOL OF SCIENCE & TECHNOLOGY

DEPARTMENT OF CHEMISTRY

DERIVATION OF KIDNEY ORGANOIDS FROM HUMAN INDUCED PLURIPOTENT STEM CELLS UNDER 3D CONDITIONS

MARIANA ISABEL BARATA MOÇO

Bachelor's degree in Biology

Supervisor: Doctor Cláudia Daniela Canelas Miranda Simões, University of Lisbon

Examination committee:

Chairperson:	Doctor Mariana da Mota Veiga de Araújo Branco.
Members of the committee:	Doctor Cláudia Daniela Canelas Miranda Simões
	Doctor Ana Cecília Afonso Roque

MASTER IN BIOTECHNOLOGY

NOVA University of Lisbon
December, 2021

Derivation of kidney organoids from human induced pluripotent stem cells under 3D conditions

ACKNOWLEDGEMENTS

Firstly, I would like to thank Professor Joaquim Cabral for accepting me as a master thesis student in the Stem Cell Engineering and Regenerative Medicine Research Group (SCERG) at Instituto Superior Técnico.

I would like to express my deep gratitude to my supervisor Cláudia for one million reasons, but primarily for all the availability, comprehension, precious guidance and care. It was a great pleasure to be accepted as your master student and my words are not enough to thank you for all the help, for your work along my side, for being so supportive and endlessly patient. Above all things, thank you for always caring about my wellbeing in various ways: the car rides, the attention about the time that I have to spent with my family (which was essential to keep me mentally healthy), the jokes, the breaks for coffee, the comprehension about exceeded deadlines and many other details… I appreciated every little thing and for sure that, every and each of them, made this journey a lot easier. I am extremely grateful since day one, since the lecture that I wasn't supposed to go but that allowed me to know you and your work. Call me cheesy, but I totally believe in destiny and I'm sure it was destined since day one. I definitely could not have asked for a better supervisor, lucky me.

I would also like to thank to all my Professors who accompanied my academic journey for all these years, but in particular to Professor Romana Santos, for all the availability, guidance and support before my journey into this master.

I'm also grateful to my lab partners Carina, Mariana and Cotovio for being always so helpful and available for my constant and unending doubts, thanks for always making me feel welcomed, for the friendship, the laughs and good moments. A special thanks to the girls for making my life a lot easier with all the car rides.

To my chiquita Maria, thank you for sharing this journey with me, for all the help and the great shared moments. Miss you a lot!

A special thanks to my dearest friend Rita for all the support, caring and help with thesis revision and constructive suggestions. Thank you for being always there for me, for the advice and for being the best friend I could ask for.

My gratitude also goes to my high school group friend "Cientistas de café" who always encouraged me and celebrated my victories. I'm sorry for the lack of time spent together during this last year but I will make it up to you! Thank you for the amazing friendship for all these years.

A heartfelt thanks to my friends Daniela and Celine for always checking up on me, for being my motivational coaches and for all the encouragement and emotional support. Love you all.

To my friends Maria and Mica from 'Consultório dos desabafos', thank you for being always there available to listen the complains about my daily life and for all the support and strength. You were the best thing that FCT gave me.

Most importantly, none of this could have been possible without my family. I must express my profound gratitude to my aunts and cousins, for always providing me with continuous support and courage.

To my brother, thank you for all of the snack prep during the time writing this dissertation, for all the times that you acted as an older brother but above all, thank you for being my partner in crime in every situation. I love you.

To my parents, thank you for being part of what I am today. Above all things, thank you for every opportunity you gave me and for always considering your children as the most important investment of your lives. I am deeply and forever thankful for everything you have done for me and I hope to never disappoint you. You are the most important people in my life and this thesis is also yours.

ABSTRACT

Human induced pluripotent stem cells (hiPSCs) have the unique potential of self-renewal and the functional capacity to give rise to any specialized cell type in the human body, including all types of renal cells. By virtue of these outstanding features, hiPSCs constitute a powerful research tool and present an immensurable clinical potential. Kidney organoids derived from hiPSCs constitute attractive three-dimensional (3D) models that may enable kidney regeneration, disease modelling and drug screening, amongst others.

The following experimental work focused on developing kidney organoids from hiPSCs under 3D conditions resorting to commercially available high-throughput microwells. For that purpose, two relevant protocols, which combine monolayer and 3D culture, were applied and adapted to a full 3D culture configuration. The conducted differentiation experiments under 3D conditions revealed temporal discrepancy of the obtained cellular stages in relation to the referred protocols. In the end, it was possible to generate immature kidney organoids.

Keywords: Human induced pluripotent stem cells; Renal differentiation; Kidney organoids; 3D culture.

RESUMO

As células estaminais pluripotentes induzidas humanas (hiPSCs) têm o potencial único de autorrenovação e a capacidade funcional de originar qualquer tipo de célula especializada no corpo humano, incluindo todos os tipos de células renais. Em virtude destas características excecionais, as hiPSCs são um poderoso instrumento de pesquisa e apresentam um potencial clínico imensurável. Os organóides de rim derivados de hiPSCs constituem modelos tridimensionais (3D) atrativos que podem permitir a regeneração do rim, modelação de doenças e triagem de fármacos, entre outros.

O seguinte trabalho experimental focou-se no desenvolvimento de organóides de rim a partir de hiPSCs sob condições 3D recorrendo a uma metodologia *high-throughput* através do uso de micropoços. Com esse propósito, dois protocolos relevantes, que combinam cultura em condições aderentes e cultura 3D, foram aplicados e adaptados a uma configuração de cultura totalmente em condições 3D. As experiências de diferenciação conduzidas sob condições 3D revelaram uma discrepância temporal dos estágios celulares obtidos em relação aos protocolos referidos. No final, foi possível gerar organóides de rim imaturos.

P**alavras-chave:** Células estaminais pluripotentes induzidas humanas; Diferenciação renal; Organóides de rim; Cultura 3D**.**

LIST OF CONTENTS

LIST OF FIGURES

LIST OF TABLES

LIST OF ABBREVIATIONS

2D Two-dimensional
3D Three-dimensional
ALKs Activin receptor-Like Kinases
AMED Agency for Medical Research and Development.
APC Adenomatous Polyposis Coli
ASCs Adult stem cells
AXIN Axis Inhibitor
bFGF basic Fibroblast Growth Factor
BMPs Bone Morphogenetic Proteins
BSA Albumin Bovine Serum
cDNA Complementary deoxyribonucleic acid
CHIR CHIR99021
CM Cap mesenchyme
CO_2 Carbon dioxide
CSB Comma-shaped body
C_T Threshold cycles
CUBN Cubilin
DAPI 4',6-Diamidino-2-Phenylindole
DMEM-F12 Dulbecco's Modified Eagle Medium: Nutrient Mixture F-12
DMSO Dimethyl Sulfoxide
DNA Deoxyribonucleic acid
DPBS Dulbecco's Phosphate Buffered Saline
ECM Extracellular matrix
ECSCs Embryonal carcinoma stem cells
EDTA Ethylenediamine Tetraacetic Acid
EGCs Embryonic germ cells
ERK Extracellular-Signal-Regulated kinase
ESCs Embryonic stem cells
FACS Fluorescence-Activated Single Cell Sorting
FBS Fetal Bovine Serum
FGF2 Fibroblast Growth Factor 2
FGFR FGF receptor
FGFs Fibroblast Growth Factors
FOXD1 Forkhead box D1
GAPDH Glyceraldehyde-3-Phosphate Dehydrogenase
GATA3 GATA binding protein 3
GDFs Growth/Differentiation Factors
GDNF Glial-Derived Neurotrophic Factor
GSK-3β Glycogen Synthase Kinase-3 β
hESCs Human embryonic stem cells
hiPSCs Human induced pluripotent stem cells
HOXD11 Homeobox D11
hPSCs Human pluripotent stem cells
ICM Inner cell mass
IGF-IR Insulin-Like Growth Factor I Receptor
IM Intermediate mesoderm
iPSCs induced pluripotent stem cells
KLF4 Krüppel-like factor 4
LEF Lymphoid Enhancer Factor
LHX1 LIM Homeobox 1
LIF Leukaemia Inhibitory Factor
LRP Lipoprotein Receptor-related Protein
MEKs Mitogen-activated proteins
MET Mesenchyme-to-epithelium transition
miRNA micro ribonucleic acid
MM Metanephric mesenchyme
mRNA messenger ribonucleic Acid
n Replicate number
NGS Normal Goat Serum
NPC Nephron progenitor cell
NPHS1 NPHS1 adhesion molecule, nephrin.

OCT 3/4 Octamer-binding transcription factor 3/4

P Passage

PAX2 Paired box 2

PAX8 Paired box 8

PDK-1 Phosphoinositide-Dependent Kinase-1

PDMS Polydimethylsiloxane

PE Phycoerythrin

PFA Paraformaldehyde

PI3K Phosphoinositide 3-Kinase

PIP2 Phosphatidylinositol (4,5)-biphosphate

PIP3 Phosphatidylinositol (3,4,5)-triphosphate

PSCs Pluripotent stem cells

PTA Pre-tubular aggregate

R-SMADs Receptor-activated SMADs

RNA Ribonucleic acid

ROCK Rho-associated Coiled-coil protein Kinase

Rpm Rotations per minute

RPMI 1640 Roswell Park Memorial Institute medium 1640

RT-PCR Real-time polymerase chain reaction

RV Renal vesicle

SCERG Stem Cell Engineering and Regenerative Medicine Research Group

SD Standard deviation

SIX2 Sine oculis-related homeobox 2

SMAD Smad and mothers against decapentaplegic related protein

SOX2 Sex determining region Y-box 2

SSB S-shaped body

SSEAs Stage Specific Embryonic Antigens

TCF T-Cell Factor

TGF-β Transforming Growth Factor β

TRAs Tumour-Rejection Antigens

UB Ureteric bud

UMOD Uromodulin

WD Wolffian duct

WNT Wingless-type mouse mammary tumour virus integration site

WT1 Wilms' tumour 1

I. INTRODUCTION

I.1. Stem Cells

A stem cell can be generically described as an undifferentiated cell which presents two major features: unlimited or prolonged self-renewal capacity and potential to differentiate towards specialized and functional cells along different lineages [1,2]. Mitotic cell divisions allow stem cells continuous proliferation generating identical uncommitted stem progeny (self-renewal). Alternatively, stem cells can also undergo differentiation through action of manifold stimuli, generating progenitor cells that develop into mature specialised descendants [2–4].

A progenitor cell, also known as a precursor cell, might be seen as an intermediate stage in the differentiation process. These cells are unspecialized or partially specialised cells that present distinguishable features from stem cells. When stem cells undergo cell division, one of the two new cells is often a stem cell with self-renewal capacity. By comparison, progenitor cells undergo cell division and yield progenitor cells or two specialised cells, neither of which is capable of replicating itself [3].

I.1.1. Stem cells potency classification

Stem cells might present distinct differentiation potentials (*i.e.* potency), and, in accordance, present distinct classifications: totipotent, pluripotent, multipotent and unipotent stem cells [3] (Figure 1.1).

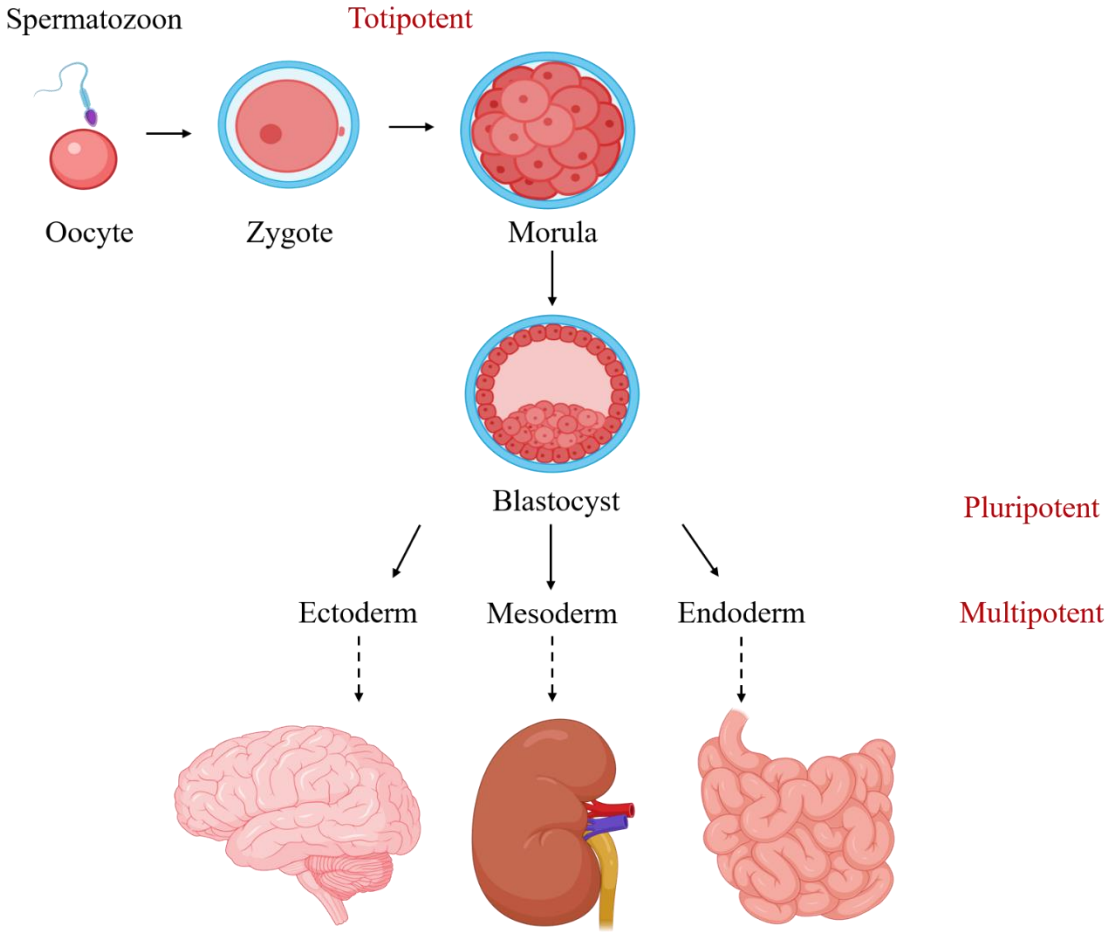

Figure 1.1| Human embryonic development paired with stem cells potency classification. Figure created with BioRender.com.

Totipotency refers to the ability of a cell to give rise to a complete embryo, including cells occurring in extra-embryonic tissues such as the umbilical cord and placenta, which support embryonic development. This classification solely includes the zygote, the first entity of life resulting from oocyte fertilisation, and cell stages until eight-cell stage [2,3,5,6].

About five to six days after fertilization takes place and, with subsequent cell divisions, the zygote develops into a blastocyst. This structure is composed of two different groups of cells: the trophoblast (outer cells of the blastocyst) and the inner cell mass (ICM). Trophoblast cells are responsible for placenta formation, whereas the ICM cells have the ability to generate the three embryonic germ layers composing an organism, namely ectoderm, mesoderm, and endoderm [2,3,5]. Embryonic stem cells (ESCs), which derive from the ICM, are pluripotent stem cells (PSCs) as

they can generate every somatic cell that develops from the three germ layers [2,3,5–7]. Therefore, when compared to totipotent stem cells, PSCs lack the ability to generate extra-embryonic tissues. As cell divisions proceed in embryonic development, cells become more restricted concerning their ability to differentiate into multiple lineages. Stem cells composing the three germ layers are classified as multipotent stem cells. Although these cells can differentiate into multiple cell types, their differentiation potential is restricted to a specific germ layer or cell lineage [2,3,5,6].

Adult individuals also present stem cells which are present in small niches in differentiated tissues and allow for somatic cells renewal in case of damage, injury and disease. Adult stem cells (ASCs) maintain the stem cell hallmarks, as they can self-renew and differentiate, however, they are multipotent, only being able to generate cell lineages in the tissue where they reside [2,3,6]. Despite being most often in a metabolic quiescent state, both intrinsic signals or extrinsic regulatory factors from the microenvironment, can influence cell behaviour when necessary and trigger self-renewal or differentiation [6,8]. These cells are rare but essential for dead cells renewing and cell homeostasis maintenance [2,3,6].

Lastly, unipotent stem cells are adult tissue-specific stem cells with self-renewal capacity but can only specialize into one cell lineage [3]. Spermatogonia stem cells are an example of unipotent stem cells, as they are only able to produce one type of differentiated cell, a spermatozoon [9].

I.1.2. Human stem cells sources

Human stem cells may also be classified according to their source, as schematised in Figure 1.2.

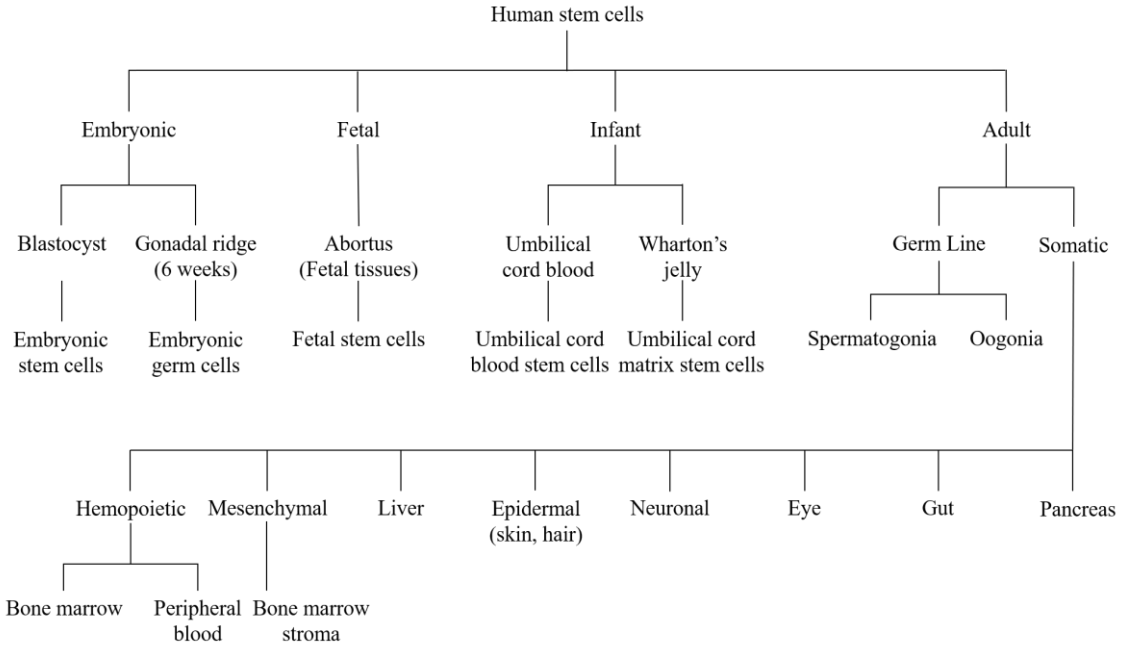

Figure 1.2| Human stem cells classification according to their source. Figure adapted from Bongso & Hin Lee, 2005 [10].

Human ESCs (hESCs) are collected from the ICM of a preimplantation stage embryo (blastocyst), whilst human embryonic germ cells (hEGCs) are derived from primordial germ cells present on the gonadal ridge of a few weeks' foetuses. Fetal stem cells, which are responsible for initial tissue development, are present in foetuses' organs and umbilical cord stem cells occur in umbilical cord blood. Lastly, adult stem cells, as referred in Section I.1.1., are undifferentiated cells with restricted potential that can be found in specialized tissues composing the human body. The two last ones present multipotent capabilities [10,11].

I.1.3. Human pluripotent stem cells

Human pluripotent stem cells (hPSCs) are, as the name suggests, PSCs of human origin. A single hPSC has the functional capacity to give rise to any fully differentiated cell type in the human body, *i.e.* it can generate all the differentiated cells derived from the three germ layers: ectoderm, mesoderm and endoderm (Figure 1.1).

Ectoderm (external layer) cells can give rise to epidermis, sensorial epithelia on face and nervous tissue which evolves to central and peripheral nervous system. Whereas mesoderm (middle layer) is able to form connective tissue (including bone and cartilage), muscles, gonads and some components of the urogenital system as genital ducts and kidneys. Finally, endoderm (internal

layer) can develop into the epithelial lining of major body tracts including the urinary, respiratory and gastrointestinal. Together, the three germ layer cells originate every tissue, organ and system of the human body [3,12].

This class of cells comprehends hESCs, hEGCs, and human induced pluripotent stem cells (hiPSCs).

Human embryonal carcinoma stem cells (ECSCs) are also included in this class and are derived from teratocarcinomas- tumours of germ cell origin [13].

I.1.3.1. Human embryonic stem cells

hESCs are derived from preimplantation human embryos (blastocysts), and thus, are defined by their origin. Figure 1.3 demonstrates hESCs derivation.

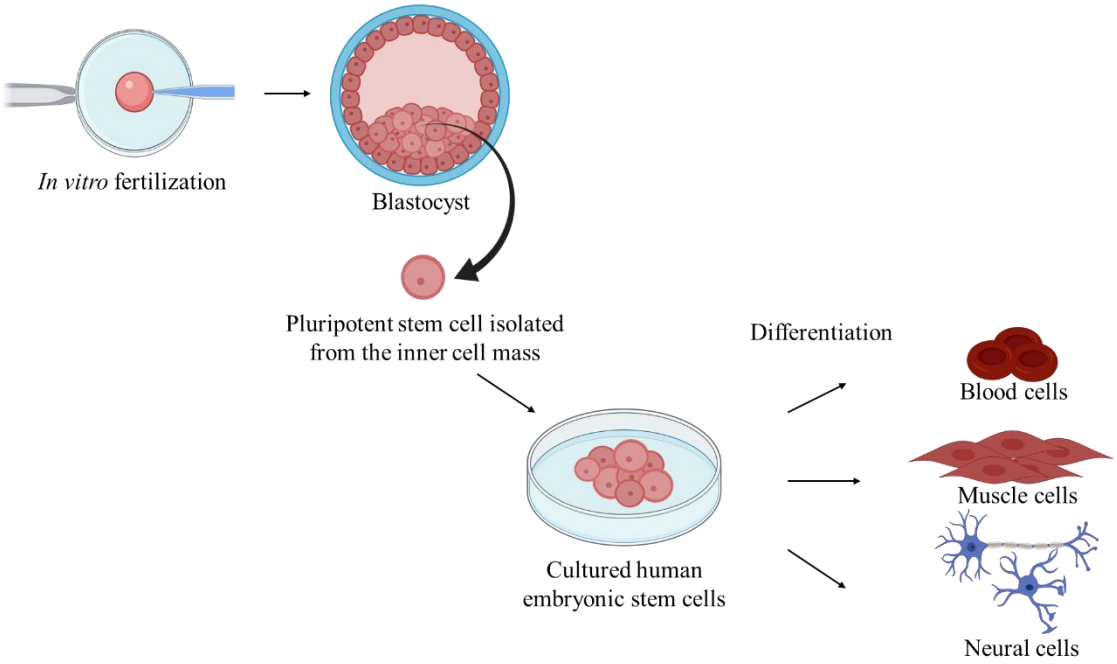

Figure 1.3| hESCs derivation. hESCs are collected from the pluripotent ICM cells of a preimplantation, blastocyst-stage embryo (embryo with 5 to 6 days of development) [3,10]. hESCs can be isolated from blastocysts obtained from *in vitro* fertilized eggs donated for research purposes [20]. Figure created with BioRender.com.

ESCs were, for the first time, isolated from the ICM of a mouse embryo, in 1981, by Martin Evans and his co-workers [14], and by Gail Martin and his co-workers [15]. More than fifteen years later, James Thomson and his colleagues reported a successful attempt of isolation and *in vitro* cultivation of hESCs (using blastocysts produced by *in vitro* fertilisation) [16].

After removal from their typical embryonic environment, and when given suitable culture conditions, hESCs will continue to proliferate indefinitely and yet retain an unrestricted pluripotent developmental potential [8]. Such pluripotency might be assessed through various

assays: *in vitro*, embryoid body formation in suspension evinces three germ layer differentiation capability; also, an *in vivo* assay might be performed when transferring ESCs to immunocompromised mice and assessing the formation of teratomas, a type of benign tumour that contains cells from the three germ layers [2,3,7,11].

hESCs are known to present high levels of alkaline phosphatase and telomerase activity [11]. With regard to the last characteristic, hESCs are accepted as a type of immortalized cells due to their ability to regenerate telomeres edges after cell divisions, which allows for genetic information protection and also, for more cell divisions and, consequently, longer lifespan [3,8].

Pluripotency maintenance in hESCs is possible due to molecular mechanisms comprising the action of several nuclear transcription factors that sustain self-renewal and suppress differentiation [17]. The three pivotal transcription factors involved in this process are Octamer-binding transcription factor 4 (OCT4), Sex determining region Y-box 2 (SOX2) and NANOG. These factors establish pluripotency by activating the expression of target pluripotency-associated genes and, simultaneously, repressing lineage-specific genes [18]. Therefore, these three transcription factors, as pluripotency markers, are commonly used for hESCs characterization and pluripotency assessment [7]. Undifferentiated hESCs also express characteristic surface markers, such as the Stage-Specific Embryonic Antigens (SSEAs) pluripotency markers SSEA-3 and SSEA-4 and Tumour-Rejection Antigens (TRAs) TRA-1-60 and TRA-1-81 [11].

When cultured *in vitro* and upon the presence of the appropriate signals, hESCs have the capacity to differentiate, forming precursor cells, into every mature cell type [19]. These features make them a powerful and promising raw material to model human embryonic development and disease, for drug testing and for cell/tissue transplantation therapy [20,21].

Despite the enormous potential of hESCs, in particular in transplantation therapy, their use in this field faces various hindrances. When transplanted into a living host, these cells can induce tumour growth- teratomas- and cause perturbations in normal tissue function. Thus, it is imperative to remove any undifferentiated hESCs or unwanted cell lineages prior to transplantation. Using these cells in transplantation also carries the risk of immune rejection by the patient. Additionally, their generation raises ethical concerns regarding human embryos creation, usage and sacrifice that limit and compromise their use in research studies and cell-based therapies [1–3].

I.1.3.2. Human induced pluripotent stem cells

Induced pluripotent stem cells (iPSCs) were first derived in 2006, by Shinya Yamanaka and his co-workers, when they made the outstanding discovery that terminally differentiated cells could be induced to revert to an embryonic-like state [22]. They were able to successfully reprogram mouse somatic cells into pluripotent cells relying on a defined method encompassing the introduction of four specific genes encoding transcription factors, namely, *OCT 3/4*, *SOX2*, Krüppel-like factor 4 (*KLF4*) and c-*MYC*.

One year later, the Kyoto University group reported hiPSCs attainment by reprogramming human adult dermal fibroblasts, targeting the same four transcription factors [23]. Figure 1.4 illustrates hiPSCs derivation from somatic, differentiated cells.

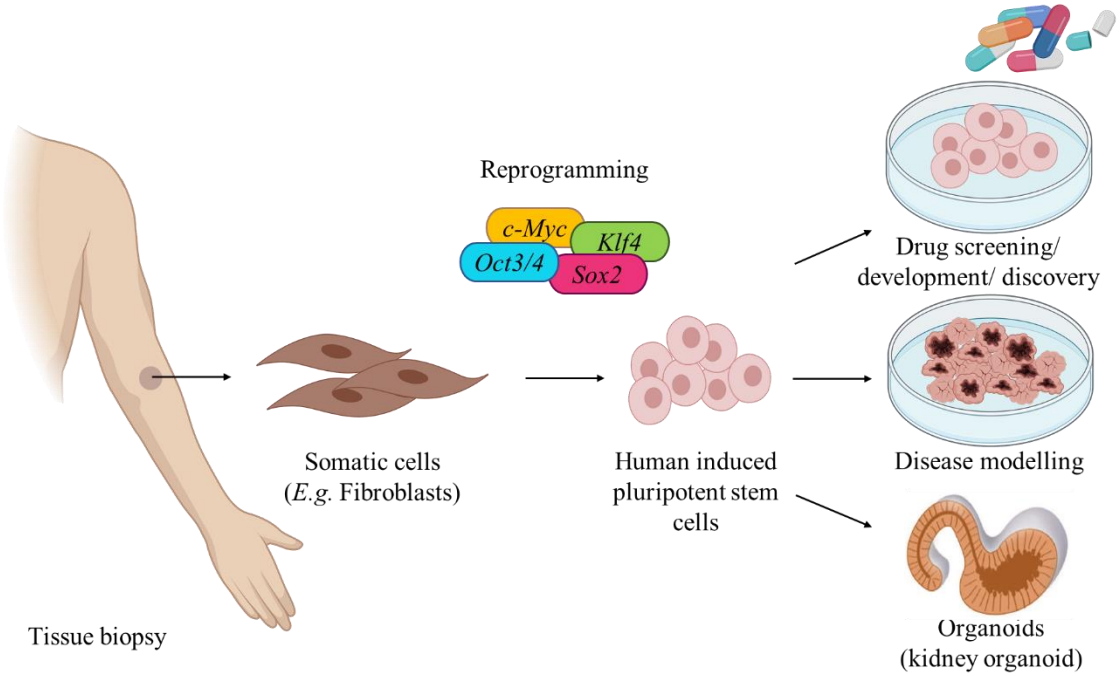

Figure 1.4| hiPSCs generation from differentiated cells. iPSCs were first obtained by retrovirus-mediated transfection of four genes encoding transcription factors: Octamer-binding transcription factor 3/4 (*OCT3/4*), Sex determining region Y-box 2 (*SOX2*), Krüppel-like factor 4 (*KLF4*) and c-*MYC*. The four selected transcription factors were chosen based on their importance in pluripotency maintenance and cell phenotype in early embryos and ESCs [22]. Figure adapted from Lancaster & Knoblich, 2014 [74]. Figure created with BioRender.com.

The same achievement was later reported by an independent group, however, targeting different genes (*OCT4*, *SOX2*, *NANOG* and *LIN28*) [24].

I.1.3.2.1. Reprogramming methods

Obtaining hiPSCs by reprogramming somatic, differentiated cells into a pluripotent state, constitutes an alternative source of hPSCs. In order to obtain hiPSCs, reprogramming factors are delivered to somatic cells through specific vectors. There are several different strategies allowing to obtain hiPSCs through reprogramming which may be divided in two main categories based on the chosen delivery vector: I) genome integrative methods; and II) non-integrative methods [25].

I.1.3.2.1.1. Genome integrative methods

Reprogramming through genome integrative methods involves the integration of exogenous genetic material by host cells. This category comprises deoxyribonucleic acid (DNA) based strategies by viral delivery (retrovirus and lentivirus) and non-viral delivery (linear fragments transfection and transposons) [25].

Integrative methods employing retroviruses and lentivirus are considered robust and efficient as they are able to infect a broad range of cell types and have a stable transgene expression [26]. Nevertheless, lentiviruses are more commonly used since lentiviral systems infect both dividing and non-dividing cells, while retroviruses infectivity is limited to dividing cells [25]. The main drawbacks concerning viral vectors are related to the unpredictable and permanent genomic modifications on host cells genome, as viral transgene insertion occurs randomly and might result in insertional mutagenesis and heterogenous hiPSC lines. Beyond the possibility of tumour formation due to transgenes reactivation during differentiation, residual transgenes expression may also affect hiPSCs and their derivates behaviour [25–28]. These problems were partially solved by the development of transgene excision strategies however, these leave a small footprint in reprogrammed cells and can also cause insertional mutagenesis [26,29].

Another alternative method is non-viral delivery in which liposomes and electroporation allow the transfection of linear DNA fragments, and transposons allow the transfection of DNA sequences [25]. The main advantage of using transposons as vectors is the fact that they allow to precisely remove transgenes, without leaving any footprint in host cells genome [26]. However, the non-viral delivery approach results in a lower transduction efficiency when compared to viral delivery, consequently, requiring a large number of host cells [25].

I.1.3.2.1.2. Non-integrative methods

Concerns regarding genome integrative methods safety prompted efforts on developing new reprogramming methodologies excluding transgene integration, the non-integrative methods. Non-integrative methods are considered to be safer as their effect is transient and they do not interfere in genome integrity, however, they are usually inefficient and poorly reproducible [25].

Among their disadvantages are the need of successive transgenes delivery and their reduced applicability to different cell types [30].

Similar to integrative methods, non-integrative methods also comprise DNA-based strategies, which encompass viral delivery (adenovirus, and Sendai virus) and non-viral delivery (plasmids, minicircles and episomal plasmids). Furthermore, Ribonucleic acid (RNA)-based (mRNAs- messenger ribonucleic acids and miRNAs- micro ribonucleic acids) and protein-based strategies are included [25,29].

Recombinant adenoviruses are capable of efficiently infecting both dividing and non-dividing cells, being able to transduce many different cell types. Notwithstanding, their use is limited due to transient expression as they are rapidly cleared from dividing cells, resulting in low reprogramming efficiency. Sendai viruses are, currently, the most popular and versatile systems being extensively used in cell reprogramming. These RNA viruses are capable of producing large amounts of proteins and exclusively replicate in the cytoplasm, not entering into the nucleus of infected cells. This method is characterised by a higher reprogramming efficiency than retrovirus-mediated reprogramming and the virus is depleted some passages after infection, generating transgene-free hiPSCs [26,30].

Conventional polycistronic plasmids allow for a transient expression of transgenes as they do not self-replicate and are rapidly lost upon cell divisions. Therefore, efficient cell reprogramming requires repeated transfection of reprogramming plasmids. Due to constraints related to their large size and in order to provide a longer and stable transgenes expression, alternative vectors have been used, the minicircle vectors. These supercoiled DNA episomal vectors lack both antibiotic resistance gene and bacterial origin of replication, which are commonly responsible for transgenes silencing in mammalian cells and thus, allow for longer expression. Equally to conventional plasmids, they do not self-replicate, enabling transgene-free hiPSCs production. In addition, using episomal plasmids as a vector seems to be a simpler method as they replicate autonomously and, consequently, only requires a single transfection for long term stable expression [26].

At last, both protein and RNA delivery allow for transgene-free and zero-footprint hiPSCs generation. Nevertheless, while protein delivery exhibits poor efficiency and slow kinetics [25], RNA delivery is able to highly efficiently reprogram multiple cell types with rapid kinetics [31]. Protein-based strategies have faced some challenges regarding the difficulty in purifying sufficient desired proteins [31] and synthetizing large amounts of bioactive proteins that can cross plasma membranes [29]. Regarding RNA delivery, there are some limitations related to short half-life and short-term expression of the delivered RNA [30].

The reprogramming process is generally characterised by a low reprogramming efficiency [32]. The above-mentioned reprogramming methods present different efficiencies which are summarized in Table 1.1.

Table 1.1| Efficiency of different reprogramming methods to obtain hiPSCs. Table adapted from Rao & Malik, 2012 [29].

Reprogramming method	Efficiency in human cells (%)
Retroviral	0.02-0.08
Lentiviral	0.02-1
PiggyBac (Transposon)	0.02-0.05
Adenoviral	0.0002
Sendai virus	0.5-1.4
Episomal	0.0006-0.05
Minicircles	0.005
mRNA	0.6-4.4
miRNA	0.002

There are several factors affecting reprogramming efficiency, namely species, donor cell type, delivery method, culture conditions, supportive cells and media composition [25]. Noteworthy, it is also quite difficult to compare reprogramming efficiencies due to the differing criteria used to calculate efficiencies, the use of different reprogramming factor combinations and the use of some molecules potentiating reprogramming efficiency such as cell-cycle regulators and compounds altering DNA methylation or chromatin modifications [25,29,32].

I.1.3.3. Human embryonic stem cells versus human induced pluripotent stem cells

Despite their distinct origins and derivation methodologies (Figure 1.3 and Figure 1.4), hiPSCs exhibit the same general characteristics as hESCs, such as cell morphology, proliferation, cell-surface marker expression, self-renewal capacity and pluripotency. Other shared features comprehend promoter and telomerase activities and the expression of the previously stated SSEAs, TRAs, as well as the transcription factors referred for hESCs (Section I.1.3.1.) [23].

hiPSCs technology provides the opportunity to produce patient-specific cells by reprogramming somatic cells of the host (autologous cells), overcoming immune rejection associated with hESCs after transplantation and thus, bypassing the need for immunosuppression [2,7]. Their derivation circumvents much of the ethical debate surrounding hESCs derivation, but similarly to hESCs, they can also form teratomas after implantation hindering their transplantation to a human patient [23,24].

hiPSCs possess unlimited resource capacity since they can be obtained through a tissue biopsy against the restricted supply capacity of hESCs derived from discarded embryos after *in vitro* fertilization [33].

Although several studies reported slight differences between hiPSCs and hESCs regarding their methylation patterns and gene expression profiles, it is really difficult to distinguish the two types of PSCs based on these features, suggesting that these variations might arise from different induction methodologies and, especially, from different culture conditions [34]. Moreover, iPSCs were reported to retain epigenetic memory from tissue of origin, which was indicated to give

preferential differentiation into tissue types remising of cell type origin [35]. Although there was evidence that modest passaging erased this memory in mouse iPSCs, the same was not verified for hiPSCs [35,36].

I.1.3.4. Pluripotency maintenance

hPSCs are characterised by being able to divide for indefinite periods and to form representative tissues of all three germ layers of the developing embryo upon differentiation, defined as self-renewal and pluripotency. These two features are tightly controlled by regulatory networks composed of signalling pathways and intrinsic transcriptional factors.

Diverse extrinsic signals are diffused through intracellular signal-transduction pathways which converge towards the activation of a core transcriptional network involving three, previously referred, transcription factors: OCT4, SOX2 and NANOG. Among the signalling pathways, three specific pathways can be highlighted, namely TGF-β/Activin/Nodal, FGF and WNT [37]. These will be followingly referred.

The overall signalling responsible for human stem cell pluripotency maintenance is schematised in Figure 1.5.

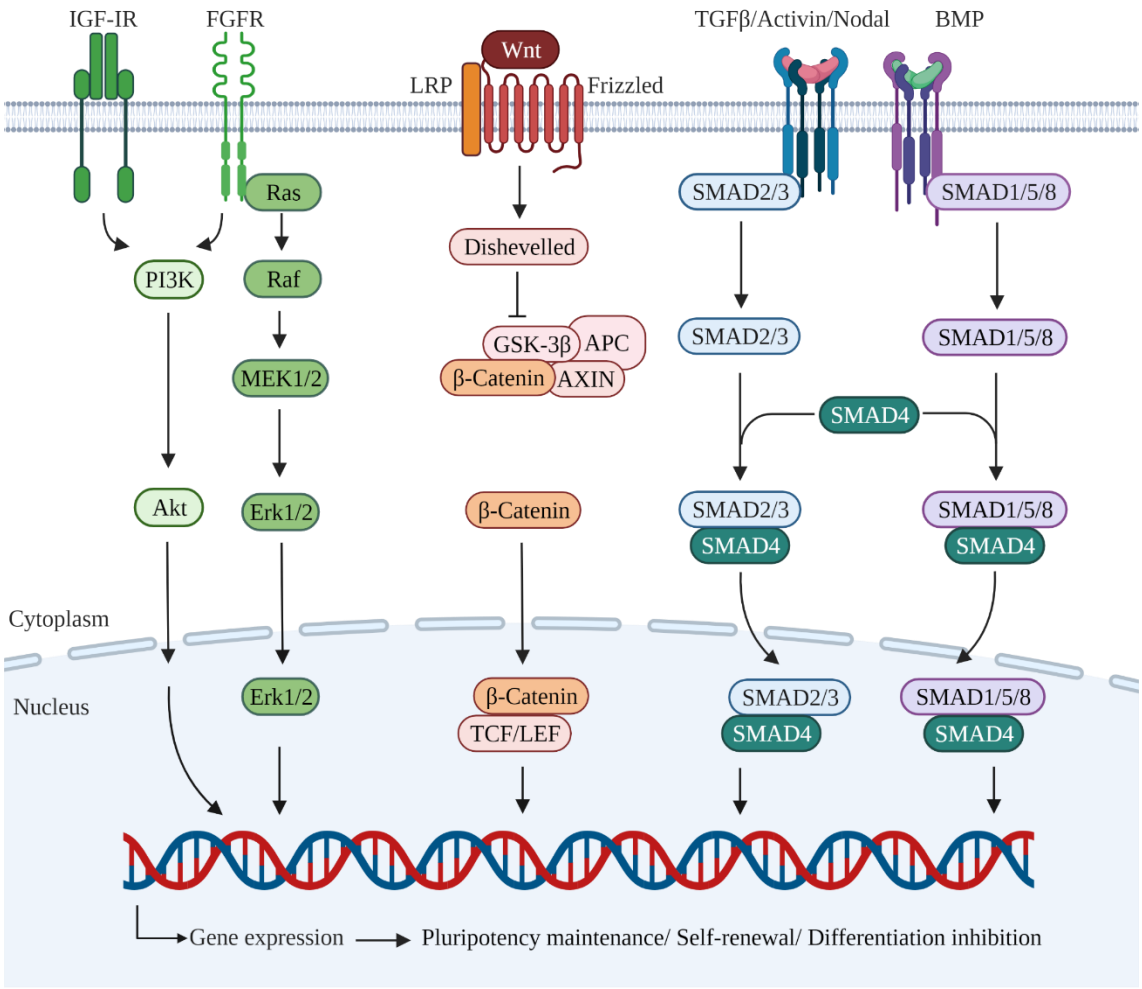

Figure 1.5| Signalling in hPSCs pluripotency regulation and maintenance. FGFR: FGF receptor; IGF-IR: Insulin-Like Growth Factor I Receptor. Figure created with Biorender.com.

The Transforming Growth Factor β (TGF-β) superfamily of morphogens includes several ligands such as TGF-βs, inhibins, myostatins, Bone Morphogenetic Proteins (BMPs), Growth/Differentiation Factors (GDFs), activin and nodal. These ligands bind to cell-surface serine/threonine kinase receptors, the TGF-β type II receptors, which in turn, phosphorylate and activate the TGF-β type I receptors, also known as activin receptor-like kinases (ALKs). TGF-β signals propagate, afterwards, through intracellular mediators, the Receptor-activated Smad and mothers against decapentaplegic related proteins (R-SMADs), through two main branches: one comprising TGF-β, activin and nodal, which plays a major role in hPSCs self-renewal and pluripotency maintenance; and one comprising BMPs and GDFs which accounts for differentiation induction.

TGF-β, activin and nodal, transduce through R-SMADs 2/3 via type I receptors ALKs 4/5/7 binding. Upon activation within the cytoplasm, R-SMADs 2/3 form a complex with the co-activator SMAD4 which is translocated into the cell nucleus and induces target gene expression, thus activating undifferentiation-associated genes supporting pluripotency maintenance, particularly, *Nanog*.

By comparison, BMPs activate R-SMADs 1/5/8, through ALKs 1/2/3/6 binding. As in the TGF-β, activin and nodal pathway, R-SMADs 1/5/8 will form a complex with SMAD4, promoting its translocation into cell nucleus, activating target gene expression, inhibiting self-renewal and stimulating differentiation [38]. BMP signalling may be suppressed not only by its antagonist, nogging, but also by Fibroblast Growth Factor 2 (FGF2), also known as basic Fibroblast Growth Factor (bFGF) [39]. When culturing hPSCs *in vitro*, culturing media must comprise FGF2 supplementation in order to prevent spontaneous differentiation [40].

Fibroblast Growth Factors (FGFs) are also responsible for hPSCs pluripotency maintenance. FGF ligands bind to tyrosine kinase receptors, resulting in the activation of intracellular signalling, namely, PI3K/AKT and/or Ras-Raf-MEK/ERK downstream pathways. In the first pathway, Phosphoinositide 3-Kinase (PI3K) catalyses the conversion of Phosphatidylinositol (4,5)-Biphosphate (PIP2) into Phosphatidylinositol (3,4,5)-Triphosphate (PIP3), through phosphorylation. A serine/threonine kinase, Akt, binds to PIP3 and is translocated to the inner cell membrane, where it suffers phosphorylation and activation by Phosphoinositide-Dependent Kinase-1 (PDK-1) action. Activated Akt is implicated in various cellular processes such as cell survival (inhibiting apoptosis), proliferation and growth [40–43]. The Ras-Raf-MEK/ERK signalling pathway is also known as MAPK-ERK. When FGFs bind to tyrosine kinase receptors, they are able to activate Ras protein which will, in turn, bind and activate a downstream effector protein, Raf. Activated Raf, phosphorylates and activates Mitogen-activated proteins (MEKs) 1/2, which have the same action in Extracellular-Signal-Regulated kinase (ERK) 1/2. Activated ERKs are capable of entering into the nucleus and directly phosphorylating some transcription factors implicated in cellular proliferation and differentiation [44].

Pluripotency maintenance in stem cells also involves Wingless-type mouse mammary tumour virus integration site (WNT) family members signalling. Canonical WNT signalling pathway controls gene expression through β-catenin, as it promotes its stabilization through glycogen synthase kinase-3 β (GSK-3β) inhibition. When WNT ligands in the cell bind to Frizzled receptors and to his co-receptors LRP (lipoprotein receptor-related protein) 5/6, provoke Dishevelled activation which prevents the Axis Inhibitor (AXIN)/ Adenomatous Polyposis Coli (APC)/ GSK-3β complex formation. As this complex induces β-catenin degradation, its non-assembly results in β-catenin accumulation and stabilization in the cytoplasm. β-catenin translocates into the nucleus and interacts with T-Cell Factor (TCF) and Lymphoid Enhancer Factor (LEF) allowing for target gene activation [45,46].

Apart from the above-mentioned signalling pathways, epigenetic changes are also known to have a crucial role in stem cell pluripotency maintenance. In particular, mechanisms like histone modifications, DNA methylation/acetylation and small RNAs are, as well, implicated in pluripotency and self-renewal associated genes expression [47].

Beyond differences concerning their morphology and proliferation rate, mouse PSCs and hPSCs also differ in their requirements for pluripotency maintenance [48]. Contrary to mouse PSCs, Leukaemia Inhibitory Factor (LIF) is not sufficient for pluripotency maintenance in hPSCs [19].

I.1.4. Applications for human induced pluripotent stem cells

Notwithstanding the previously stated problems regarding hiPSCs handling, the capacity of unlimited self-renewal and ability to differentiate into cells of all three embryonic germ layers, renders these cells ideal candidates for various applications in the area of regenerative medicine, disease modelling, drug screening and organoid models, amongst others [49–53] (Figure 1.4).
hiPSCs are attractive candidates for cell therapy-based regenerative medicine as they own the ability to provide large quantities of cells and generate functional tissue to replace diseased or damaged tissue [53,51]. Furthermore, hiPSCs hold great promise for the minimization of immune rejection in this area, as they can be harvested from individual patients and transplanted autologously [51,52]. PSCs have been tested in a great number of clinical trials for regenerative medicine applications but mainly directed towards treatment of ophthalmologic, neurological and neurodegenerative diseases. In fact, the majority of these clinical trials use hESCs, but the number of clinical trials using hiPSCs is growing [54,55]. A list of some hiPSC-based products on-going clinical trials is shown in Table 1.2.

Table 1.2| hiPS cell-based products in clinical trials. The status of trials is indicated as September 2021.Table adapted from Yamanaka, 2020 [55].

Disease	Company/sponsor	ID	Status	Country	Type of therapy
Age-related macular degeneration	National Eye Institute	NCT04339764	Phase I/II	USA	Autologous
Cancer	Fate Therapeutics	NCT03841110	Phase I	USA	Allogenic
Cartilage defect	AMED	jRCTa050190104	Interventional	Japan	Allogenic
Heart failure	Help Therapeutics	NCT03763136	Phase I/II	China	Allogenic
Spinal cord injury	AMED	jRCTa031190228	Interventional	Japan	Unknown
Thrombocytopenia	AMED	jRCTa050190117	Interventional	Japan	Autologous

AMED: Agency for Medical Research and Development.

Other major applications for hiPSCs *in vitro* are disease modelling and drug screening. Although human diseases are conventionally studied *in vivo* using animal models such as rodents [49], hiPSCs may provide more accurate responses, since unlike animal models they do not lack human disease relevance, providing better understanding of the human body complexity and physiology [50]. This field may use hiPSCs as they retain unique genetic and epigenetic signatures of the patient from whom they were derived, enabling to recapitulate a patient-specific disease. Thereby, after

reprogramming and subsequent differentiation into a specific cell type of interest [51], cells may be characterized revealing disease mechanisms, thus allowing to develop therapeutic methodologies and target drugs.

The early stages of drug discovery and screening may also benefit from hiPSC technology [52], as these cells provide a human-specific testing platform that may decrease and complement the use of animal models, while at the same time provide personalized treatments using patient-specific hiPSCs [49].

The great potential of hiPSCs in organoids generation will be addressed further in Section I.3.

I.2. The urinary system

The human urinary system consists of two kidneys from which extend two ureters, a bladder and an urethra as schematized in Figure 1.6, A.

This system is essentially responsible for excretion of metabolism end products and excess water, through its primary excretion organs, the kidneys. The combination of excretory products forms urine, which is carried by the ureters to the bladder, where it is stored and then excreted through the urethra.

Beside its main function, this system plays an important role in a wide range of physiologic processes such as osmoregulation, red blood cell synthesis, calcium absorption, blood volume and pressure regulation, among others [56–58].

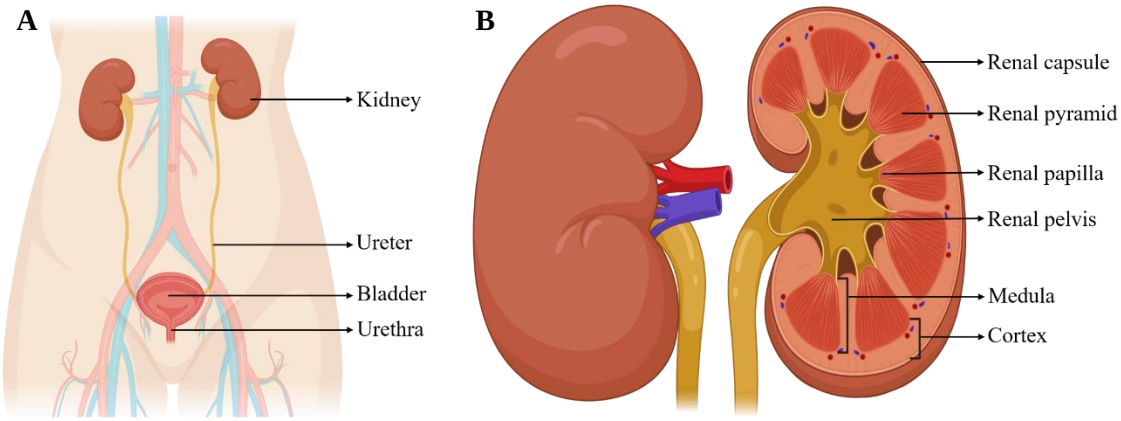

Figure 1.6| Urinary system and kidneys. A) Urinary system components; **B)** Kidneys external anatomy (left) and internal anatomy (right). Figure created with BioRender.com.

I.2.1. Kidneys

The paired bean-shaped organs are located on either side of the human spine and present about 12 cm in length. Each kidney has an indention on its concave medial side, the hilum, wherethrough various structures enter and exit the kidney, while renal artery and nerves enter each kidney, renal vein and ureters exit the kidney [56–58] (Figure 1.6).

Kidneys are responsible for blood filtration which reaches this organ through the renal arteries. This process ensures homeostasis maintenance, as it regulates the body fluid composition through water and waste removal and also, through control of electrolytes and non-electrolytes abundance [56–58].

I.2.1.1. Kidney external anatomy

Regarding kidney external anatomy (Figure 1.6, B), this excretory organ is enveloped in three layers of distinct tissues: I) the renal capsule, a thin outer layer of fibrous connective tissue that provides support to the organ; II) a thick layer of adipose tissue responsible for its protection; and III) the renal fascia, a thin layer of connective tissue, which surrounds the fat and anchors the kidney to the abdominal wall [56–58].

I.2.1.2. Kidney internal anatomy

The kidney parenchyma corresponds to functional tissue and presents two major regions: the outer cortex and an inner medulla, which in turn is also divided in inner and outer medulla (Figure 1.6, B and Figure 1.7).

Medulla is composed of 12-18 cone-shaped structures, the renal pyramids, which consist of a collection of tubules and ducts responsible for fluid modification and transport throughout the organ. Renal pyramids broad bases are adjacent to the cortex and the apex regions- renal papilla- are directed to the centre of the kidney, being connected to a large cavity designated as renal pelvis. This cavity receives the urine transported by tubules and ducts on the renal pyramids that flows, afterwards, out of the kidney into the ureters [56–58].

Throughout its parenchyma, each kidney contains over a million functional and structural units: the nephrons (Figure 1.7). The nephrons are composed of five segments with distinct functions in urine production: the renal or Malpighian corpuscle, a proximal tubule (convoluted and straight), descending and ascending loops of Henle, a distal convoluted tubule and a collecting duct [56–58].

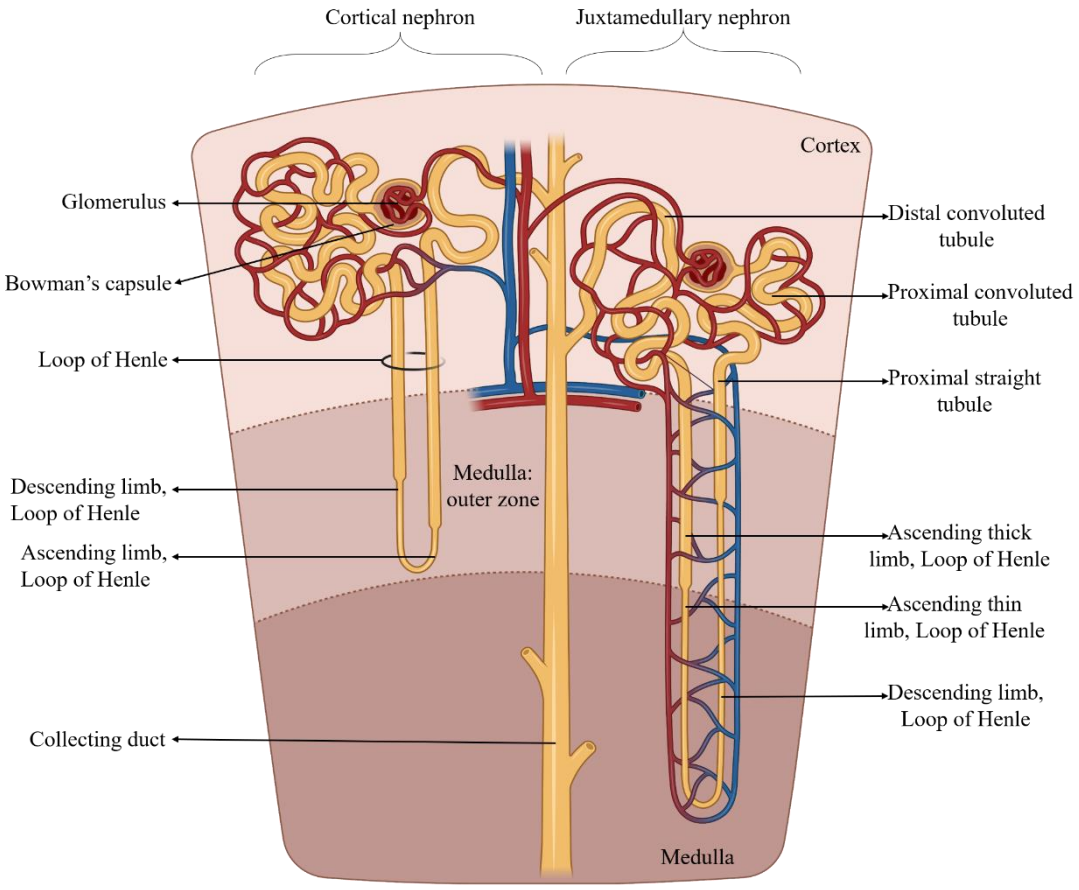

Figure 1.7| Kidneys functional and structural units: nephrons. Loops of Henle of juxtamedullary nephrons extend deep into the medulla, while cortical nephrons present loops of Henle that do not extend deep into the medullary region [59]. Figure created with BioRender.com.

The renal corpuscle consists of a cluster of blood capillaries, the glomerulus, that is enclosed by Bowman's capsule. This vascularized structure is located at the cortex and accounts for blood filtering. The filtrate flows towards the proximal tubule (at the cortex) which returns filtered substances to the blood, such as glucose, amino acids, water, and calcium and phosphate ions. Loops of Henle are present in both the cortex and the medulla and connect the proximal and distal tubules. These u-shaped segments contribute to water conservation in the body as they absorb water from the filtrate and influence urine concentration. Thereafter, the filtered fluid goes through the cortical distal tubule, where some additional waste might be scoured, and empties into a collecting duct. This structure conducts the newly formed urine from the kidney cortical region to the renal papilla [57,58] (Figure 1.7).

I.2.1.3. Kidney embryonic development

As formerly referred, the three embryonic germ layers forming an organism arise from the ICM of an embryo. During human embryonic development, the ICM cells segregate into a cluster of cells called epiblast and a layer of primitive endoderm [59]. Ectoderm, mesoderm and endoderm emerge from the epiblast as a result of a complex process involving various cellular movements, the gastrulation. During this event, epiblast cells migrate through the primitive streak- a furrow stretching that extends from the posterior end of the embryo- to form the three germ layers [59]. Gastrulation is proceeded by organogenesis, where kidney development takes place [59]. In mammals, kidney develops from the intermediate mesoderm (IM) (Figure 1.8, A), progressing through three major stages: pronephros, mesonephros and metanephros (Figure 1.8, B). The first two stages are transient whereas metanephric kidney persists as a mature and functional kidney in mammals [60,61].

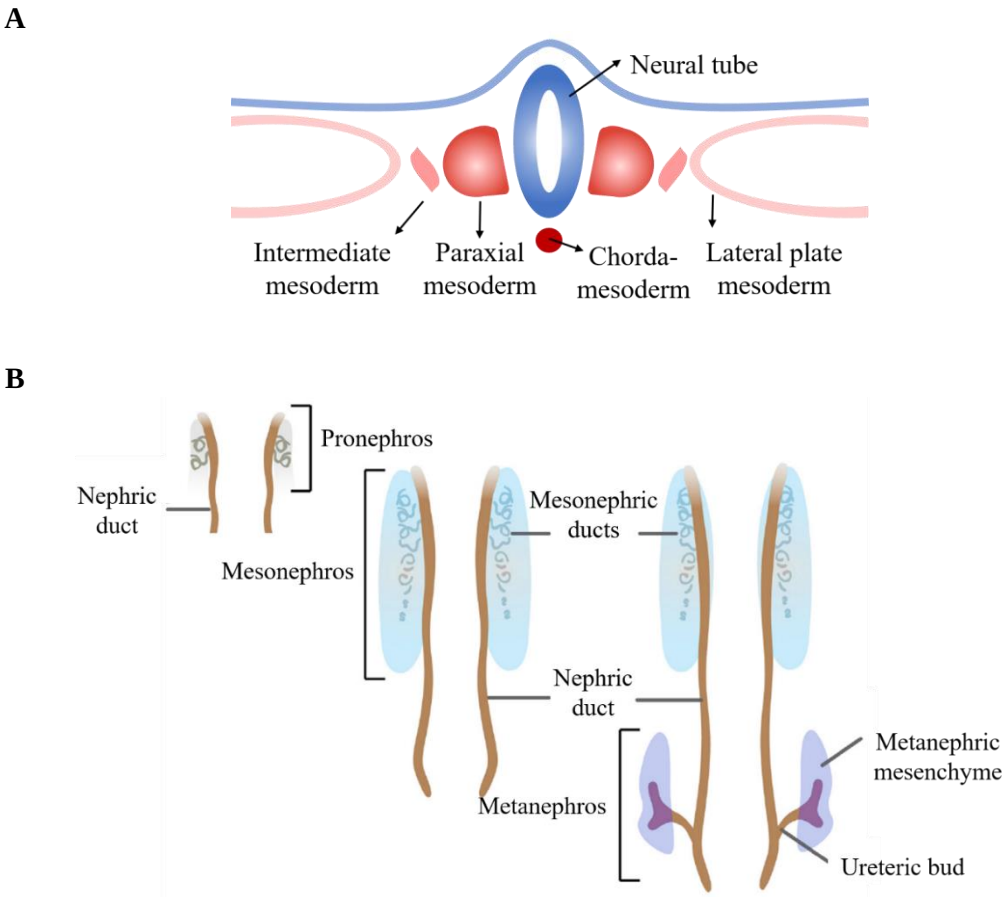

Figure 1.8| Intermediate mesoderm and its derivates. A) Intermediate mesoderm is located between the lateral plate mesoderm and paraxial mesoderm and gives rise to the urogenital system which consists of the kidneys, the gonads, and their associated ducts [59]; **B)** Pronephros, mesonephros and metanephros develop sequentially in cranial to caudal sequence as the body plan elongates [60]. Figure adapted from Little, 2017 [60].

Pronephros is formed around gestational day 22 in humans, as the nephric duct, the first epithelial component of the urogenital system, arises [59,62]. The duct forming cells migrate caudally and its anterior region induces the formation of tubular structures from the adjacent mesenchyme, originating pronephros. This structural stage is very rudimentary and degenerates, while the posterior portion of the nephric duct remains, continues to elongate and becomes the wolffian duct (WD), thenceforth playing a central role in kidney development [59,63]. With pronephros regression, mesonephros develops caudal to the pronephros, presenting well developed mesonephric tubules with glomeruli and convoluted-like structures [61,64].

Metanephric kidney derives from the reciprocal interactions of two primordial mesodermal tissues, the epithelial ureteric bud (UB) and the metanephric mesenchyme (MM) [65,66], both generated through FGF and WNT signalling pathways [59]. The UB and the MM are known to present distinct origins in the IM: the former arises from the anterior portion of the IM whereas, the latter arises from the posterior portion of the IM [67]. The UB gives rise to renal collecting system epithelial cells, whereas MM gives rise to nephron epithelial cells as well as endothelial and stromal cell precursors [68,69].

Kidneys functional units, the nephrons, arise from MM cells in a process denominated nephrogenesis, which is schematically represented in Figure 1.9.

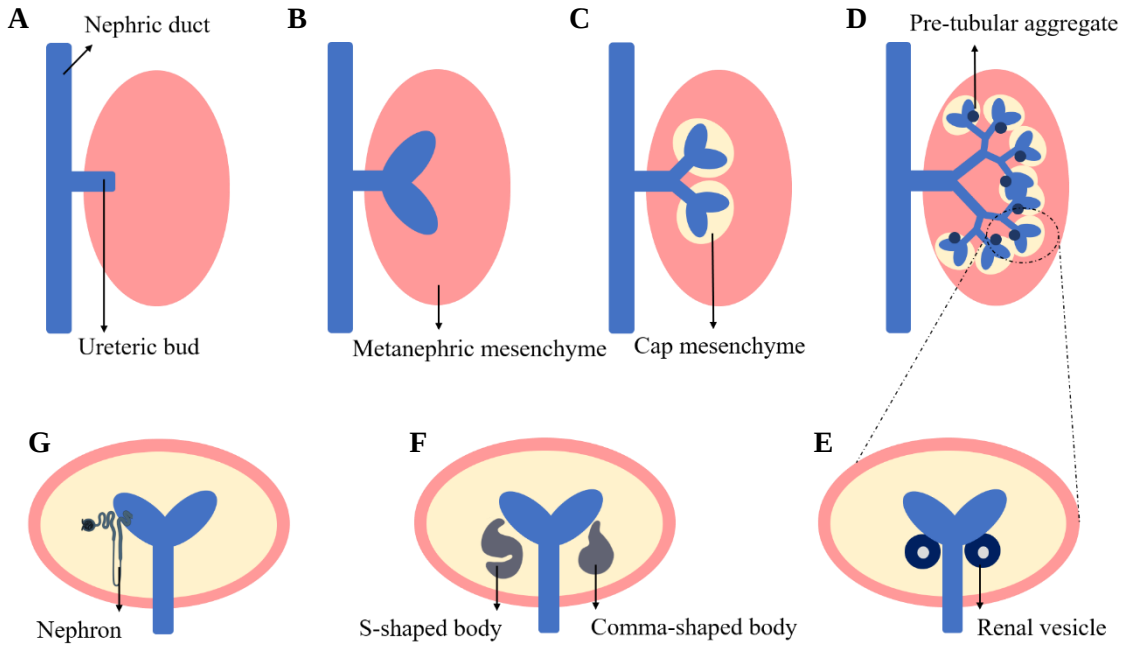

Figure 1.9| Schematic representation of sequential nephrogenesis. A) The UB arises at the posterior end of the nephric duct and progressively invades the surrounding MM; **B-D)** Signals from the MM cause the ureteric epithelium to branch and grow giving rise to the arborized renal collecting system; **C)** UB invasion induces some mesenchymal cells to condense around the tips of newly formed branches. Other mesenchymal cells generate the interstitial stroma; **D)** A subset of this condensed mesenchyme further aggregates to form pre-tubular aggregates (PTA) around the bud tips; **E)** PTAs become polarized as they undergo a mesenchyme-to-epithelium transition (MET), forming the renal vesicle (RV); **F)** Nephron segmentation into glomerular and tubular domains initiates with the sequential formation of two clefts in the RV, forming the comma-shaped body (CSB) followed by the S-shaped body (SSB); **G)** While the distal end of the SSB fuses with the UB-derived collecting ducts, the more proximal cleft is infiltrated by endothelial cells and forms the renal corpuscle. Figure created with BioRender.com.

At the 28th day of gestation, the UB outgrows from the posterior portion of the WD, as an aggregate of epithelial cells, that invades the surrounding MM [62,66]. Thereafter, the UB gives rise to the renal collecting system (cortical and medullary collecting ducts, renal calyces and renal pelvis) through branching morphogenesis [68]. This process comprises UB growth and repeated bifurcation [64] and is driven by continued Glial-Derived Neurotrophic Factor (GDNF) production by a restricted mesenchymal population, the cap mesenchyme (CM) [65,66]. This cell population constitutes a self-renewing nephron progenitor cell (NPC) population, which is characterized by Sine oculis-related homeobox 2 (*SIX2*) transcription factor expression [62,66]. CM cells condense around the growing tip of the UB due to branch tips induction. Thereat, a group of cells detach itself from the condensate and form a pre-tubular aggregate (PTA) [59], where the composing cells proliferate and undergo through a mesenchyme-to-epithelium transition (MET), forming a spherical polarized structure with a central lumen, the renal vesicle (RV) [62,63,65]. UB is known to secret factors such as FGF2, FGF9 and BMP7 in order to prevent mesenchymal apoptosis and allow for proliferation [59] and WNT canonical signalling had been identified as having a critical role in condensation and epithelization, in particular, the Wilms' tumour 1 (*WT1*) gene [65].

Afterwards, the RV primitive epithelium experiences segmentation and reorganizational proximal-distal patterning as it bends, elongates and forms a 'comma-shaped' (CSB) and a subsequent 'S-shaped' body (SSB) [63]. The distal portion of the SSB forms the distal convoluted tubule, the centre portion develops into the proximal tubule, loop of Henle and distal straight tubule and, at last, the proximal portion evolves to the renal corpuscle [61]. Cell fate establishment along the proximal-distal axis of the SSB is under the charge of *WT1* and Paired box 2 (*PAX2*) genes: the former accounts for glomerular cell fate, whereas the latter induces tubular cell fate [68]. As patterning occurs, and by the SSB stage, the distal portion of RV forms a connection with the UB [70], allowing for communication between the ureteric bud' lumen and the internal cavity of the renal vesicle [62,68].

Glomerulus formation initiates when the SSB forms a cup-like structure: endothelial and mesangial cells migrate into the proximal SSB cleft, creating a capillary tuft which results in SSB deformation. The epithelial cells lining the inner wall of this cup, the visceral glomerular epithelium, originate podocytes, while cells lining the outer wall, the parietal glomerular epithelium, line Bowman's capsule [68]. The visceral epithelium envelops the capillary tuft and starts to differentiate into podocytes and to form a filtration barrier [61,64]. Podocytes also take part in the formation of the glomerular basement membrane, which is responsible for separating the capillary tuft from the urinary space and is formed through fusion between podocytes and glomerular capillaries basement membranes [61].

Interstitial spaces, surrounding the forming nephrons and UB branches, are occupied by stromal cells [68], that provide structural support [69]. These cells, which are characterized by expression of

the transcription factor *FOXD1* (Forkhead box D1) [71], arise from the posterior IM, and interfere in UB branching and CM differentiation by GDNF secretion [71,72].

Nephrogenesis process ceases around the 36th week of gestation [62]. The postnatal human kidney lacks a nephron progenitor population, as this population is terminally differentiated prior to birth [66], consequently, adult kidney is unable to generate new nephrons [73].

I.3. Human organoids

Organoids are *in vitro* three-dimensional structures with several different cell types, which arise from stem and progenitor cells differentiation and that are capable of self-organization into a structure resembling an *in vivo* organ, exhibiting similar organ structure and functionality [74,75]. These multicellular structures can be generated from PSCs, ASCs or fetal stem cells by mimicking the assumed *in vivo* signalling events during human development [75,76]. More precisely, during organoid formation and consequent stem cells differentiation, correct regional identity establishment is achieved through application of morphogens and signalling inhibitors, as they permit to activate or inhibit, respectively, key signalling pathways responsible for regulating developmental patterning [76].

Over the past years, human organoids have been established for a wide range of organs, including stomach, intestine, pancreas, liver, lung, brain and kidney [75].

This type of model system is endued of a myriad of applications, which include human development modelling, disease modelling, drug development and screening, replacement strategies, biobanking, medicine precision, among others [74–79].

Human organoids may prove very useful as human models, arising as a complement to *in vivo* animal models and *in vitro* human cell-based models. Although animal models have been extensively used and have been a source of valuable information, there are significant differences between human and animal physiology, which limit the applicability of animal-sourced results, as well as some human-specific biological processes such as metabolism and drug efficacy. Another relevant aspect concerns the notorious contrast between genetic homogeneity of inbred animal models and human genetic diversity, as this feature has a great impact on drug response and disease onset and progression. Also, organoids are more amenable to manipulation of niche components, signalling pathways and genome editing than *in vivo* models [75]. Overall, organoids could provide an attractive alternative to animal models for both ethical and economic reasons [76].

In Table 1.3, benefits and limitations of organoid systems are listed [74–76,80].

Table 1.3| Benefits and limitations of organoid systems.

Benefits
Represent human physiology as they are human-derived; Can be derived from various sources: adult and fetal tissues, hESCs and hiPSCs; Can be derived from minimal amounts of tissue biopsies and be cultured indefinitely without genomic alterations for multiple applications; Pave the way to personalized medicine as they can be obtained from specific individuals, providing robust and personalized data; An organoid model, for a specific disease, can be directly generated from affected patients without prior knowledge of the specific cause of the disease or involved genes; Can be easily and rapidly established; Relatively easy to handle; Amenable to a wide variety of established experimental techniques and genetic manipulation;
Limitations
Relatively costly; Standardization of protocols for organoid establishment and quality control are lacking; Unable to mimic *in vivo* signalling gradients and biochemical forces; Heterogeneous (size, shape, cell type ratios, etc.) between cell lines, experiments, groups and consequently, not reproducible; Only reproduce organ-specific or tissue-specific microphysiology as there is lack of inter-organ communication- only represent a part of the human body; Lack of vascularization (affecting nutrient supply and consequent organ maturation) and immune cells (do not reflect interactions with the immune system).

Organoid development is a recent technology and still is under further improvement [76], howsoever, it is already considered a matter of ethical concerns, especially regarding the extent of organoid maturation, chimera research, the use of gene-editing technologies in organoid research and the provenance of human materials [81].

I.3.1. Human kidney organoids

Kidney disease affects around 15% of the global population [82] and arises as a result of congenital, acute or chronic causes that impair renal function [83]. Considering this information, kidney organoids may allow to screen for new therapies and improve our understanding of some renal pathologies such as interstitial fibrosis, diabetic nephropathy or glomerulosclerosis [84].

There have been several successful attempts of deriving *in vitro* kidney organoids, in both two-dimensional (2D) [85–88] and three-dimensional (3D) [89–92] cultures. Primitive kidney morphogenesis has been accomplished through application of a defined cocktail of growth factors and small molecules, in a timed sequence, to both ASCs and PSCs [76].

Human kidney organoids derived from hiPSCs might be attractive 3D models for different purposes, namely, to model kidney embryonic development, kidney disease, high-throughput

drug screening and potential implementation in renal regeneration and replacement therapies [73,82,84].

Regarding homeostasis maintenance, the adult kidney shows a low rate of proliferation [82], however, this organ possesses an intrinsic, but limited, capacity to self-repair following injury [73]. In case that the induced damage surpasses the kidney regenerative capacity, damage can become irreversible, resulting in a permanent loss of nephrons, leading to end-stage renal disease. One possible cause for acute kidney injury is the accumulation of nephrotoxic agents. Therefore, kidney organoids may constitute an accurate system for drug screening/development, with special impact on drug safety assessment (nephrotoxicity) [82].

I.4. Derivation of kidney organoids from human induced pluripotent stem cells under 3D conditions

I.4.1. Pluripotent stem cells culture

Stem cells have the capacity for long self-renewal as well as the potential for differentiation into a variety of specialized cell types. This cell behaviour is strongly dictated by the complex 3D microenvironment wherein cells reside, the niche. Cell niches are spatially and temporally dynamic and provide the structural, biochemical, mechanical, and stimulatory cues essential for cell homeostasis and physiological change. Several constituents contribute to the stem cell niche, including extracellular matrix (ECM), cell-to-cell interactions, soluble and immobilized signalling factors, the physicochemical environment and mechanical forces [2,93].

In particular, the extrinsic signals provided by cell-to-cell and cell-to-ECM interactions are indispensable for hPSCs survival, growth and pluripotency maintenance [94]. Therefore, when culturing hPSCs and to assure pluripotency maintenance, it is necessary to mimic these aspects [2].

During hiPSCs culture, some procedures imply cell detachment and dissociation, which leave them vulnerable to anoikis, an apoptosis process initiated by lack of cell-to-cell and cell-to-matrix contact [95].

The rho-associated coiled-coil protein kinase (ROCK) signalling pathway, which is responsible for a plethora of cell behaviours such as motility, proliferation, adhesion and cytokinesis, is also of a paramount importance in hPSCs' anoikis event under single-cell conditions [96,97].

The addition of a ROCK inhibitor (for instance, Y-27632) prevents single cells from entering apoptosis, maintaining them viable and promoting cell survival after singularisation [98,99].

I.4.2. Three-dimensional culture versus two-dimensional culture

Two distinct configurations might be adopted for culturing hiPSCs *in vitro*: two-dimensional or three-dimensional.

In the first approach, cells are cultured on planar, rigid plastic surfaces, usually coated with adhesion substrates [100], which mimic ECM composition, promoting cell adhesion and growth. These substrates are composed of several adhesion molecules playing a crucial role in the long-term maintenance and self-renewal of adherent cells like hiPSCs, as well as in cell differentiation [2,101]. When culturing hiPSCs resorting to a 2D configuration, cells are maintained as an adherent monolayer, exposing cells to a homogeneous amount of nutrients, oxygen and physical stimulation [100]. Although this aspect enables the formation of genotypic and phenotypic uniform cell populations [102], the absence of oxygen/nutrients and waste removal diffusional gradients does not reflect *in vivo* tissues [100,103]. Also, cells grown in a 2D environment lack the *in vivo* cell-to-cell and cell-to-ECM interactions that rely on 3D architecture. This can influence many cellular processes including cell proliferation, differentiation, apoptosis, and gene/protein expression [100].

The 3D approach includes different cell culture techniques: spheroids, organoids, scaffold-based 3D culture, organ-on-chip and 3D bioprinting [104].

Cells grown in 3D culture agglomerate into cellular aggregates or spheroids to seek for support. This way, cells are allowed to grow and interact with their environment in all the three dimensions and, thus, cell-to-cell and cell-to-ECM interactions are potentiated [100,103]. Therefore, 3D cell culture, in contrast to 2D culture, is thought to closely resemble the complex microenvironment surrounding cells *in vivo*, and thus the behaviour of 3D-cultured cells is more reflective of *in vivo* cellular responses [100,103,105]. As a consequence, 3D configuration is thought to better simulate a wide range of cellular functions such as proliferation, morphology, differentiation, gene/protein expression, and cellular response to external stimuli [100].

In opposition to 2D configuration, cellular aggregates display diffusional gradients, which may yield cellular heterogeneity (proliferating, quiescent, apoptotic, hypoxic, and necrotic cells) characteristic of *in vivo* tissues [100].

Cell culture configuration is particularly important in drug discovery/development process, as drug testing in 2D configuration often provides misleading information [100], which may be explained by signalling network alteration in 2D culture [106]. Culturing cells in a 3D environment enables drug testing regarding pharmacodynamics, efficacy and safety, in a more *in vivo*-like context than in traditional monolayer culture [100,104,107]. This culture configuration may contribute to a bigger success of novel drugs, identifying toxic and ineffective substances at an earlier stage of the drug discovery pipeline [108].

Provided that 3D cell culture shows a greater stability and a longer lifespan than 2D, this culture configuration might be more appropriate for long-term studies as a way to access drug-derived long-term effects [103].

I.4.3. From pluripotent stem cells to nephron progenitor cells and kidney organoids

Two protocols were used in this work to direct hiPSCs differentiation into NPCs and kidney organoids under 3D conditions: the Morizane protocol [109] and the Takasato protocol [110].
A timeline of the events occurring during the Morizane differentiation protocol is schematically presented in Figure 1.10.

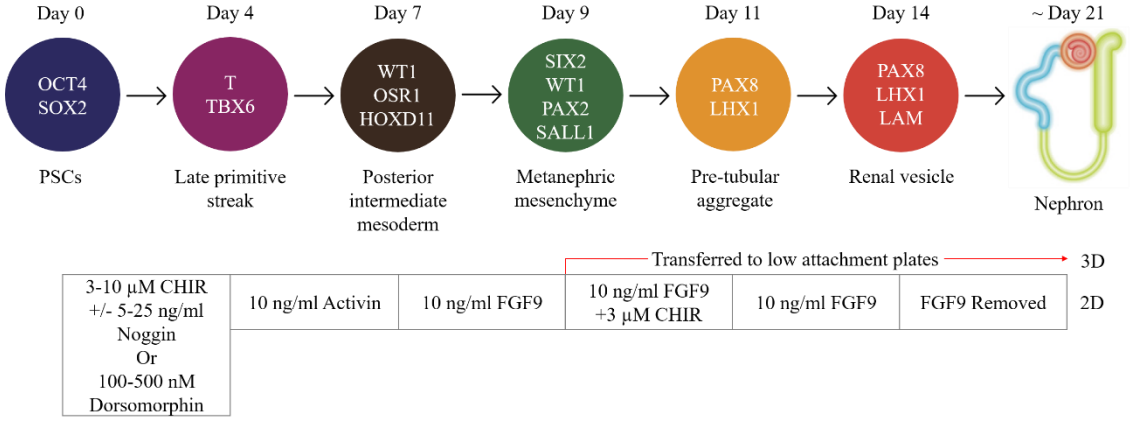

Figure 1.10| Timeline of events, cellular stages and cell marker phenotype during Morizane differentiation protocol. Figure adapted from Morizane & Bonventre, 2016 [109].

A timeline of the events occurring during Takasato differentiation protocol is schematically presented in Figure 1.11.

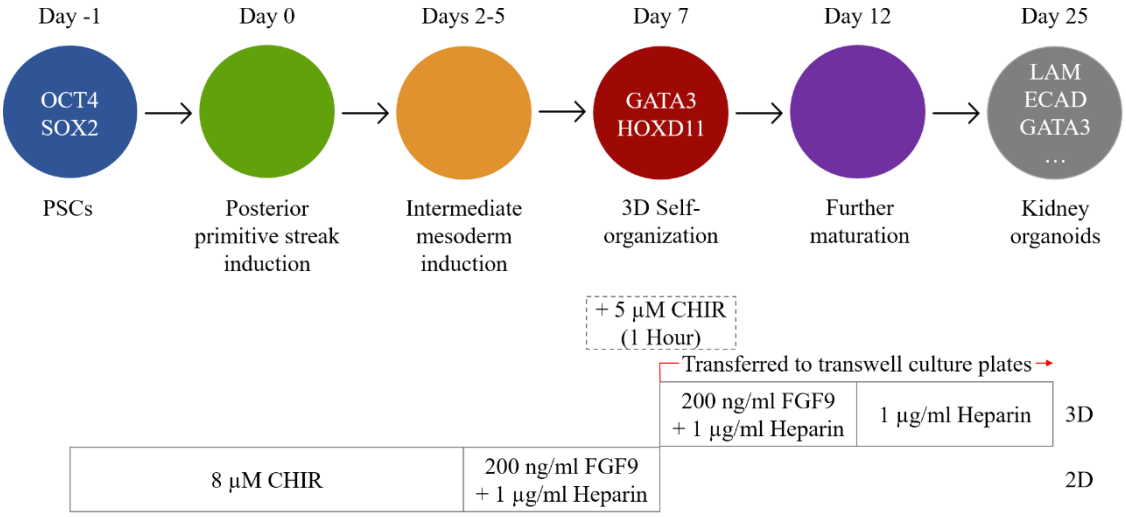

Figure 1.11| Timeline of events, cellular stages and cell marker phenotype during Takasato differentiation protocol. Figure adapted from Takasato *et al.*, 2016 [110].

These two differentiation protocols combine monolayer and 3D culture and essentially differ in the used growth factors/small molecules, length of culture and the employed 3D culture approach.

Generation of kidney organoids from hiPSCs, just as the embryonic kidney, depends on cell-to-cell interactions between four distinct progenitor cell populations, namely, NPCs, UB progenitor cells, endothelial progenitor cells and stromal progenitor cells [69].

As referred in Section I.2.1.3., UB and MM cell populations are both generated through FGF and WNT signalling pathways. More precisely, *in vivo*, primitive streak cells migrate from the caudal to the rostral direction, being exposed to canonical WNT signals, followed by FGF9 and retinoic acid. Hence, early migrating cells are briefly exposed to WNT signals and give rise to the anterior IM (becoming the ureteric epithelium), whereas, late migrating cells are exposed longer to WNT signals and form the posterior IM (becoming the kidney-forming mesenchyme) [59,90,110]. Pursuant to this aspect, when driving hiPSCs differentiation, and apart from the signalling pathways manipulation, the timing, level and duration of a particular signal must be considered as these variables influence cellular responses [111].

In both of the referred protocols, CHIR99021, a GSK-3 inhibitor, is used to induce late primitive streak via canonical WNT signalling pathway activation. The duration of WNT signalling exposure determines whether the UB or MM cell population becomes the dominant population. A shorter phase of CHIR99021 administration results in the predominant induction of the anterior IM and consequent predominance of the UB cell population whereas a longer phase results in predominant induction of the posterior IM and consequent predominance of the MM cell population [110].

Then UB and MM cell populations interact with one another, resulting in further differentiation and self-organization into nephron structures [82].

I.4.4. Aggregate size and lineage specification

When driving hiPSCs differentiation under 3D conditions, the initial aggregate size directly affects growth and subsequent cell trajectories [112,113]. The aggregate size has a special impact on cell-to-cell and cell-to-soluble factors interactions [113], thus influencing signalling in pluripotency and differentiation [114].

During differentiation, cell aggregates can grow to a size where they display oxygen and nutrient gradients similar to *in vivo* tissue [105] however, as aggregates increase in size, they face diffusional limitations that may result in cell death at aggregates centre and influence differentiation [114]. On the other hand, aggregates of a reduced size tend to compromise cell survival due to lack of support [113].

II. AIM OF STUDIES

There have been several successful attempts of deriving *in vitro* kidney organoids, in both 2D [85–88] and 3D [89–92] cultures.

The existing protocols for human kidney organoids generation under 3D conditions strongly differ between each other and in relation to various aspects such as: length of culture, the used growth factors/small molecules and the employed 3D culture techniques.

Another important aspect falls into the fact that some protocols are not fully conducted under 3D conditions, instead, they combine monolayer culture and 3D cell culture configuration [89,92,109,110].

Furthermore, different protocols committed to exclusively and efficiently generate a specific renal cell population (and correspondent derivative cell types) or a specific renal structure [67,89,92,109].

These different protocols also present different induction efficiencies of these tissues/structures.

In addition, a relevant feature refers to the need of co-culture human renal cells with mouse cells [67,89,92], which precludes the use of these renal cells for clinical applications.

This project set out the aim of generating kidney organoids from hiPSCs under fully 3D conditions. For this purpose, two different protocols regarding renal differentiation were used: I) Morizane protocol; and II) Takasato protocol.

These approaches which combine monolayer and 3D culture, were applied and adapted to 3D cell culture configuration in order to guide this process in a more *in vivo* similar context.

The first protocol is specific for NPCs efficient induction, generating kidney organoids without inducing collecting ducts or other nonepithelial renal cell types [91], whereas the second protocol is able to simultaneously induce ureteric epithelium and MM [90]. Therefore, as a remarkable goal, and apart from protocol optimization to 3D culture conditions, this work aimed to simultaneously induce these two renal cell populations, which was attained by optimizing the duration of CHIR99021 exposure. Along with that, the concentration of the different molecules used to induce kidney organoids was also optimized.

Kidney organoids were generated resorting to a commercially available methodology consisting on the use of microwells, which provides an easy and standardized way to produce a large number of size-specified cellular aggregates [112].

Considering the fact that the initial aggregate size directly affects growth and subsequent cell trajectories [112,113], one initial objective of this work was to evaluate the effect of the initial aggregate size towards the efficiency of hiPSCs derivation into IM. With this in view, different initial aggregate sizes were tested.

This methodology is particularly important insofar as it enables the conduction of the whole differentiation process under 3D conditions, which in turn, is extremely relevant as, a functional differentiation is known to depend on a 3D architecture [106].

Along with that, this microwell-based system is a high throughput methodology that may be able to generate 3D kidney organoids for various applications. Particularly, kidney organoids generated in microwells display a great potential as a high throughput drug testing platform.

In summary, the specific objectives in this work consist of:

I) Conduct and adapt both of the differentiation protocols entirely on 3D conditions, in particular, in microwells;

II) Simultaneously induce ureteric epithelium and MM cell populations;

III) Evaluate the effect of the initial aggregate size towards the efficiency of hiPSCs derivation into IM.

III. MATERIALS AND METHODS

III.1. Expansion of human induced pluripotent stem cells

III.1.1. Cell culture

III.1.1.1. Cell lines

The experiments presented in this work were performed using three different commercially available hiPSC lines: Gibco™ Episomal (iPSC6.2), WT-F002.1A.13 and DF6-9-9T.B.
The Gibco™ Episomal hiPSC line (Gibco™) is a zero-footprint, viral-integration-free hiPSC line generated using cord blood-derived CD34+ progenitors with seven episomally expressed reprogramming factors (*OCT4*, *SOX2*, *KLF4*, *MYC*, *NANOG*, *LIN28*, and *SV40 T*).
The WT-F002.1A.13 hiPSC line (Tecnologias Celulares para Aplicação Médica, Unipessoal, Lda.) was obtained through retroviral reprogramming of fibroblasts by ectopic expression of four reprogramming factors (*OCT4*, *SOX2*, *KLF4* and C-*MYC*).
The DF6-9-9T.B hiPSC line (DF6, by WiCell® Bank) is a vector-free hiPSC line generated from foreskin fibroblasts with seven reprogramming factors (*OCT4*, *SOX2*, *NANOG*, *LIN28*, L-*MYC*, *KLF4* AND *SV40 T*).
From now on, these cell lines will be designated as GEpi, TCLab and DF6, respectively.
Cells with passages (P) between P34 and P61 were used for the presented results.

III.1.1.2. Culture plates coating with adhesion substrate

III.1.1.2.1. Matrigel®

Matrigel® (Corning®) is a basement membrane preparation extracted from the Engelbreth-Holm-Swarm mouse sarcoma, a tumour rich in ECM molecules. This preparation is composed of laminin, collagen IV, heparan sulfate proteoglycans, entactin and several growth factors [115,116].
Matrigel® was used as an adhesion substrate in hiPSCs feeder-free culture, for expansion and differentiation.
For Matrigel® matrix preparation, an aliquot of stock solution was thawed on ice. This solution was then diluted in a 1:100 (v/v) proportion using Dulbecco's Modified Eagle Medium: Nutrient Mixture F-12 (DMEM-F12, by StemCell Technologies™) and applied to multiwell tissue culture plates (Tissue Culture Plates Flat Bottom with Low Evaporation Lid, by Falcon®), in such a way that the surface of the well was completely coated. After incubation for, at least, two hours at room temperature, Matrigel® solution was removed prior to cell seeding, or plates could be stored at 4°C up to two weeks.

III.1.1.3. Culture media

III.1.1.3.1. Washing medium

Washing medium was used for different purposes and moments, namely, for cell processing in suspension and for ceasing enzymatic cell dissociation. Washing medium basal formulation includes DMEM/F-12, 10% (v/v) of KnockOut™ Serum Replacement (Gibco™), 1% (v/v) MEM Non-essential Amino Acids Solution (Gibco™), 2.4 g/L of Sodium Bicarbonate (Sigma-Aldrich®) and 0.5% (v/v) of Penicillin/Streptomycin (Gibco™).
This medium was stored at 4°C and pre-warmed at room temperature prior to use.

III.1.1.3.2. mTeSR™ Plus

mTeSR™ Plus (StemCell Technologies™) was used for hiPSCs maintenance on Matrigel® matrix. This culture medium is a defined serum-free, stabilized cell culture medium designed for *in vitro* feeder-free maintenance and expansion of hESCs and hiPSCs.
mTeSR™ Plus 5X Supplement (StemCell Technologies™) was thawed overnight at 4°C and mixed with mTeSR™ Plus Basal Medium in order to generate mTeSR™ Plus complete medium. Thereupon, the complete medium was stored in 40 mL aliquots at -20°C. When necessary, mTeSR™ Plus aliquots were thawed, stored at 4°C and supplemented with 0.5% (v/v) Penicillin/Streptomycin solution before use (Penicillin/Streptomycin supplementation allowed to culture hiPSCs without bacterial contaminations). mTeSR™ Plus was pre-warmed at room temperature prior to use.

III.2. Human induced pluripotent stem cells' general manipulation techniques

III.2.1. Thawing of cryopreserved human induced pluripotent stem cells

Selected cryovials (Cryo Tube™ Vials, by Thermo Scientific™) containing hiPSCs were removed from liquid nitrogen tank and immersed on a 37°C-water bath, being gently swirled until its content appeared to be around 50% thawed. Then, 1 mL of pre-warmed washing medium was added dropwise to the cell vial with a pipette. After cell mixing, the total cell volume was transferred to a 15 mL Falcon® tube (Corning®) containing pre-warmed washing medium. Cells were pelleted by centrifugation (HERAEUS™ Megafuge™ 8, by Thermo Scientific™) for 3 minutes at 1,000 rpm (rotations per minute) and the supernatant discarded. Lastly, the cell pellet was resuspended into mTeSR™ Plus supplemented with 10 μM ROCK inhibitor (Y-27632, by StemCell Technologies™) and cell suspension was uniformly distributed on previously Matrigel®-coated wells. Cell culture plates were kept at a 5% Carbon dioxide (CO_2) humidified incubator (Series 8000 Water-Jacketed, by Thermo Scientific™) at 37°C.

III.2.2. Human induced pluripotent stem cells' harvesting and passaging

Cells were grown in Matrigel®-coated plates and passaged when they achieved around 70-80% of confluence. For this purpose, two different treatments were applied: an enzyme-free treatment and an enzymatic treatment.

III.2.2.1. Non-enzymatic treatment

PSCs are routinely passaged resorting to a non-enzymatic treatment with Ethylenediamine tetraacetic acid (EDTA), which is a chelating agent that promotes partial cell dissociation in small cellular aggregates [117].

Firstly, the exhausted culture medium was fully aspirated and cells were rapidly washed with 0.5 mM EDTA solution, that consists of 0.1% (v/v) Ultrapure™ 0.5M EDTA, pH 8.0 (Invitrogen™) and 1.8 g/L of Sodium Chloride (Sigma-Aldrich®) in DPBS. The following step was an incubation with the same solution for 5 minutes at room temperature. After this step, EDTA solution was removed and cells were detached from the wells by rinsing twice with mTeSR™ Plus. The remaining volume of culture medium was added to the resulting cell suspension for replating. When replating cells, cell suspension was homogenized and the desired volume transferred to previously Matrigel®-coated wells. Cell culture plates were kept at a 5% CO_2 humidified incubator at 37°C.

III.2.2.2. Enzymatic treatment

Alternatively, the enzymatic approach leads to the full individualization of cells by promoting cell dissociation from the surface and from other cells. Single-cell passaging is usually applied to enable an accurate cell count, and thus allowing a better control of the initial cell number on experiments.

As in the previously mentioned treatment, culture medium was aspirated and cells were rapidly washed with Dulbecco's Phosphate-Buffered Saline (DPBS, by Gibco™) solution. The following step was an incubation with Accutase® (Sigma-Aldrich®) solution for 5 minutes at 37°C, which led to colonies dissociation into single cells. Subsequently, cells were flushed with washing medium, inactivating enzymatic digestion action. The resulting cell suspension was collected to a 15 mL tube and centrifuged for 3 minutes at 1,000 rpm. The supernatant was discarded and the pellet was resuspended in mTeSR™ Plus supplemented with 10 μM of ROCK inhibitor. When re-plating cells, cell suspension was homogenized and the desired volume transferred to previously Matrigel®-coated wells. Cell culture plates were kept at a 5% CO_2 humidified incubator at 37°C.

III.2.3. Cell counting

When performing a cell count, the protocol for cell passaging with Accutase® treatment was applied. Thereafter, the resulting cell suspension was treated with a 1:10 (v/v) Trypan Blue Stain (Gibco™) solution (in DPBS solution) - which colours dead cells blue, enabling to only count live cells, which remain uncoloured. Thereupon, 10 µL of Trypan Blue-treated cell suspension were collected, loaded into a haemocytometer (Neubauer-improved, by Superior Marienfield™), and observed through an inverted optical microscope (CKX31, by Olympus®). For each condition, at least two independent counts were performed.

Total cell number was calculated considering haemocytometer square number whereat cells were counted, the applied dilution (in Trypan Blue stain), each square volume (10^{-4} cm^3) and the original cell suspension total volume; as indicated in the following equation:

$$Total\ cell\ number = \frac{\sum Counted\ cells}{\#\ Independent\ counts} \times \frac{Dilution\ factor}{\#\ Squares \times Square\ volume} \times Sample\ volume$$

III.2.4. Cryopreservation of human induced pluripotent stem cells

Cryopreservation allows long-term storage and preservation of hiPSCs, while maintaining their structural and functional integrity [118,119].

The first step of cryopreservation consisted of a washing step with EDTA solution and then, cells were incubated with 1 mL of EDTA solution for 5 minutes at room temperature. After incubation, cells were detached from wells' surface using washing medium and the resulting cell suspension was collected to a 15 mL tube and centrifuged for 3 minutes at 1,000 rpm. The supernatant was discarded and the resultant cell pellet was resuspended in freezing medium, which consists of 90% (v/v) culture medium and 10% (v/v) of Dimethyl sulfoxide (DMSO, by Sigma-Aldrich®)- a permeant cryoprotective agent which avoids cell rupture due to ice crystals formation [118,120]. Freezing medium was prepared on ice.

Each 1 mL cryovial was loaded with 250 µL of cell suspension and then placed in a freezing container (Mr. Frosty™, by Nalgene®) for controlled freezing (cooling rate of -1°C per minute) and stored in a -80°C freezer for, at least, 24 hours and afterwards transferred into a liquid nitrogen tank (-196°C; Biorack 3000, by Statebourne) for long-term storage until further use.

III.3. Differentiation of human induced pluripotent stem cells into nephron progenitor cells and kidney organoids

III.3.1. Culture media

III.3.1.1. RPMI 1640 and Advanced RPMI 1640

Roswell Park Memorial Institute medium 1640 (RPMI 1640, by Gibco™) and Advanced Roswell Park Memorial Institute medium 1640 (Advanced RPMI 1640, by Gibco™) were used to generate nephron progenitor cells and kidney organoids upon hiPSCs differentiation.
RPMI 1640 is a serum-free medium, containing high concentration of vitamins, but lacking lipids, proteins and growth factors, thus requiring supplementation to allow for cell growth.
Advanced RPMI is a widely used basal medium that allows the culture of mammalian cells with reduced Fetal Bovine Serum (FBS) supplementation.
Both media were stored at 4°C and supplemented with 1% (v/v) GlutaMAX™-I (100X) (Gibco™) and 0.5% (v/v) Penicillin/Streptomycin solution before use. These media were pre-warmed at room temperature prior to use.
Complete media formulation from both, RPMI 1640 and Advanced RPMI 1640, is presented in Table 8.1 and Table 8.2 (Annexes, Section VIII.).

III.3.1.2. STEMdiff™ APEL™ 2

STEMdiff™ APEL™ 2 (StemCell Technologies™) medium was used to generate nephron progenitor cells upon hiPSCs differentiation. This is a fully defined, serum and animal component-free medium suitable for hESCs and hiPSCs differentiation.
STEMdiff™ APEL™ 2 medium was stored in 10 mL aliquots at -20°C and, when necessary, aliquots were thawed, stored at 4°C and supplemented with 0.5% (v/v) Penicillin/Streptomycin solution before use. STEMdiff™ APEL™ 2 medium was pre-warmed at room temperature prior to use.

III.3.2. 3D culture: cell aggregates

The initial step towards generating organoids consists in promoting hiPSCs assembly into a 3D structure [121].
In this particular case, this assembly process was accomplished through a commercially available high-throughput methodology- AggreWell™ 800 plates (StemCell Technologies™)- which provides an easy and standardized way to produce a large number of size-specified cellular aggregates [112]. Each well of a 24 well plate contains 300 V-shaped bottom microwells of a defined size (800 μm), allowing for uniform aggregates production (Figure 3.1). This scaffold-free 3D

methodology takes advantage of the self-assembly properties of PSCs [121] and the lack of cell attachment surfaces to promote aggregation of cells and the formation of cellular aggregates. Scaffold-free methodologies such as AggreWell™ 800 plates are amenable to cellular and physiological gradients however, they are unable to proper mimic cell-to-ECM interactions [105].

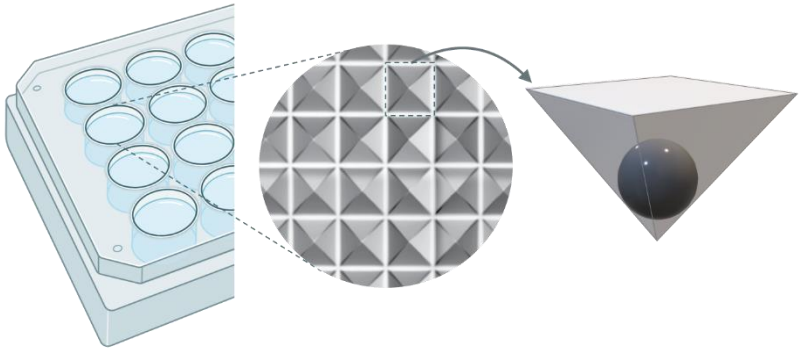

Figure 3.1| Schematic representation of AggreWell™ 800 plates and its V-shaped microwells. Each well of a 24 well plate contains 300 V-shaped bottom microwells. Figure created with BioRender.com.

Prior to cell seeding, each well of AggreWell™800 plates was rinsed with DMEM-F12 and 500 µL of mTeSR™ Plus supplemented with 10 µM of ROCK inhibitor were added to each well.
Plates were centrifuged for 3 minutes at 3,500 rpm to remove any possible formed air bubbles on microwells.
In order to study the effect of the initial aggregate size on the efficiency of renal commitment, different initial cell densities were used to generate aggregates inside each microwell (Table 3.1).

Table 3.1| Initial cell number (per well) and correspondent aggregate size (number of cells per aggregate/microwell) tested during this work.

Cell number	Number of cells per aggregate
$0.9x10^6$ Cells	3,000 Cells per aggregate
$1.2x10^6$ Cells	4,000 Cells per aggregate
$1.5x10^6$ Cells	5,000 Cells per aggregate

After single-cell seeding, mTeSR™ Plus supplemented with 10 µM of ROCK inhibitor was added to each well, up to a final volume of 1.5 mL per well.
At last, uniform cellular aggregates were rapidly established after a rotational force is applied to the plate: plates were centrifuged, for 3 minutes at 1,000 rpm, for cell settlement in each microwell and transferred to a 5% CO_2 humidified incubator at 37°C for 24 hours.
Throughout hiPSCs differentiation, various cell samples were collected at different time points (Days 0, 4, 7, 8, 9 and 14) and analysed through immunofluorescence staining and real-time polymerase chain reaction (RT-PCR) regarding different renal differentiation markers, in order to access their temporal fluctuation.

III.3.3. 3D cellular aggregate size measurement and analysis

For the purpose of determining aggregates size, several bright-field images of hiPSCs aggregates were acquired at various time points. In particular, to evaluate the effect of initial aggregate size towards the efficiency of hiPSCs derivation into intermediate mesoderm, bright-field images were acquired at *t*=24 hours (Day 0). The images were then analysed using an imaging processing software, ImageJ (Fiji®) to determine the area of each aggregate. Considering the aggregates as spheroids, their diameter was calculated according to the following equation:

$$D = 2 \times \sqrt{\frac{A}{\pi}}$$

In which *D* represents the aggregate's diameter, in μm, and *A* represents its area, in μm^2.

III.3.4. Cellular aggregates cryosectioning

When collecting cellular aggregates for cryosectioning, the first step was cell fixation, which was accomplished by washing aggregates with DPBS solution and incubating them with 4% (v/v) Paraformaldehyde (PFA, by Sigma-Aldrich®) solution (in DPBS) for 20 minutes at 4°C.
Previously fixed aggregates were first incubated in a 15% (w/v) Sucrose (Sigma-Aldrich®) solution (in DPBS solution), overnight at 4°C. In the following step, aggregates were left to incubate for 1 hour at 37°C, in a Gelatin solution composed of: 15% (w/v) Sucrose and 7.5% (w/v) Gelatin from porcine skin (Sigma-Aldrich®) (in DPBS solution). Afterwards, Gelatin blocks were obtained by transferring cell aggregates to the top of a formerly settled thin Gelatin layer and by being covered with the same solution. These were frozen by vitrification through submersion in Isopentane (VWR™) at -80°C.
The frozen aggregates were stored at -80°C and later, were cut resorting to a cryostat-microtome (CM3050 S, by Leica) at -24°C with a view to proceeding with immunofluorescence staining later. Organoids were serially sectioned at 12 μm thickness and placed on adhesive Superfrost® Plus (Thermo Scientific™) glass slides. Glass slides were stored at -20°C until further use.

III.3.5. Renal commitment of hiPSCs into nephron progenitor cells and kidney organoids

As previously referred, two different protocols were applied and adapted in order to obtain kidney organoids. Both protocols were applied to 2D and 3D conditions.

III.3.5.1. Morizane protocol

The differentiation protocol was initiated with late primitive streak induction by a GSK-3 inhibitor, CHIR99021 (Stemolecule™ CHIR99021; CHIR, by Stemgent™). This molecule was added to RPMI/Advanced RPMI medium, at a concentration of 5-11 µM, with or without 100-500 nM Dorsomorphin (Sigma-Aldrich®)- a BMP4 inhibitor [109]. This initial step took 3 or 4 days and the differentiation medium was refreshed at day 2. It was followed by Activin A (R&D Systems®) addition at a concentration of 10 ng/mL, for 2 or 3 days. Following that period, cells were treated with 10 ng/mL of FGF9 (R&D Systems®) for 2 days in order to induce NPCs. At this point, and to induce PTAs, 3 µM CHIR and 10 ng/mL FGF9 were added for 2 days. Afterwards, cells were cultured for 3 days with 10 ng/mL FGF9 to get differentiated into RVs. Subsequently, cells were cultured in growth factor-free medium until day 21 of differentiation, refreshing the differentiation medium every 2 days.

III.3.5.2. Takasato protocol

Equal to the previous protocol, the first step comprised culturing hiPSCs in Stemdiff™ APEL™ 2 medium supplemented with CHIR, however, here, this molecule was applied at a concentration of 8-10 µM with or without 100 nM Dorsomorphin for 3 or 4 days. Cells were then cultured with 200 ng/mL FGF9 and 1µg/mL Heparin (Sigma-Aldrich®) until day 7 of differentiation, refreshing the differentiation medium every 2 days. On day 7, a 5 µM CHIR pulse was applied for 1 hour. After this incubation, 200 ng/mL FGF9 and 1µg/mL Heparin were added to the differentiation medium. Cells were cultured for 5 days, refreshing the differentiation medium every 2 days. The final step of this protocol consisted of culturing cells with 1µg/mL Heparin-containing medium until day 25 of differentiation, refreshing the differentiation medium every 2 days.

III.4. Characterisation of human induced pluripotent stem cells, nephron progenitor cells and kidney organoids

hiPSCs characterization was performed resorting to immunofluorescence staining and flow cytometry analysis.

In order to understand if the different stages of renal differentiation were being reached by the cells, a characterization of those cell populations was needed. For that purpose, immunofluorescence staining analysis, flow cytometry analysis and RT-PCR were the three performed techniques.

III.4.1. Immunofluorescence staining

Stained cells were observed resorting to two different microscopes: a fluorescence optical microscope (Leica DFC7000 T digital camera and a Leica Kubler CODIX fluorescence illuminator, associated to a Leica DMI 3000 B microscope) and images were acquired with Las X (Leica Application Suite X, by Leica).
The acquired images were treated in an imaging processing software, ImageJ, whenever needed.

III.4.1.1. Immunofluorescence staining for human induced pluripotent stem cells' pluripotency assessment

III.4.1.1.1. Surface staining

Firstly, the culture medium present in wells was removed. Primary antibody (Table 3.2) was diluted in staining solution (5% (v/v) Normal goat serum (NGS, by Sigma-Aldrich®) and 0.1% (v/v) of Triton-X-100 (Sigma-Aldrich®) in DPBS solution) and cells were treated with this solution for 90 minutes at room temperature. Cells were washed three times with 1 mL of DPBS solution to remove any excess of the primary antibody. The staining solution containing the secondary antibody (Table 3.2) was placed on wells, and left to incubate for 60 minutes at room temperature, in the dark. Following this, cells were once more washed thrice with DPBS solution and left in this solution. Cells were stored, for later observation, at 4°C in the dark.

III.4.1.1.2. Intracellular staining of fixed cells

Intracellular staining procedure required cell fixation, which was accomplished by removing culture medium, washing cells with DPBS solution and incubating cells with 250 µL of 4% (v/v) PFA solution for 20 minutes at 4°C. After this incubation step, PFA solution was removed and DPBS solution was added to each well.
When initiating cell intracellular staining, DPBS solution was aspirated and cells were incubated for 30 minutes at room temperature with blocking solution (10% (v/v) NGS and 0.1% (v/v) Triton-X-100 in DPBS solution) in order to reduce backgrounds staining. Cells were placed on primary antibody (diluted in staining solution) for 90 minutes at room temperature (Table 3.2). Afterwards, three washing steps with DPBS solution were performed followed by an incubation with secondary antibody (also diluted in staining solution) (Table 3.2) for 60 minutes at room temperature, in the dark. Once more, cells were washed to remove any exceeding secondary antibody with DPBS solution and nuclear-stained using a 15:10,000 (v/v) 4',6-Diamidino-2-Phenylindole (DAPI, by Sigma-Aldrich®) solution (in water)- a nuclei counterstaining that binds strongly to adenine-thymine rich regions of DNA [122] for 2 minutes at room temperature. As an

ending step, DAPI was removed, cells were washed thrice with DPBS solution to remove any remaining DAPI crystals and left in DPBS solution. Cells were stored, for later observation, at 4℃ in the dark.

III.4.1.2. Immunofluorescence staining of nephron progenitor cells and kidney organoids

III.4.1.2.1. Intracellular staining of nephron progenitor cells and kidney organoids

Immunofluorescence staining protocol slightly differs depending on being applied to nephron progenitor cells or kidney organoids as for the former, it is performed on cell culture plates and, for the later, on glass slides. In the first case, DPBS solution was aspirated from fixed cells while in the second case, slides with sectioned aggregates were de-gelatinized through an incubation with pre-warmth PBS for 1 hour at 37°C.

From this initial step forward, the immunofluorescence staining protocol was equally applied.

PFA residues were washed with 0.1 M Glycine (Sigma-Aldrich®) solution (in DPBS solution) and cells were afterwards permeabilized with 0.1% (v/v) of Triton-X-100 solution (in DPBS solution), both for 10 minutes at room temperature. Following this, two washing steps were performed with DPBS solution for 5 minutes each and cells were then incubated for 30 minutes with blocking solution which consists of 10% (v/v) FBS (VWR™) in TBS-T solution. TBS-T solution is comprised of 20 mM of Trizman® hydrochloride solution, pH 8.0 (Sigma-Aldrich®), 150 mM Sodium chloride and 0.05% (v/v) Tween-20 (Sigma-Aldrich®). Cells were then left to incubate with primary antibody (diluted in blocking solution) (Table 3.2) for 1-2 hours at room temperature or overnight at 4℃. Afterwards, three washing steps with TBS-T solution were performed, followed by an incubation with secondary antibody (also diluted in blocking solution) (Table 3.2) for 30 minutes at room temperature, in the dark. Once more, cells were washed thrice with TBS-T solution and nuclear-stained with DAPI for 5 minutes at room temperature. Lastly, cells were washed thrice with TBS-T solution.

Culture plates were left in DPBS solution whereas glass slides were mounted with Mowiol® 4-88 (Sigma-Aldrich®) and a coverslip. In both cases, and for later observation, storage was done at 4℃ in the dark.

III.4.1.3. Antibodies

In Table 3.2, a list of antibody solutions used in immunofluorescence staining assays throughout this work, is presented.

Table 3.2| List of antibody solutions and correspondent dilutions used on immunofluorescence assays during this work.

Marker	Primary Antibody	Dilution	Secondary Antibody	Dilution
Intracellular markers				
FOXD1	Anti-FOXD1 Mouse IgG2b (Santa Cruz Biotechnology)	1:50	Alexa Fluor™ 488 Goat Anti-Mouse IgG2b	1:500
GATA3	Anti-GATA3 Mouse IgG1 (Santa Cruz Biotechnology)	1:50-500	Alexa Fluor™ 488 Goat Anti-Mouse IgG1	
HOXD11	Anti-HOXD11 Mouse IgG2a (Santa Cruz Biotechnology)	1:50-150	Alexa Fluor™ 488 Goat Anti-Mouse IgG2a (Invitrogen™)	
LHX1	Anti-LHX1 Mouse IgG2a (Santa Cruz Biotechnology)	1:50		
NANOG	Anti-NANOG Rabbit IgG (Thermo Scientific™)	1:500	Alexa Fluor™ 546 Goat Anti-Rabbit IgG	
OCT4	Anti-OCT4 Mouse IgG (Millipore®)	1:750	Alexa Fluor™ 546/488 Goat Anti-Mouse IgG	
PAX8	Anti-PAX8 Rabbit IgG (Proteintech®)	1:50	Alexa Fluor™ 488 Goat Anti-Rabbit IgG	
SIX2	Anti-SIX2 Rabbit IgG (Invitrogen™)	1:50		
SOX2	Anti-SOX2 Mouse IgG (R&D Systems®)	1:500	Alexa Fluor™ 546 Goat Anti-Mouse IgG	
WT1	Anti-WT1 Rabbit IgG (Invitrogen™)	1:50-500	Alexa Fluor™ 546/488 Goat Anti-Rabbit IgG	

III.4.2. Flow cytometry

Flow cytometry was performed to identify different cell subpopulations based on their surface antigens expression. This procedure was firstly performed to assess cell pluripotency and afterwards, to assess the percentage of WT1-positive cells obtained after the initial steps of differentiation.

Prepared cell samples were analysed on FACSCalibur™ flow cytometer (Becton Dickinson Biosciences®), using CellQuest™ software (Becton Dickinson Biosciences®) for data acquisition. The obtained results were analysed in Flowing Software 2.5.1 (Turku Centre for Biotechnology).

III.4.2.1. Sample collection and preparation

Cultured cells were firstly washed with DPBS solution and singularised by an incubation with Accutase® solution for 5 minutes at 37℃. After incubation, cells were detached from wells

surface using washing medium and the resulting cell suspension was collected to a 15 mL tube and centrifuged for 3 minutes at 1,000 rpm. The supernatant was discarded, and the cells were fixed through pellet resuspension in 1 mL of 2% (v/v) PFA solution (in DPBS solution). Cells were kept in PFA solution at 4°C.

III.4.2.2. Flow cytometry analysis for human induced pluripotent stem cells' pluripotency assessment

III.4.2.2.1. Intracellular staining of fixed cells

Eppendorf® tubes were coated with 1% (v/v) Bovine Serum Albumin (BSA, by Invitrogen™) (in DPBS solution) solution for 15 minutes at room temperature, prior to their utilization. Cell suspension samples, previously stored in PFA 2% (v/v) solution, were centrifuged for 3 minutes at 1,000 rpm (Z-300k, by Hermle Labortechnik GmbH), the supernatant was removed and a washing step with 1% (v/v) Normal Goat Serum (NGS, by Sigma-Aldrich®) solution (in DPBS solution) was performed. Once more, cell samples were centrifuged for 3 minutes at 1,000 rpm and resuspended in 3% (v/v) NGS (in DPBS solution).

After BSA removal from the tubes, cell suspension was equally distributed to each tube and centrifuged for 3 minutes at 1,000 rpm. After supernatant removal, cell membrane permeabilization was achieved by an incubation with 1:1 (v/v) solution of 3% (v/v) NGS and 1% (v/v) Saponin (Sigma-Aldrich®) (in water) for 15 minutes at room temperature. Afterwards, tubes were centrifuged for 3 minutes at 1,000 rpm, the supernatant was removed and the resultant cell pellet was treated with a 3% (v/v) NGS solution for 15 minutes at room temperature. After cell centrifugation (for 3 minutes at 1,000 rpm) and supernatant removal, the resultant pellet was incubated with primary antibody (diluted in 3% (v/v) NGS solution) (Table 3.3) for 90 minutes at room temperature.

The negative control sample was incubated with 3% (v/v) NGS solution. Following incubation, all cell samples were centrifuged for 3 minutes at 1,000 rpm and washed twice with 1% (v/v) NGS solution, and incubated for more 45 minutes in the dark, at room temperature, with the secondary antibody (also diluted in 3% (v/v) NGS solution) (Table 3.3). Finally, and after centrifugation for 3 minutes at 1,000 rpm, another two washing steps with 1% (v/v) NGS solution were performed. Cell samples were resuspended in DPBS solution and transferred to FACS (Fluorescence-Activated Single Cell Sorting) tubes for further analysis.

III.4.2.2.2. Extracellular staining of fixed cells

For extracellular staining, cell samples were firstly centrifuged for 3 minutes at 1,000 rpm, the supernatant was removed and cells were left to incubate with primary antibody (diluted in 3% (v/v) NGS solution) (Table 3.3) for 15 minutes at room temperature, in the dark.
When evaluating extracellular markers, a cell sample was also tagged with an isotype control which acted as a negative control (for 15 minutes at room temperature, in the dark).
Afterwards, a washing step was performed twice: 2 mL of DPBS solution were added to each tube (without removing any previous content), tubes were centrifuged for 3 minutes at 1,000 rpm and the supernatant was removed. DPBS solution was used to resuspend cell pellets and the resultant cell suspensions were transferred to FACS tubes for further analysis.

III.4.2.3. Flow cytometry analysis of nephron progenitor cells and kidney organoids

Firstly, cell samples were centrifuged for 3 minutes at 1,000 rpm and the supernatant was removed. Cells were then resuspended in 1 mL of 90% (v/v) Methanol (Sigma-Aldrich®) solution and placed for 1 hour at -20°C. After incubation, and in order to remove the Methanol, a washing step was performed twice: 2 mL of Flow Buffer 2 (0.5% (w/v) of BSA and 0.1% (v/v) Triton-X-100 in DPBS solution) were added to each tube which was then centrifuged for 3 minutes at 1,000 rpm. The following step was an incubation with 100 µL of primary antibody (diluted in Flow Buffer 2) for 1 hour at room temperature (Table 3.3). Afterwards, cell samples were washed twice with Flow Buffer 2 and resuspended in 100 µL of secondary antibody (also diluted in Flow Buffer 2) for 30 minutes at room temperature (Table 3.3). At last, cells were, once more, washed twice, resuspended in 300 µL of Flow Buffer 1 (0.5% (w/v) of BSA in DPBS solution) and transferred to FACs tubes for further analysis.

III.4.2.4. Antibodies

In Table 3.3, a list of antibody solutions used in flow cytometry analysis throughout this work, is presented.

Table 3.3| List of antibody solutions and correspondent dilutions used on flow cytometry analysis throughout this work. For the intracellular markers containing an asterisk (*), it was used a phycoerythrin (PE)-conjugated antibody, which does not require a secondary antibody. For these antibodies, an isotype control is listed instead of a secondary antibody.

Marker	Primary Antibody	Working Dilution	Secondary Antibody/ Isotype control	Working Dilution
Intracellular markers				
OCT4	Anti-OCT4 Mouse IgG (Millipore®)	1:300	Alexa Fluor™ 488 Goat Anti-mouse IgG	1:500
SOX2	Anti-SOX2 Mouse IgG (R&D Systems®)	1:200		
WT1	Anti-WT1 Rabbit IgG (Invitrogen™)	1:500	Alexa Fluor™ 488 Goat Anti-Rabbit IgG	1:500
Extracellular markers				
SSEA-1*	Anti-human SSEA-1-PE (PioLegend)	1:10	REA control (S)-PE (Miltenyi Biotec)	2:10
SSEA-4*	Anti-human SSEA-4-PE (Miltenyi Biotec)			
TRA-1-60*	Anti-human TRA-1-60-PE (Miltenyi Biotec)			

III.4.3. Real time polymerase chain reaction

RT-PCR allows to determine the expression of a particular gene present in a cell sample. This procedure was applied to evaluate gene expression during renal differentiation, namely, of the following genes: *WT1, PAX2, SIX2, GATA3* (GATA binding protein 3) and *HOXD11* (Homeobox D11**)**. Glyceraldehyde-3-phosphate Dehydrogenase (*GAPDH*) was used as an endogenous control gene.

Cell samples from sequential stages of renal differentiation were collected, singularised and stored at -80℃. Later, total RNA from the collected samples was extracted resorting to a High Pure RNA Isolation Kit (Roche) according to manufacturers' instructions. RNA concentration was, afterwards, quantified using a NanoVue™ Plus Spectrophotometer (GE Healthcare).

For complementary deoxyribonucleic acid (cDNA) synthesis, 1 µg of the previously extracted RNA was reverse transcribed into cDNA with a High Capacity cDNA Reverse Transcription Kit (Applied Biosystems®) also following the provided instructions. The RNA-cDNA conversion was done resorting to a T100™ Thermal Cycler (Bio-Rad) with the following program: 10 minutes at 25℃, 120 minutes at 37℃, 5 minutes at 85℃ and then, 4℃ until storage (at -20℃).

RT-PCR was run using 12.5 ng of cDNA, Speedy qPCR Green Master Mix (2x) ROX plus (NZYtech), and forward and reverse-primers at 250 µM each. The used primers are listed in Table 8.3 (Annexes, Section VIII.).

Reactions were run in triplicate using StepOnePlus™ RT-PCR System (Applied Biosystems®) and data were analysed using StepOne Software V2.2.2 (Applied Biosystems®). The threshold cycles (C_T) obtained for each sample were compared with C_T from the endogenous control gene *GAPDH*, resulting in ΔC_T. These values were normalized with C_T obtained at day 0, $\Delta\Delta C_T$, and the final results of gene expression are represented as $2^{-\Delta\Delta C_T}$.

IV. RESULTS AND DISCUSSION

IV.1. Pluripotency assessment of hiPSCs

Since the quality of the obtained differentiated cells is directly influenced by the quality of the starting hiPSCs [123], cultured hiPSCs were firstly evaluated regarding their pluripotency.

One important aspect to consider when evaluating hiPSCs pluripotency is cellular morphology. In order to evaluate it, a single-cell suspension of hiPSCs was seeded in Matrigel®-coated plates using mTeSR™ Plus supplemented with ROCK inhibitor, which was added to promote cell survival.

Images of hiPSCs morphology at 24, 48 hours and 120 hours (5 days), after single-cell seeding, are presented in Figure 4.1.

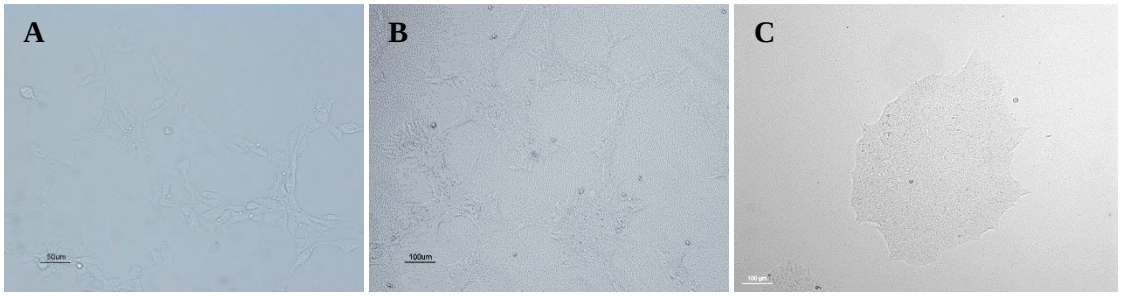

Figure 4.1| Representative brightfield images of cultured hiPSCs. Cells (GEpi, P45) were previously expanded on Matrigel®-coated culture plates in mTeSR Plus™ medium at a density of 15,000 cells/cm^2. **A)** 24 hours after single-cell seeding, image at 200x magnification (scale bar: 50 µm); **B)** 48 hours after single-cell seeding; **C**) 120 hours (5 days) after single-cell seeding, images at 100x magnification (scale bars: 100µm).

Considering the images corresponding to 24 and 48 hours of culture, it is possible to identify individual cells with a high nuclear to cytoplasmic ratio, as well as a prominent single nucleolus, both typical features of hPSCs [124]. Also, 24 hours after cell seeding, cells display an elongated morphology due to ROCK inhibitor presence.

hiPSCs depend on cell-to-cell interactions for survival, therefore, these cells grow as adherent colonies in culture [94]. Thus, as cells grow, divide and get more confluent, individual cells are indistinguishable, as cells get closely attached to each other (Figure 4.1, C). In Figure 4.1,C is possible to identify a hiPSCs colony in the centre of the image exhibiting a hPSCs typical morphology which is characterized by flat and densely packed colonies with a round shape and defined borders [124].

Apart from cellular morphology, hiPSCs pluripotency can also be assessed by analysing pluripotency markers expression, such as the cell surface markers SSEA-3, SSEA-4, TRA-1-60, TRA-1-81 and the transcription factors OCT4, SOX2 and NANOG [7,11]. When evaluating pluripotency, it is also important to consider another surface marker, SSEA-1, which opposite to what occurs in mouse PSCs, should have low expression [1].

Considering that, cultured cells were firstly characterized concerning the expression of intracellular pluripotency markers (OCT4, SOX2 and NANOG) by immunofluorescence staining. The obtained results were merged with DAPI and are presented in Figure 4.2.

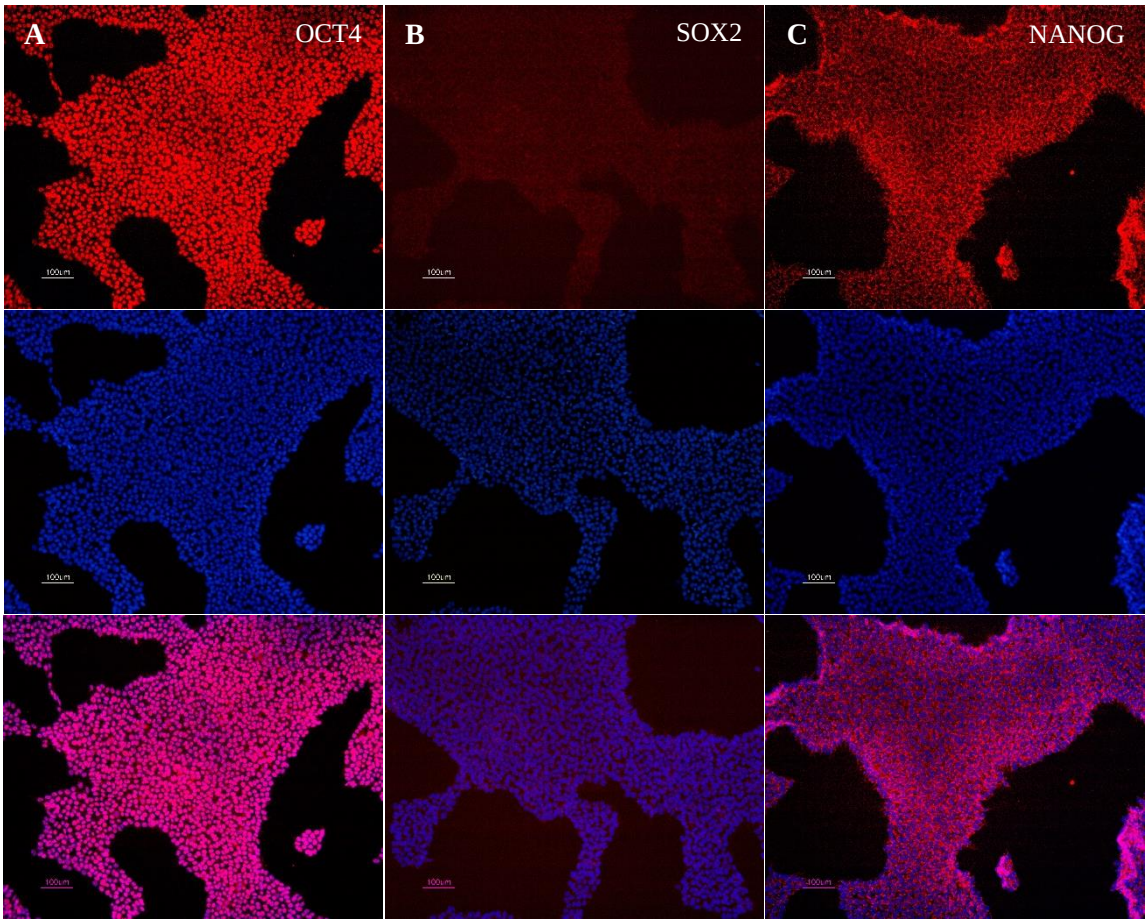

Figure 4.2| Immunofluorescence staining analysis of GEpi hiPSCs pluripotency markers. Cells (GEpi, P45) were previously expanded on Matrigel®-coated culture plates in mTeSR Plus™ medium at a density of 15,000 cells/cm^2. Immunofluorescence staining with DAPI counterstain discloses positive expression of endogenous pluripotency markers in the nuclei. **A)** Immunofluorescence staining of the transcription factor OCT4 (top), nuclear staining with DAPI (centre) and merge between OCT4 and nuclear staining with DAPI (bottom); **B)** Immunofluorescence staining of the transcription factor SOX2 (top), nuclear staining with DAPI (centre) and merge between SOX2 and nuclear staining with DAPI (bottom); **C)** Immunofluorescence staining of the transcription factor NANOG (top), nuclear staining with DAPI (centre) and merge between NANOG and nuclear staining with DAPI (bottom). Images were acquired with a fluorescence optical microscope. Images at 100x magnification (scale bars: 100 µm). DAPI: 4',6-Diamidino-2-Phenylindole; OCT4: Octamer-binding transcription factor 4; SOX2: Sex determining region Y-box 2.

Although immunofluorescence staining analysis allowed to confirm the presence of pluripotency markers throughout the entire area of cell colonies- qualitative analysis, flow cytometry analysis was also performed in order to quantify pluripotency markers expression (OCT4 and SOX2 for cell intracellular markers, and SSEA-4, SSEA-1, and TRA-1-60 as a cell surface markers). Results are presented in Figure 4.3.

Flow cytometry histograms exhibit the percentage of cells in the population expressing each pluripotency marker. The use of a negative control allowed to distinguish between specific antibody signal and non-specific background signal as, in each case, the negative control signal was subtracted from the signal of the target labels.

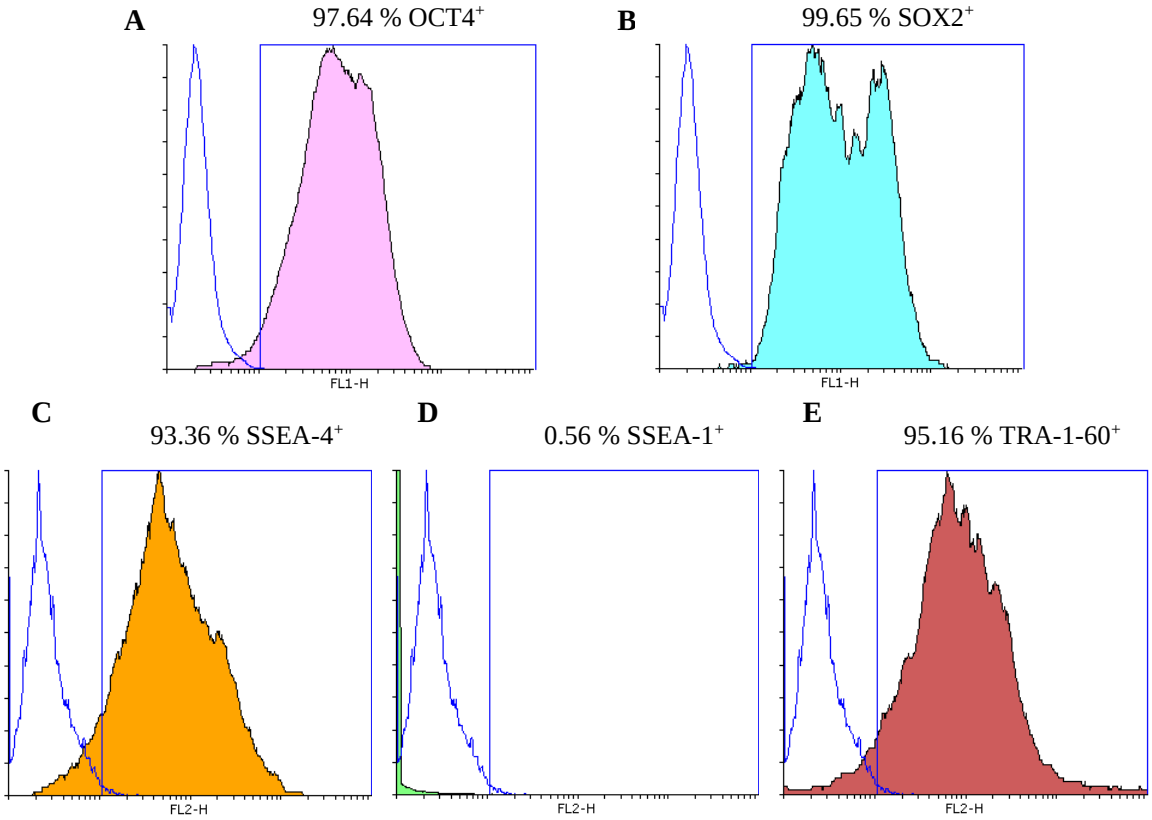

Figure 4.3| Flow cytometry analysis of GEpi hiPSCs intracellular and extracellular pluripotency markers. Cells (GEpi, P45) were previously expanded on Matrigel®-coated culture plates in mTeSR Plus™ medium at a density of 15,000 cells/cm^2. The areas under the blue curves represent the negative control and the coloured areas correspond to the analysed samples. The percentage of analysed cells expressing each pluripotency marker is shown above bars. **A)** OCT4; **B)** SOX2; **C)** SSEA-4; **D)** SSEA-1; **E)** TRA-1-60. (*n*=1). OCT4: Octamer-binding transcription factor 4; SOX2: Sex determining region Y-box 2; SSEA-4/1: Stage Specific Embryonic Antigen 4/1; TRA-1-60: Tumour-Rejection Antigen 1-60.

Flow cytometry histograms reveal high levels of expression for the four pluripotency markers, confirming hiPSCs pluripotency. In accordance, the expression of the differentiation marker SSEA-1 is restricted to a low percentage of cells (0.56%).

IV.2. Derivation of kidney organoids from human induced pluripotent stem cells under 3D conditions

This work constituted the first approach in conducting renal differentiation from hiPSCs in SCERG's laboratory, therefore, the referred differentiation protocols used throughout this work (Morizane and Takasato) were not optimized for the available cell lines.

On this account, there was the need to test several different culture conditions (mainly in terms of small molecule concentrations and seeding cell densities) during the course of this work. As a consequence, the different tested culture conditions were mainly implemented once, meaning that the performed studies have limited statistical relevance.

Throughout this work various experiments regarding renal differentiation were conducted in both adherent monolayer and 3D culture conditions.

Taking the previous information into consideration, the results obtained when conducting all experiments in this work will be presented and discussed in the following sections.

IV.2.1. From pluripotent stem cells to nephron progenitor cells and kidney organoids

IV.2.1.1. Morizane protocol: Monolayer culture #1

The first experiment in this work consisted in carrying Morizane protocol with GEpi cells and intended to adapt some culture conditions to this cell line, on monolayer culture.

Morizane and Bonventre [109] state that the initial cell density substantially affects the differentiation efficiency and recommend adjusting cell density to obtain around 50% confluency when differentiation is initiated. For that reason, one of the initial steps in this work was the test of different cell densities, namely, densities of ~10,000, 15,000, 20,000 and 25,000 cells/cm^2 were tested.

The differentiation protocol was initiated 48 hours after seeding and, thenceforward, cells were cultured in RPMI 1640 medium. The first step comprised the optimization of CHIR concentration, as the authors of both protocols state that different cell lines respond differently to CHIR and consequently, CHIR dose requires an adjustment for each cell line [109,110]. The authors recommend applying a dose of CHIR between 3-10 µM for 4 days [109].

Therefore, cells were exposed to 5 or 8 µM of CHIR for a period of 4 days (96 hours).

The authors also observed some changes in cellular morphology during this process, defending that at the fourth day of the differentiation protocol, corresponding to late primitive streak stage, cells should form 'loosely dense' clusters in order to proceed with a successful renal differentiation [109]. Figure 4.4 depicts the cellular morphology obtained by the authors on day 4 of the differentiation protocol.

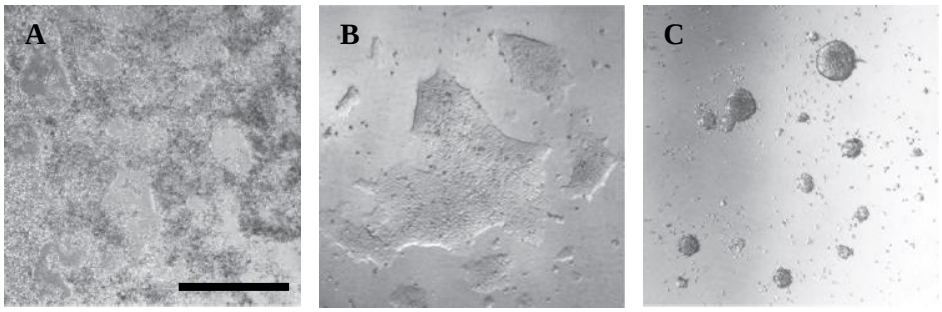

Figure 4.4| Cellular morphology on day 4 of the differentiation protocol. A) 'Too lose' cellular clusters morphology; **B)** 'Loosely dense' cellular clusters morphology; **C)** 'Too dense' cellular clusters morphology. Scale bar: 100 µm. Figure adapted from Morizane & Bonventre, 2016 [109].

This morphology should indicate the best moment to proceed with the next step in differentiation, which involved treating cells with Activin A (10 ng/mL) for 3 days.

Figure 4.5 shows cells on day 0 and 4 of the differentiation protocol, for the different seeded cell densities.

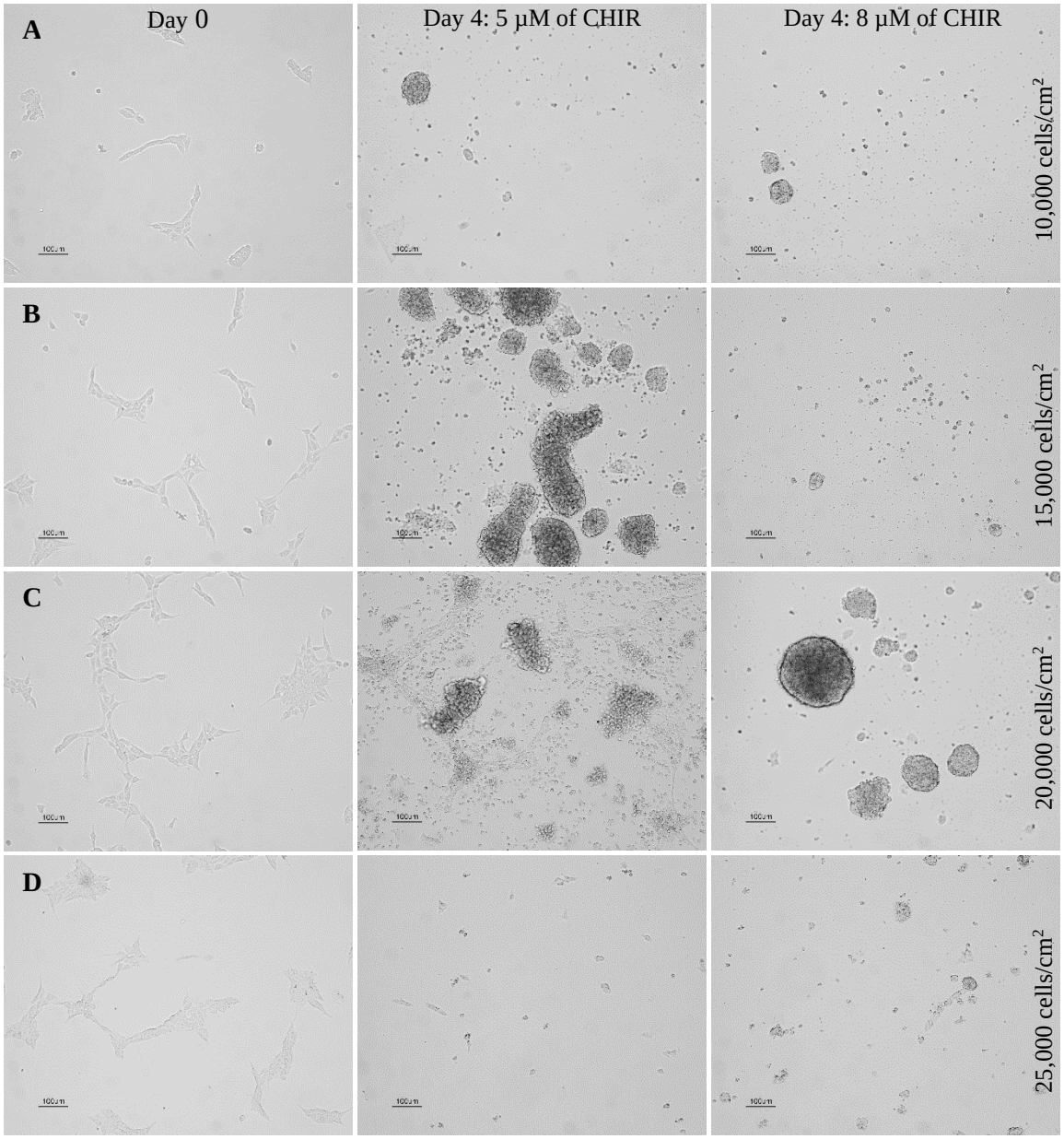

Figure 4.5| Representative brightfield images of hiPSCs seeded at different cell densities on day 0 and 4 of the differentiation protocol. Cells (GEpi, P46) were seeded at a density of 10,000, 15,000, 20,000 and 25,000 cells/cm^2 in Matrigel®-coated wells in mTeSR Plus™ medium. At day 0 of the differentiation protocol, the culture medium was changed to RPMI 1640 medium. **A)** Cells seeded at a density of 10,000 cells/cm^2 on day 0 of the differentiation protocol (left); Cells on day 4 of the differentiation protocol, when exposed to 5 µM of CHIR for 96 hours (centre); Cells on day 4 of the differentiation protocol, when exposed to 8 µM of CHIR for 96 hours (right); **B)** Cells seeded at a density of 15,000 cells/cm^2 on day 0 of the differentiation protocol (left); Cells on day 4 of the differentiation protocol, when exposed to 5 µM of CHIR for 96 hours (centre); Cells on day 4 of the differentiation protocol, when exposed to 8 µM of CHIR for 96 hours (right); **C)** Cells seeded at a density of 20,000 cells/cm^2 on day 0 of the differentiation protocol (left); Cells on day 4 of the differentiation protocol, when exposed to 5 µM of CHIR for 96 hours (centre); Cells on day 4 of the differentiation protocol, when exposed to 8 µM of CHIR for 96 hours (right); **D)** Cells seeded at a density of 25,000 cells/cm^2 on day 0 of the differentiation protocol (left); Cells on day 4 of the differentiation protocol, when exposed to 5 µM of CHIR for 96 hours (centre); Cells on day 4 of the differentiation protocol, when exposed to 8 µM of CHIR for 96 hours (right). Images at 100x magnification (scale bars: 100 µm).

By paying close attention to cellular morphology on the fourth day of differentiation, it is possible to say that 'loosely dense' cell clusters were not observable. Instead, 'too dense' clusters were formed when cells were seeded at densities of 10,000, 15,000 and 20,000 cells/cm^2. This suggests that the applied CHIR concentrations were not adequate to induce the intended 'loosely dense' cell morphology, and thus, not adequate to induce the late primitive streak stage.

Although the resultant morphology was not the ideal morphology to proceed with the differentiation protocol, Activin A (10 ng/mL) was followingly applied. Cells were cultured for another 3 days and fixed on day 7 of the differentiation protocol in order to get characterized through immunofluorescence staining.

Cells were then characterized through immunofluorescence staining against WT1 expression. At day 7 of the differentiation protocol, cells should express WT1, a posterior IM marker [109]. Immunofluorescence staining revealed that cells presented a negative expression of this intermediate mesodermal marker, as it was expected.

IV.2.1.2. Morizane protocol: Monolayer culture #2

The authors suggest that one possible cause for unsuccessful induction of IM is that CHIR treatment might induce endogenous production of BMP4, which could promote cell differentiation into the posterior primitive streak and, subsequently, into lateral plate mesoderm [91]. BMP4 is known to be expressed in the lateral plate mesoderm and to promote lateral plate mesoderm development. However, when in low concentration, this molecule is able to induce IM [109,110] (Figure 1.8, A).

Their results also showed that the efficacy of posterior IM induction was highly sensitive to the presence of BMP4 signalling at the primitive streak stage [91,109]. In light of this information, authors suggest testing different antagonist concentrations in order to suppress BMP4 to an optimal level, where it can induce IM [91,109].

As the previous attempt was not successful in inducing IM, the following step comprised the addition of a BMP4 antagonist, Dorsomorphin. In this experiment, cells were seeded at a density of 25,000 cells/cm^2 and exposed to either 5 or 8 µM of CHIR and, simultaneously, different Dorsomorphin concentrations, ranging 0, 100, 300 or 500 nM of Dorsomorphin.

Morizane and Bonventre defend that exposing cells to WNT signalling for 96 hours allows an efficient induction of the late primitive streak [109]. However, and as formerly stated, varying the exposure time to WNT signalling, enables to determine the predominant population during kidney development [110] (Section I.4.3.). For this reason, in addition to different CHIR and Dorsomorphin concentrations, cells were also exposed to WNT signalling for different periods of time, for 72 or 96 hours.

By exposing hiPSCs to WNT signalling for different periods of time, we intended to assess the adequate exposure time resulting in simultaneous induction of both cell populations: ureteric epithelium and MM. The differentiation protocol was initiated 48 hours after seeding and, thenceforward, cells were cultured in RPMI 1640 medium.

Figure 4.6 depicts brightfield images of cells exposed to 5 µM of CHIR and different concentrations of Dorsomorphin, and Figure 4.7 depicts brightfield images of cells exposed to 8 µM of CHIR and different concentrations of Dorsomorphin, both on day 4 of the differentiation protocol.

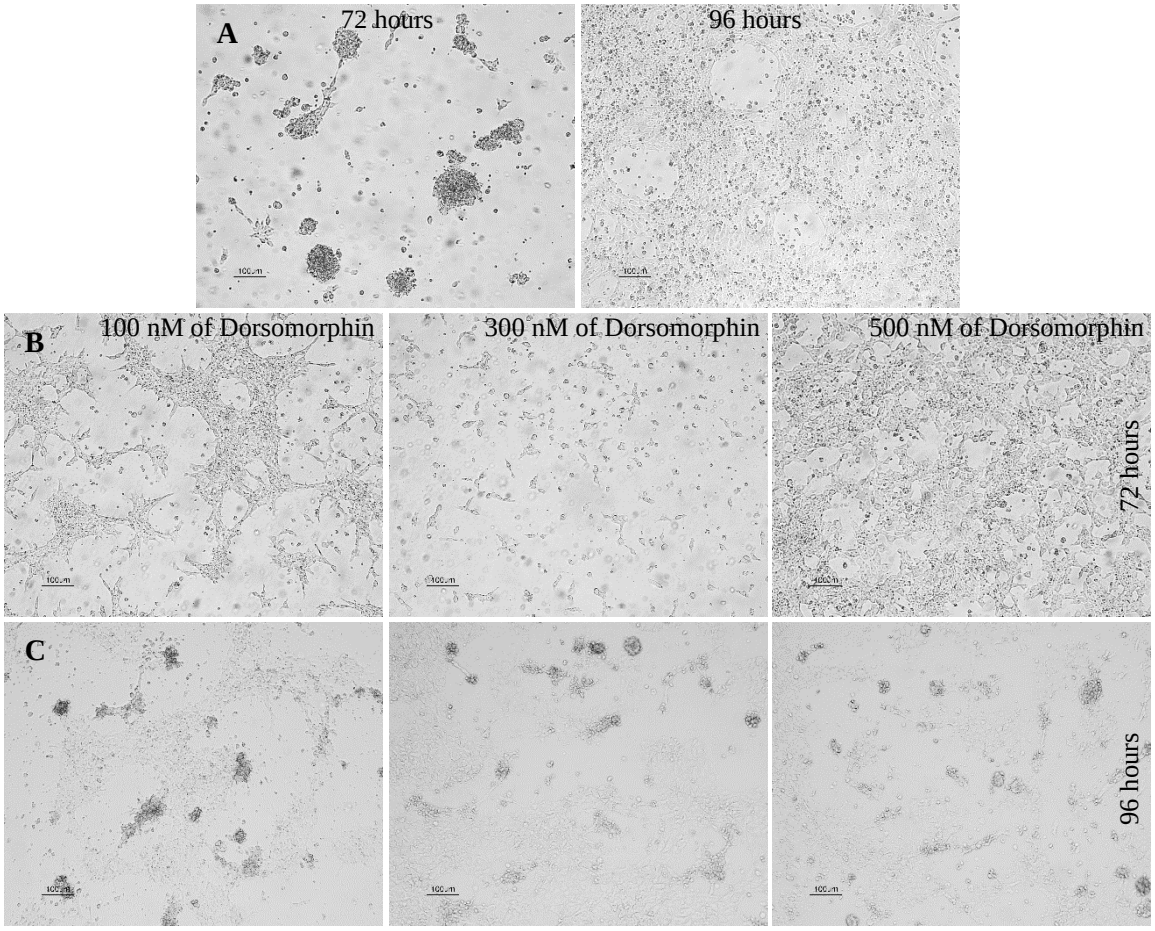

Figure 4.6| Brightfield images of hiPSCs exposed to 5 µM of CHIR and different Dorsomorphin concentrations, on day 4 of the differentiation protocol. Cells (GEpi, P52) were seeded at a density of 25,000 cells/cm^2 in Matrigel®-coated wells in mTeSR Plus™ medium. At day 0 of the differentiation protocol, the culture medium was changed to RPMI 1640 medium. **A)** Cells were exposed to 5 µM of CHIR for 72 (left) or 96 hours (right); **B)** Cells were exposed to 5 µM of CHIR and 100, 300 or 500 nM of Dorsomorphin (from left to right, respectively) for 72 hours; **C)** Cells were exposed to 5 µM of CHIR and 100, 300 or 500 nM of Dorsomorphin (from left to right, respectively) for 96 hours. Images at 100x magnification (scale bars: 100 µm).

Brightfield images of hiPSCs-derived cells show that cells did not present a 'loosely dense' clusters like morphology independently of the different tested culture conditions.

The tested culture conditions resulted in cells with a predominant 'loose' morphology.

These images also reveal morphological differences between cells only exposed to CHIR (A) and cells exposed to both CHIR and Dorsomorphin (B and C). One aspect that draws attention is that cells only exposed to CHIR exhibit a 'too dense' like cell morphology when exposed to this molecule for 72 hours. Contrastingly, cells exposed to both CHIR and Dorsomorphin only exhibit a 'too dense' like cell morphology when exposed to these molecules for 96 hours.

In addition, cells only exposed to CHIR for 96 hours (A, right) and cells exposed to CHIR and 500 nM of Dorsomorphin for 72 hours (B, right), display a similar morphology and resemble the cellular morphology defined by the authors as 'too loose'.

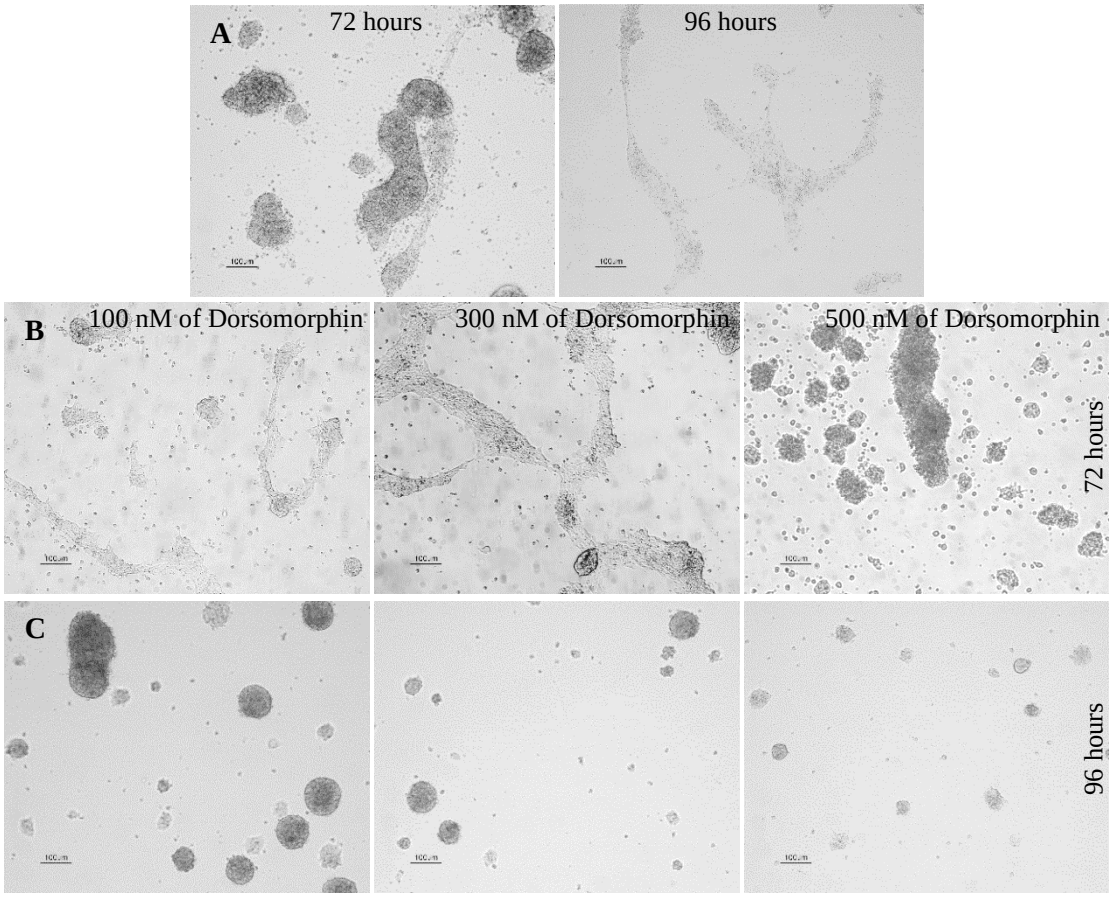

Figure 4.7| Brightfield images of hiPSCs exposed to 8 µM of CHIR and different Dorsomorphin concentrations, on day 4 of the differentiation protocol. Cells (GEpi, P52) were seeded at a density of 25,000 cells/cm^2 in Matrigel®-coated wells in mTeSR Plus™ medium. At day 0 of the differentiation protocol, the culture medium was changed to RPMI 1640 medium. **A)** Cells were exposed to 8 µM of CHIR for 72 (left) or 96 hours (right); **B)** Cells were exposed to 8 µM of CHIR and 100, 300 or 500 nM of Dorsomorphin (from left to right, respectively) for 72 hours; **C)** Cells were exposed to 8 µM of CHIR and 100, 300 or 500 nM of Dorsomorphin (from left to right, respectively) for 96 hours. Images at 100x magnification (scale bars: 100 µm).

Brightfield images corresponding to cells exposed to 8 µM of CHIR for 96 hours (Figure 4.7, A, right) and cells exposed to 8 µM of CHIR and 100 nM of Dorsomorphin for 72 hours (Figure 4.7, B, left), show that cells present the intended 'loosely dense' like morphology. Furthermore, cells exposed to 8 µM of CHIR and 300 nM of Dorsomorphin for 72 hours (Figure 4.7, B, centre)

display a combination of a ‘loosely dense’ like morphology and small portions of ‘too dense’ clusters.

The tested culture conditions resulted in cells with a predominant ‘dense’ morphology.

Moreover, morphological differences between cells only exposed to CHIR (A) and cells exposed to both CHIR and Dorsomorphin (B and C) are also observable. Cells only exposed to CHIR present a ‘too dense’ like cell morphology when exposed to this molecule for 72 hours (A, left). Contrastingly, cells exposed to both CHIR and Dorsomorphin only exhibit a ‘too dense’ like cell morphology when exposed to these molecules for 96 hours (C).

When comparing images of cells exposed to both CHIR concentrations (Figure 4.6 and Figure 4.7), it is clear that cells exposed to 8 µM of CHIR tend to present a ‘denser’ morphology.

Considering the above presented results, it is possible to say that Dorsomorphin application allowed to obtain the pretended cell morphology to proceed with a successful renal differentiation on adherent conditions.

Cells were fixed at day 6 or 7 of the differentiation protocol, when exposed to WNT signalling for 72 or 96 hours, respectively, and were characterized through immunofluorescence staining against WT1 expression. However, this characterization revealed no expression of this mesodermal marker.

IV.2.1.3. Morizane protocol: 3D Culture #1

Although it was not possible to fully define the adequate culture conditions in monolayer culture, the next step in this work involved carrying the differentiation protocol in 3D culture conditions. For this purpose, AggreWell™ 800 plates were used.

As previously stated, the initial aggregate size during hiPSCs differentiation under 3D conditions, affects growth and subsequent cell trajectories. Thus, the initial aggregate size will influence the efficiency of induction of a specific lineage.

In particular, in this project, as we intended to evaluate the effect of the initial aggregate size (which depends on the initial number of seeded cells) towards the efficiency of hiPSCs derivation into IM, three initial conditions were tested: 3,000, 4,000 and 5,000 cells per aggregate.

Beyond different number of cells per aggregate, different culture conditions were followingly tested, which included different concentrations of CHIR (5 or 8 µM) and different concentrations of Dorsomorphin (0, 250 and 500 nM). The combination of these different parameters resulted in 18 distinct culture conditions, as schematically represented in Figure 4.8 (See Annexes, Section VIII., Table 8.4).

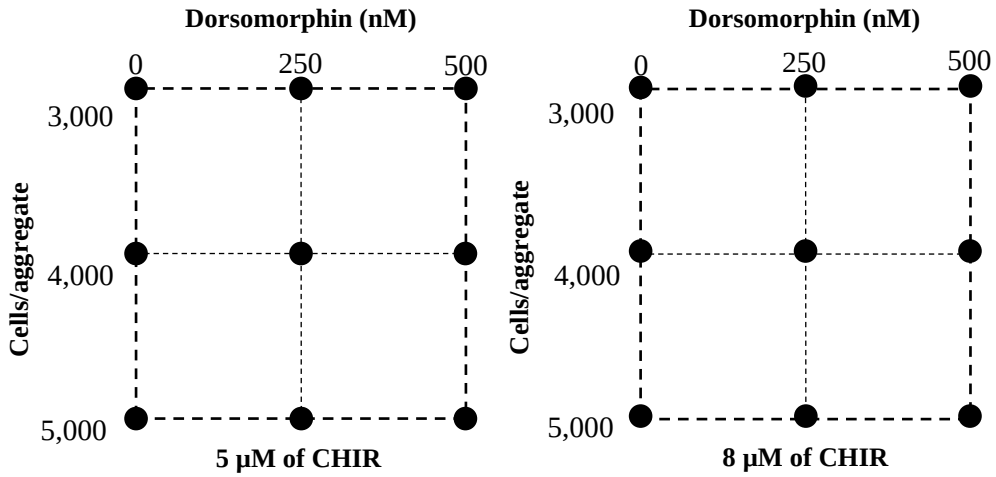

Figure 4.8| Schematic representation of the 18 tested experimental conditions.

The differentiation protocol was initiated 24 hours after seeding and, thenceforward, cells were cultured in RPMI 1640 medium. Cells were exposed to the different CHIR and Dorsomorphin concentrations for 96 hours and on day 9 of the differentiation protocol (supposed MM stage), cells were fixed in order to proceed with flow cytometry analysis.

IV.2.1.3.1. Cellular aggregates size evaluation

During the differentiation protocol, several brightfield images were acquired in order to assess aggregates size fluctuation along time.
Table 4.1 summarizes aggregates diameter 24 hours after cell seeding which corresponded to day 0 of Morizane differentiation protocol.

Table 4.1| Aggregate size (number of cells per aggregate/microwell) and correspondent aggregate diameter mean value 24 hours after cell seeding/day 0 of the differentiation protocol. (*n*=1).

Number of cells per aggregate	Diameter mean (µm)	Standard Deviation (SD)
3,000 Cells per aggregate	257	10
4,000 Cells per aggregate	313	13
5,000 Cells per aggregate	306	13

Regarding the obtained mean values for aggregate diameter on day 0 of the differentiation protocol, and considering the previously stated information that aggregate size depends on the initial number of seeded cells, it would be expected that the diameter mean value increased with the number of seeded cells. Consistently, aggregates diameter mean value when seeding 3,000 cells per microwell (257 µm) is inferior to aggregates diameter mean value when seeding 4,000 cells per microwell (313 µm). However, this is not true when comparing diameter mean values for 4,000 and 5,000 cells per microwell, as the former is superior to the latter (313 µm and 306

µm, respectively). This result is likely to be related to the fact that cellular aggregates resulting from seeding 4,000 cells per microwell present great heterogeneity in their size. Additionally, the presented values result from measuring a reduced number of cellular aggregates (12). However, this difference does not seem to be significant, since diameter mean values are within the standard deviation range.

The aggregates diameter distribution along time is depicted in Figure 4.9 (for cellular aggregates exposed to 5 µM of CHIR) and Figure 4.10 (for cellular aggregates exposed to 8 µM of CHIR).

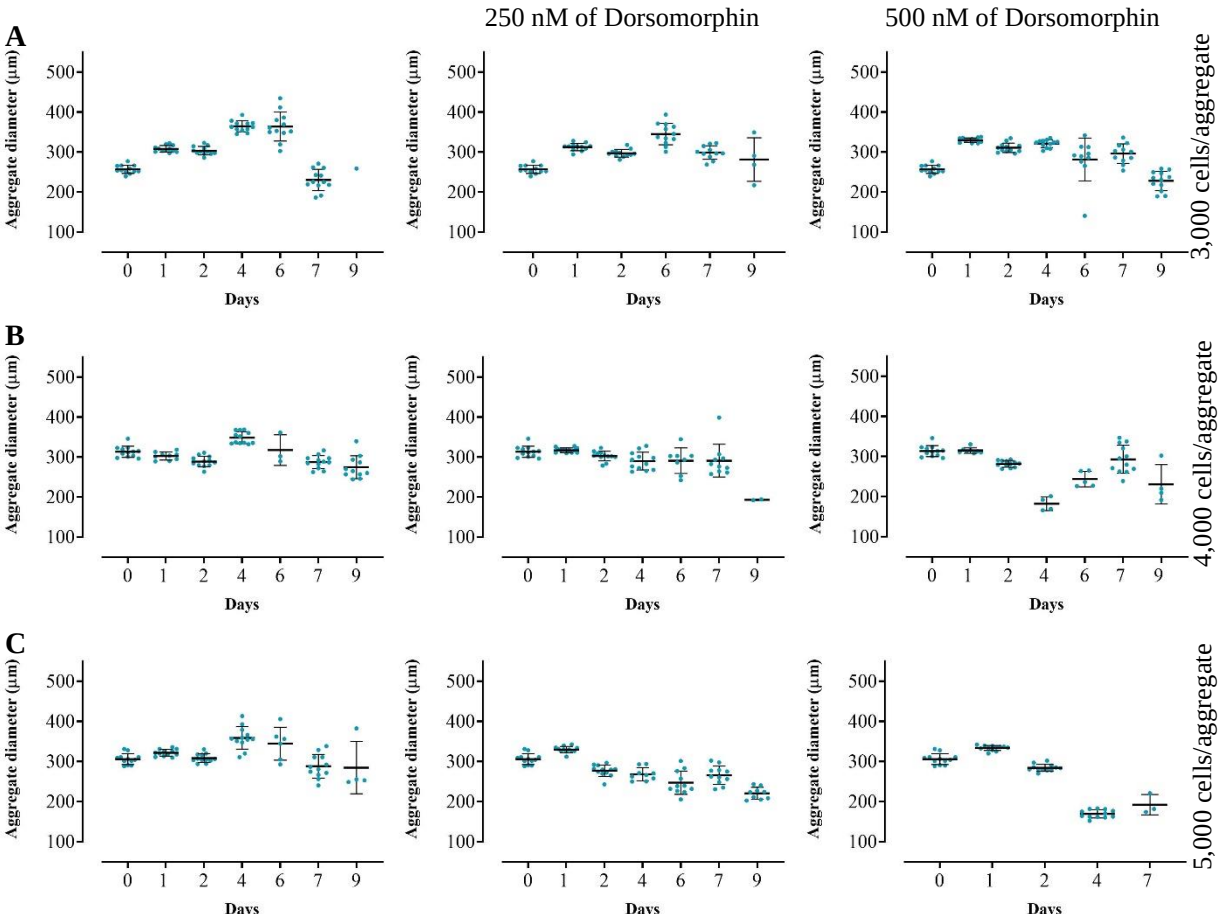

Figure 4.9| Aggregates diameter distribution along time when cellular aggregates were exposed to 5 µM of CHIR and different Dorsomorphin concentrations. Cells (GEpi, P46) were seeded at a density of 3,000, 4,000 or 5,000 cells/ aggregate in AggreWell™ 800 plates in mTeSR Plus™ medium. At day 0 of the differentiation protocol, the culture medium was changed to RPMI 1640 medium. **A)** 3,000 cells/aggregate; **B)** 4,000 cells/aggregate; **C)** 5,000 cells/aggregate. Cells were exposed to 5 µM CHIR (left); Cells were exposed to 5 µM CHIR and 250 nM of Dorsomorphin (centre); Cells were exposed to 5 µM CHIR and 500 nM of Dorsomorphin (right). The black bars represent the diameters mean values and error bars represent SD. (*n*=1).

One common observable feature of aggregates diameter distribution along time for every tested culture condition is that aggregates diameter tended to diminish along time.

These results also demonstrate that the diameter distribution patterns along time are not similar between each tested culture condition.

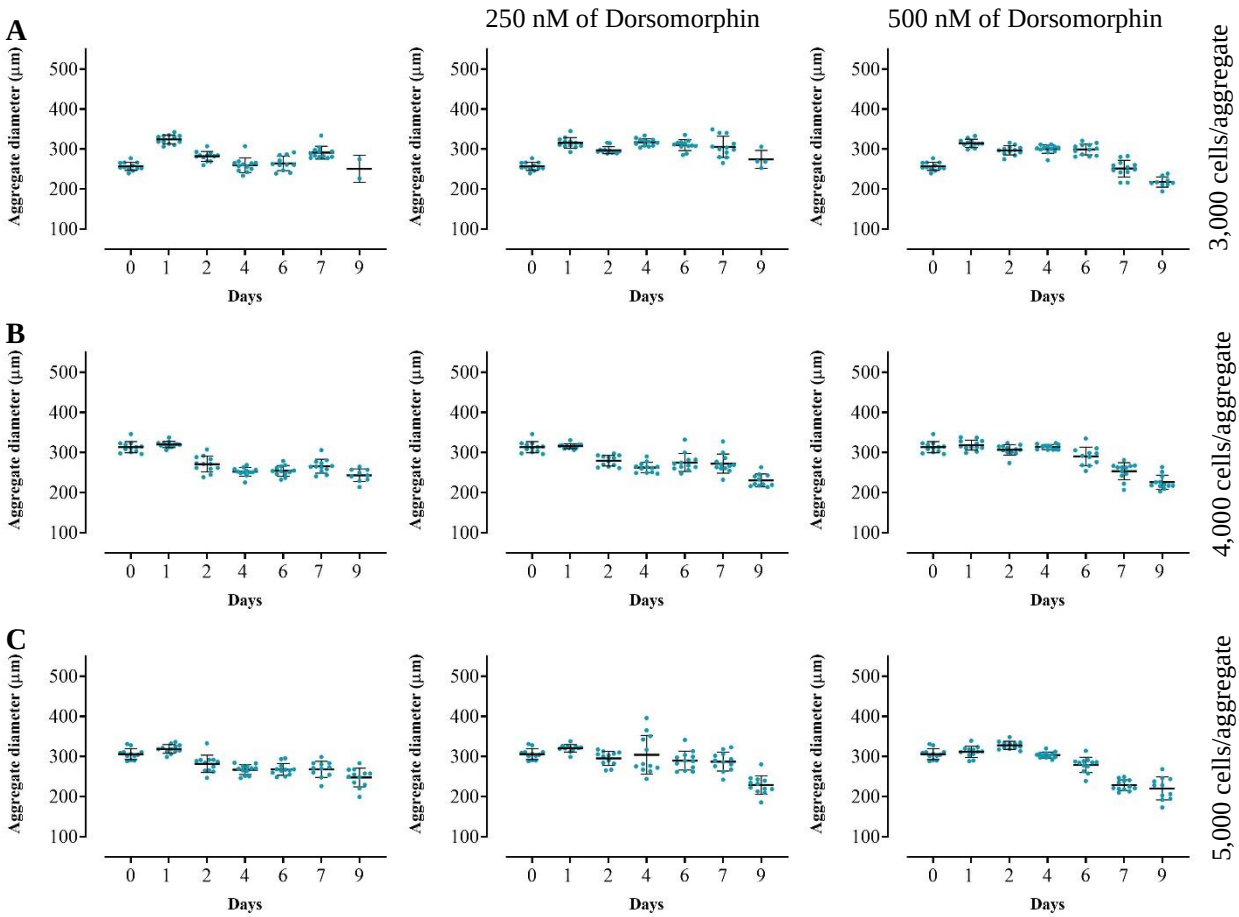

Figure 4.10| Aggregates diameter distribution along time when cellular aggregates were exposed to 8 µM of CHIR and different Dorsomorphin concentrations. Cells (GEpi, P46) were seeded at a density of 3,000, 4,000 or 5,000 cells/ aggregate in AggreWell™ 800 plates in mTeSR Plus™ medium. At day 0 of the differentiation protocol, the culture medium was changed to RPMI 1640 medium. **A)** 3,000 cells/aggregate; **B)** 4,000 cells/aggregate; **C)** 5,000 cells/aggregate. Cells were exposed to 8 µM CHIR (left); Cells were exposed to 8 µM CHIR and 250 nM of Dorsomorphin (centre); Cells were exposed to 8 µM CHIR and 500 nM of Dorsomorphin (right). The black bars represent the diameters mean values and error bars represent SD. (*n*=1).

Similar to cellular aggregates exposed to 5 µM of CHIR and different Dorsomorphin concentrations (Figure 4.9), the diameter of cellular aggregates exposed to 8 µM of CHIR and different Dorsomorphin concentrations (Figure 4.10) also tended to diminish along time. This feature may be attributable to cell size reduction as cells get differentiated.

One observable characteristic of cells exposed to 8 µM of CHIR and different Dorsomorphin concentrations, is that from day 6 of the differentiation protocol, aggregates display a darker appearance, which may result from an increase in the cellular density within each aggregate. Further characterization regarding cell counting on days 4 and 6 would be important to ascertain this aspect. By comparison, cells exposed to 5 µM of CHIR and different Dorsomorphin concentrations, seem to exhibit a darker appearance later in the differentiation protocol by day 7 or 9.

Nevertheless, in opposition to the previous culture conditions, the diameter distribution patterns along time are similar between each tested culture condition.

In the presented aggregate diameter distribution graphics, every point represents the diameter of one single aggregate. For each condition, and at every assessed time point, 12 different aggregates were measured. The total of 12 independent measurements was not always possible, as aggregates tended to disaggregate along time in culture and consequently did not present a round/circular shape. Figure 4.11 depicts one example of this situation.

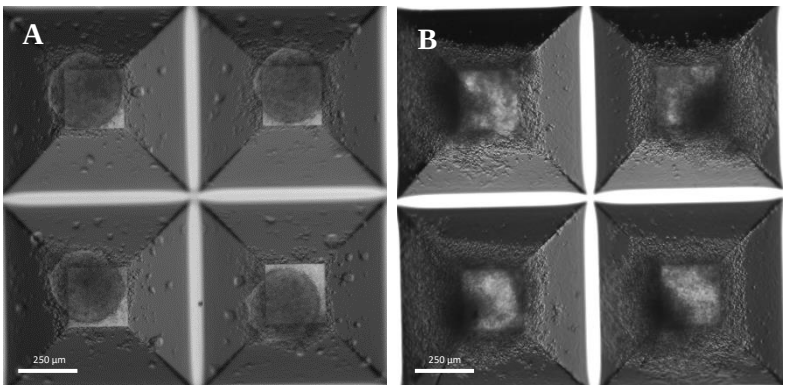

Figure 4.11| Representative brightfield images of cellular aggregates at day 0 and 9 of the differentiation protocol. Cells (GEpi, P46) were seeded at a density of 3,000 cells/ aggregate in AggreWell™ 800 plates in mTeSR Plus™ medium. At day 0 of the differentiation protocol, the culture medium was changed to RPMI 1640 medium. **A)** Cells on day 0 of the differentiation protocol; **B)** Cells on day 9 of the differentiation protocol, when exposed to 5 µM of CHIR and 250 nM of Dorsomorphin for 96 hours. Images at 40x magnification (scale bars: 250 µm).

IV.2.1.3.2. Flow Cytometry characterization

Cell samples of the 18 different tested culture conditions were characterized through flow cytometry in order to assess WT1 (characteristic marker of IM) expression on day 9 of the differentiation protocol. The obtained results are presented in Figure 4.12.

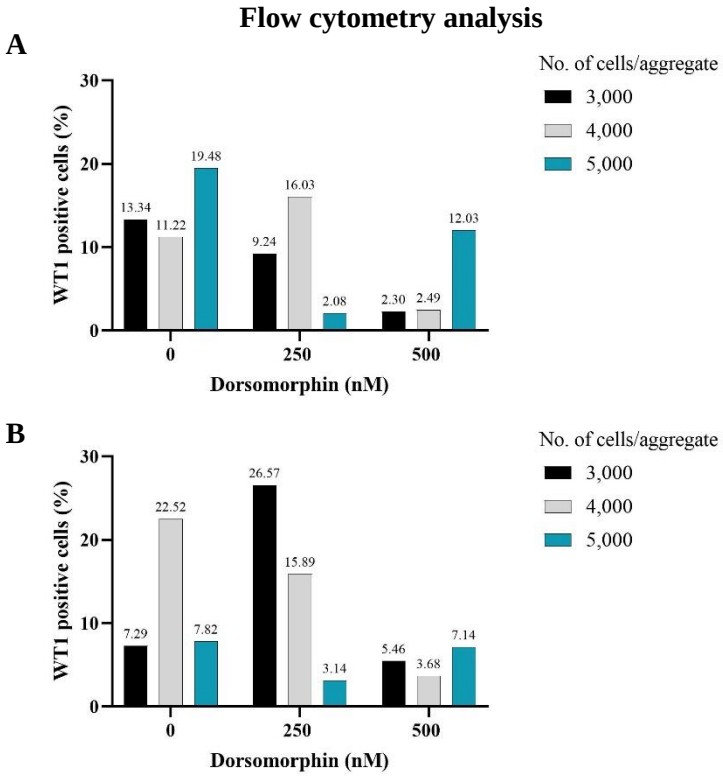

Figure 4.12| Flow cytometry analysis of WT1 expression of cells on day 9 of the differentiation protocol. Cells (GEpi, P46) were seeded at a density of 3,000, 4,000 and 5,000 cells/ aggregate in AggreWell™ 800 plates in mTeSR Plus™ medium. At day 0 of the differentiation protocol, the culture medium was changed to RPMI 1640 medium. **A)** Cells were exposed to 5 µM CHIR and different Dorsomorphin concentrations (0, 250 and 500 nM) for 96 hours; **B)** Cells were exposed to 8 µM CHIR and different Dorsomorphin (0, 250 and 500 nM) concentrations for 96 hours; (*n*=1). WT1: Wilms' Tumour 1.

The obtained results reveal low percentages of WT1 positive cells in every sample of the 18 tested culture conditions. The different 18 conditions expressed between 2.08% and 26.57% of positive cells for WT1 expression.

As it can be observed, the percentage of cells expressing WT1 is not similar between cells exposed to 5 µM (Figure 4.12, A) and 8 µM of CHIR (Figure 4.12, B). While cells exposed to 5 µM of CHIR present higher percentages of WT1 positive cells for an aggregate size of 5,000 cells/aggregate and when cells were not exposed to Dorsomorphin (19.48 %), cells exposed to 8 µM of CHIR present higher percentages of WT1 positive cells for cells exposed to 250 nM of Dorsomorphin and for an aggregate size of 3,000 cells/aggregate (26.57 %). On the other hand, cells exposed to both 5 µM and 8 µM of CHIR present the lowest percentages of WT1 positive

cells, when cells were exposed to 500 nM of Dorsomorphin, for aggregate sizes of 3,000 and 4,000 cells/aggregate.

By looking at the obtained results, does not seem to exist any correlation between aggregate size and WT1 expression.

Taking into account the obtained results revealing low percentages of WT1 positive cells, it is likely that the applied range of CHIR concentration was not the most suitable, and thus, following experiments included higher CHIR concentrations.

Considering the obtained results until this moment, it was hypothesized that the unsuccessful induction of IM could be attributed to the use of RPMI 1640 medium instead of Advanced RPMI 1640 medium, which was used originally by the authors of the differentiation protocol [109].

IV.2.1.4. Takasato protocol: 3D Culture #2

Regarding the Takasato protocol, two experiments were firstly conducted on 3D conditions with two different cell lines: GEpi and TCLab.

These experiments combined 3D culture on AggreWell™ 800 plates and 3D culture on porous membranes (Corning®). The second approach consists of the employed 3D culture strategy in Takasato protocol [110].

In these two experiments, cells were seeded in AggreWell™ 800 plates at a density of 4,000 cells/ aggregate and were exposed to 8 µM of CHIR for 72 hours. At day 7 of the differentiation protocol, cells were collected from AggreWell™ 800 plates, singularized and $5x10^5$ cells were transferred as an aggregate to a porous membrane, which provided a liquid-air interface for further differentiation. This procedure provides an increased cell density and volume, within which cells are able to positionally reorganize with respect to each other, and thus, form intact renal structures [110].

The differentiation protocol was followed for 18 more days, until day 25 of the differentiation protocol. Organoids on the porous membrane were collected and analysed through immunofluorescence staining against WT1, GATA3 and FOXD1 expression, which revealed no expression of these markers for both cell lines.

IV.2.1.5. Morizane protocol: 3D Culture #3

This experiment combined 3D culture on AggreWell™ 800 plates and 3D culture on 96-well, round-bottom, Ultra-Low Attachment Multiple Well Plates (Corning ®), which consists of the employed 3D culture strategy in Morizane protocol [109].

TCLab and GEpi cells were seeded in AggreWell™ 800 plates at a density of 4,000 cells/ aggregate, and the differentiation protocol was initiated 24 hours after seeding. Cells were cultured on Advanced RPMI 1640 medium (a more robust culture medium specifically designed for serum-free cultures) supplemented with 8 µM of CHIR and 0, 250 and 500 nM of Dorsomorphin or 10 µM of CHIR and 100 nM of Dorsomorphin, for 96 hours.

At day 9 of the differentiation protocol, cells were collected from AggreWell™ 800 plates, singularized and 100,000 cells were transferred to each well of Ultra-Low Attachment Multiple Well Plates. After cell transfer it was possible to observe some considerable cellular death.

Cells were fixed on day 21, but the characterization of all the tested conditions was not possible due to difficulties in cell collection. TCLab cells exposed to 10 µM of CHIR and 100 nM of Dorsomorphin were characterized through immunofluorescence staining against GATA3 expression and co-expression of WT1 and FOXD1.

By the end of the differentiation protocol, at day 21, collecting ducts should express GATA3 and podocytes should co-express WT1 and FOXD1 [110].

However, in Figure 4.13, results display negative expression of GATA3 and FOXD1 and positive expression of WT1, and there is no evidence of segmented nephrons.

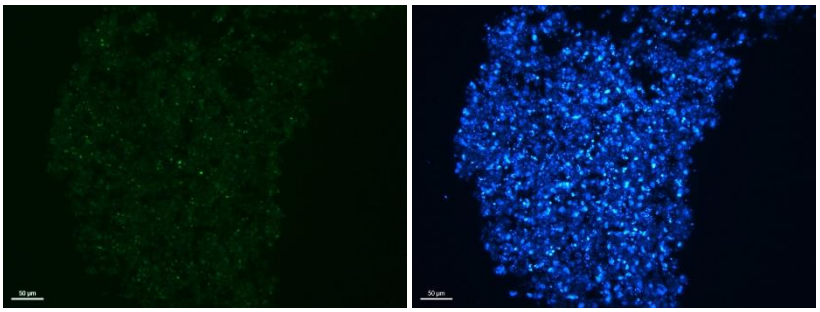

Figure 4.13| Immunofluorescence staining of cells exposed to 10 µM of CHIR and 100 nM of Dorsomorphin for 96 hours. Immunofluorescence staining of WT1 (left) and nuclear staining with DAPI (right). Images were acquired with a fluorescence optical microscope. Images at 200x magnification (scale bars: 50 µm). WT1: Wilm's Tumour 1; DAPI: 4',6-Diamidino-2-Phenylindole.

IV.2.1.6. Morizane protocol: Monolayer culture #3

This experiment intended to conduct the differentiation protocol applying the culture strategies described by Morizane and Bonventre: monolayer culture followed by 3D culture on Ultra-Low Attachment Multiple Well Plates [109].

TCLab and GEpi cells were, then again, cultured under monolayer culture and exposed to different CHIR and Dorsomorphin concentrations. Cells were seeded at a density of 25,000 cells/cm^2. The differentiation protocol was initiated 24 hours after seeding and, thenceforward, cells were cultured on Advanced RPMI 1640 medium and exposed to four different culture conditions for 96 hours: 6, 8, 11 µM of CHIR or 10 µM of CHIR and 100 nM of Dorsomorphin. At Day 9, TCLab cells were collected, singularized and 100,000 cells were transferred to each well Ultra-Low Attachment Multiple Well Plates. There were not enough GEpi cells to be transferred. Both cell lines were replated at day 9, fixed on the following day in order to proceed with immunofluorescence staining characterisation. Due to high cellular death, TCLab cells were not enough to proceed with immunofluorescence staining, and GEpi cells were characterized through immunofluorescence staining against WT1 and GATA3 (anterior IM marker) [110], which revealed a negative expression of both markers.

Cells went through the differentiation process until day 21 and were fixed on this day. The characterization of all the tested conditions was not possible due to difficulties in cell collection. TCLab cells exposed to 8 µM of CHIR for 96 hours were characterized through immunofluorescence staining against GATA3 expression and co-expression of WT1 and FOXD1 (Figure 4.14).

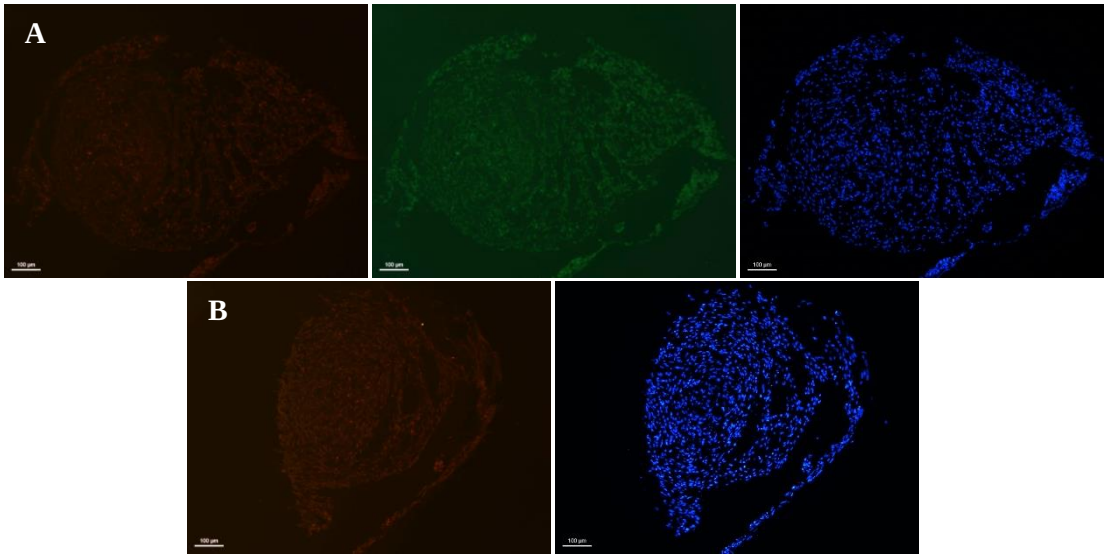

Figure 4.14| Immunofluorescence staining of cells exposed to 8 µM of CHIR 96 hours. A) Immunofluorescence staining of FOXD1 (left), WT1 (centre) and nuclear staining with DAPI (right); **B)** Immunofluorescence staining of GATA3 (left) and nuclear staining with DAPI (right). Images were acquired with a fluorescence optical microscope. Images at 100x magnification (scale bars: 100 µm). FOXD1: Forkhead box D1; WT1: Wilm's Tumour 1; DAPI: 4',6-Diamidino-2-Phenylindole; GATA3: GATA binding protein 3.

IV.2.1.7. Morizane protocol: Monolayer culture #4

It was, then, hypothesized that using a cell line previously known to efficiently differentiate into mesoderm-derived cells could result in an efficient induction of IM. Thus, the following experiments were performed with another cell line - DF6 - which had demonstrated differentiation potential towards mesoderm [125].

DF6 cells were seeded at a density of 25,000 cells/cm^2 and the differentiation protocol was initiated 48 hours after seeding.

Cells were exposed to four different culture conditions: 10 µM of CHIR and 100 nM of Dorsomorphin, either for 72 or 96 hours, followed by 10 ng/mL of Activin A either for 48 or 72 hours.

At day 7 of the differentiation protocol, cells were fixed for immunofluorescence staining and flow cytometry analysis.

Cells were characterized through immunofluorescence staining against expression of WT1 and GATA3 which revealed no expression of these two mesodermal markers.

Although immunofluorescence staining revealed no expression of the mesodermal marker, WT1, it was hypothesized that the antibodies dilution could not be adequate to detect expression of these markers.

Cell samples of the 4 different tested culture conditions were characterized through flow cytometry in order to assess WT1 (characteristic marker of IM) expression (Figure 4.15).

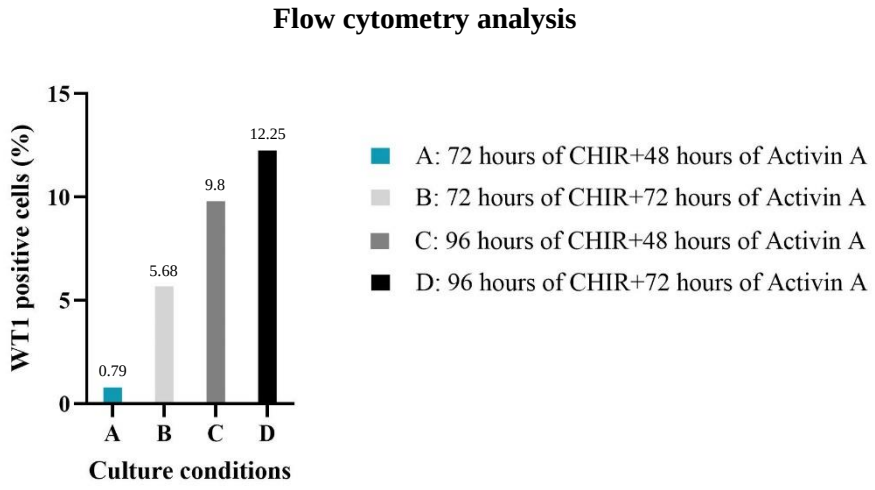

Figure 4.15| Flow cytometry analysis of WT1 expression of cells on day 7 of the differentiation protocol. Cells (DF6, P59) were seeded at a density of 25,000 cell/cm^2 in mTeSR Plus™ medium. At day 0 of the differentiation protocol, the culture medium was changed to RPMI 1640 medium. Cells were cultured under four different culture conditions: **A)** 72 hours of CHIR and Dorsomorphin + 48 hours of Activin A; **B)** 72 hours of CHIR and Dorsomorphin + 72 hours of Activin A; **C)** 96 hours of CHIR and Dorsomorphin + 48 hours of Activin A; **D)** 96 hours of CHIR and Dorsomorphin + 72 hours of Activin A. (*n*=1). WT1: Wilms' Tumour 1.

Flow cytometry analysis allowed to confirm WT1 expression, although in a reduced percentage of cells, which ranged between 0.79 % to 12.25%, where culture condition D (96 hours of CHIR and Dorsomorphin + 72 hours of Activin A) was the most successful in inducing IM.

When adapting the differentiation protocol to a hiPSC line (HDF-α), authors tested a similar culture condition to the above presented condition D. Cells were exposed to 10 µM of CHIR and 5 ng/mL of Noggin (a BMP4 antagonist) for a period of 96 hours, followed by 10 ng/mL of Activin A for 72 hours. At day 7 of the differentiation protocol, they were able to generate $WT1^+$ $HOXD11^+$ posterior IM cells with 80-90% efficiency [91].

Regardless of the similarity between culture conditions, efficiency values strongly differ between them, with culture condition D generating a significantly lower percentage of positive cells.

Moreover, further characterization against HOXD11 expression would be necessary to confirm if the obtained cells corresponded to posterior IM. On the other hand, cells could also have been characterized against co-expression of LHX1 and PAX2 markers in order to verify if the obtained cells were, instead, anterior IM [91].

IV.2.1.8. Morizane protocol: 3D Culture #4-6

Although DF6 cells did not efficiently generate IM under adherent conditions, experiments under 3D conditions were performed with this cell line.

During hiPSCs routine expansion, and before the followingly presented experiments, some spontaneous and undesired differentiation events have been observed. These events may happen due to various reasons, namely high cell confluency during culture or even poor/incomplete DMSO dilution when thawing hiPSCs [118]. Spontaneous differentiation may affect the renal differentiation process, as it can bias cells towards a specific lineage, and thus compromise their ability to differentiate into renal cells.

DF6 cells were seeded in AggreWell™ 800 plates at a density of 3,000 cells/ aggregate. The differentiation protocol was initiated 24 hours after seeding and, thenceforward, cells were cultured on Advanced RPMI 1640 medium.

Cells were cultured under different culture conditions, being exposed to WNT signalling for two different periods of time: 72 or 96 hours. Cells of both culture conditions were exposed to Activin A for 72 hours. The concentration of CHIR was also increased to 11 µM, as described in the initial steps of mesoderm derivation [125].

<u>WNT signalling exposure for 96 hours</u>

Cells were exposed to 10 µM of CHIR and 100 nM of Dorsomorphin or 11 µM of CHIR for 96 hours and cultured until day 14 of the differentiation protocol.

Cellular aggregates were collected at days 0, 4, 7, 9 and 14 for RT-PCR characterization and for immunofluorescence staining characterization.

WNT signalling exposure for 72 hours

Cells were exposed to 8 µM of CHIR, 10 µM of CHIR and 100 nM of Dorsomorphin or 11 µM of CHIR for 72 hours and cultured until day 8 of the differentiation protocol.

Cellular aggregates were collected at days 0 and 8 for RT-PCR characterization.

IV.2.1.8.1. Aggregates size evaluation

During the differentiation protocols, several brightfield images were acquired in order to assess aggregates size fluctuation along time.

Table 4.2 summarizes aggregates diameter 24 hours after cell seeding, which corresponded to day 0 of Morizane differentiation protocol.

Table 4.2| Aggregate size (number of cells per aggregate/microwell) and correspondent aggregate diameter mean value 24 hours after cell seeding/day 0 of the differentiation protocol. (*n*=2).

Culture condition	Diameter mean value (µm)	Standard Error of mean (SEM)
3,000 Cells per aggregate	274	7

The aggregate diameter distribution along time upon exposure to WNT signalling for 96 and 72 hours is depicted in Figure 4.16 and Figure 4.17, respectively.

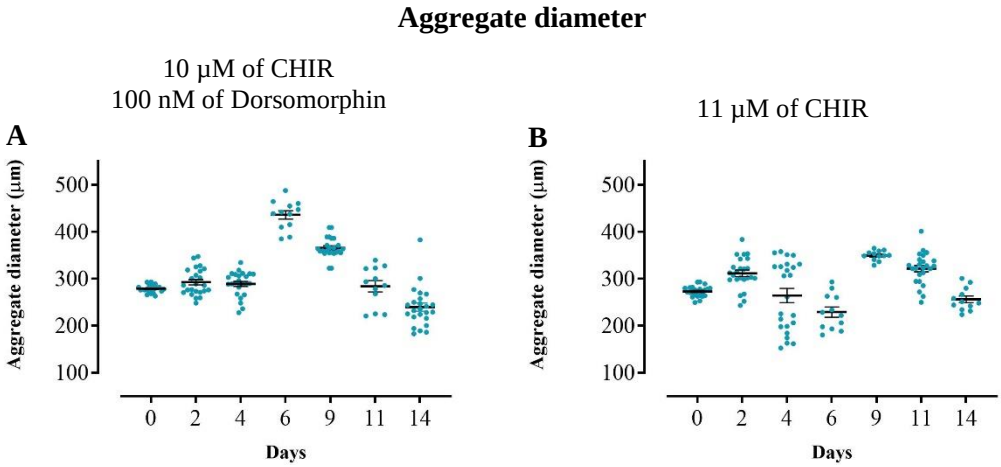

Figure 4.16| Aggregate diameter distribution along time upon exposure to WNT signalling for 96 hours. Cells (DF6, P50,51 and 61) were seeded at a density of 3,000 cells/aggregate in AggreWell™ 800 plates in mTeSR Plus™ medium. At day 0 of the differentiation protocol, the medium was changed to Advanced RPMI 1640 medium. **A)** Cells were exposed to 10 µM of CHIR and 100 nM of Dorsomorphin for 96 hours; **B)** Cells were exposed to 11 µM of CHIR for 96 hours. The black bars represent the diameters mean values and error bars represent SD. (*n*=2).

These results reveal high oscillations in aggregates diameter in different days along the time for both tested culture conditions (Figure 4.16, A and B).

In addition, the diameter distribution pattern along time is not similar between the two conditions. When cellular aggregates were exposed to 10 µM of CHIR and 100 nM of Dorsomorphin (Figure 4.16, A), its diameter ranged from 183 and 488 µm along time. Aggregate diameter increased with time in culture until reaching the highest values at day 6 of the differentiation protocol and decreasing after that time point.

When cellular aggregates were exposed to 11 µM of CHIR (Figure 4.16, B), its diameter ranged from 152 to 401 µm. In opposition to the previous condition, aggregates diameter decreased with time in culture until reaching the lowest values at day 6 of the differentiation protocol, however, after this time point, aggregates diameter went through an increment followed by a decline.

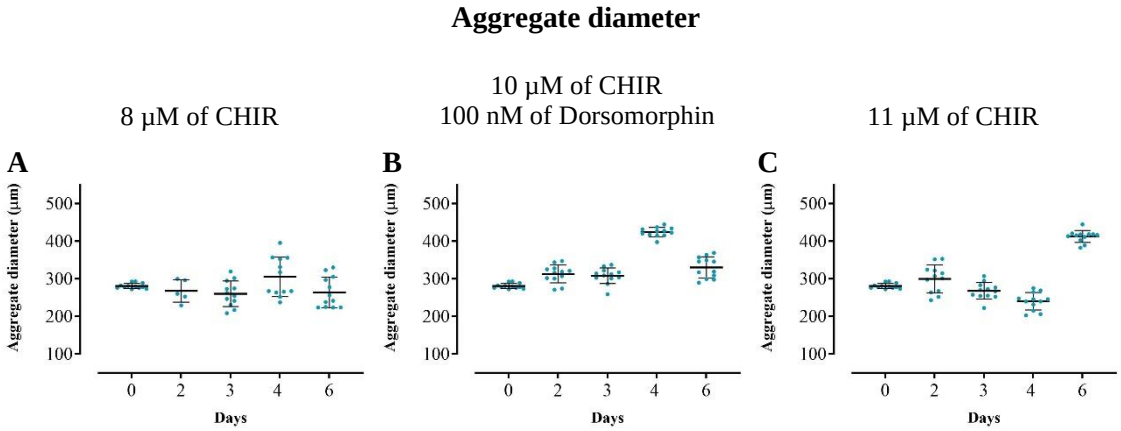

Figure 4.17| Aggregate diameter distribution along time upon exposure to WNT signalling for 72 hours. Cells (DF6, P61) were seeded at a density of 3,000 cells/aggregate in AggreWell™ 800 plates in mTeSR Plus™ medium. At day 0 of the differentiation protocol, the medium was changed to Advanced RPMI 1640 medium. **A)** Cells were exposed to 8 µM of CHIR for 72 hours; **B)** Cells were exposed to 10 µM of CHIR and 100 nM of Dorsomorphin for 72 hours; **C)** Cells were exposed to 11 µM of CHIR for 72 hours. The black bars represent the diameters mean values and error bars represent SD. (*n*=1).

Regarding Figure 4.17, aggregate diameter distribution patterns present similarities between the three culture conditions until day 3 of the differentiation protocol, as the aggregates diameter displays low oscillations for the three culture conditions during this period.

When comparing aggregates diameter distribution of cellular aggregates exposed to WNT signalling for different periods of time, namely 96 hours (Figure 4.16) and 72 hours (Figure 4.17), it is apparent that aggregates exposed to WNT signalling for 96 hours present more accentuated diameter oscillations along time.

It is worth pointing out that, during these experiments, cellular aggregates were quite heterogeneous in size between different wells of the same condition and sometimes within each well. This heterogeneity may have influenced the differentiation process, as heterogeneity in size and shape can lead to an inefficient and uncontrolled differentiation [126,121].

Regarding shape, heterogeneity in aggregates shape was also perceptible. Beyond influencing the differentiation process, shape heterogeneity and lack of circularity and roundness leads to some difficulties/errors in diameter measurement.

IV.2.1.8.2. Quantitative real-time polymerase chain reaction characterisation

Expression of *WT1*, *PAX2*, *SIX2*, *GATA3* and *HOXD11* genes were assayed through RT-PCR along the differentiation protocol, and normalised against expression at day 0 and expression of the endogenous control gene, *GAPDH*.

Figure 4.18 depicts the relative expression profiles of these genes during renal differentiation of cells exposed to WNT signalling for 96 hours.

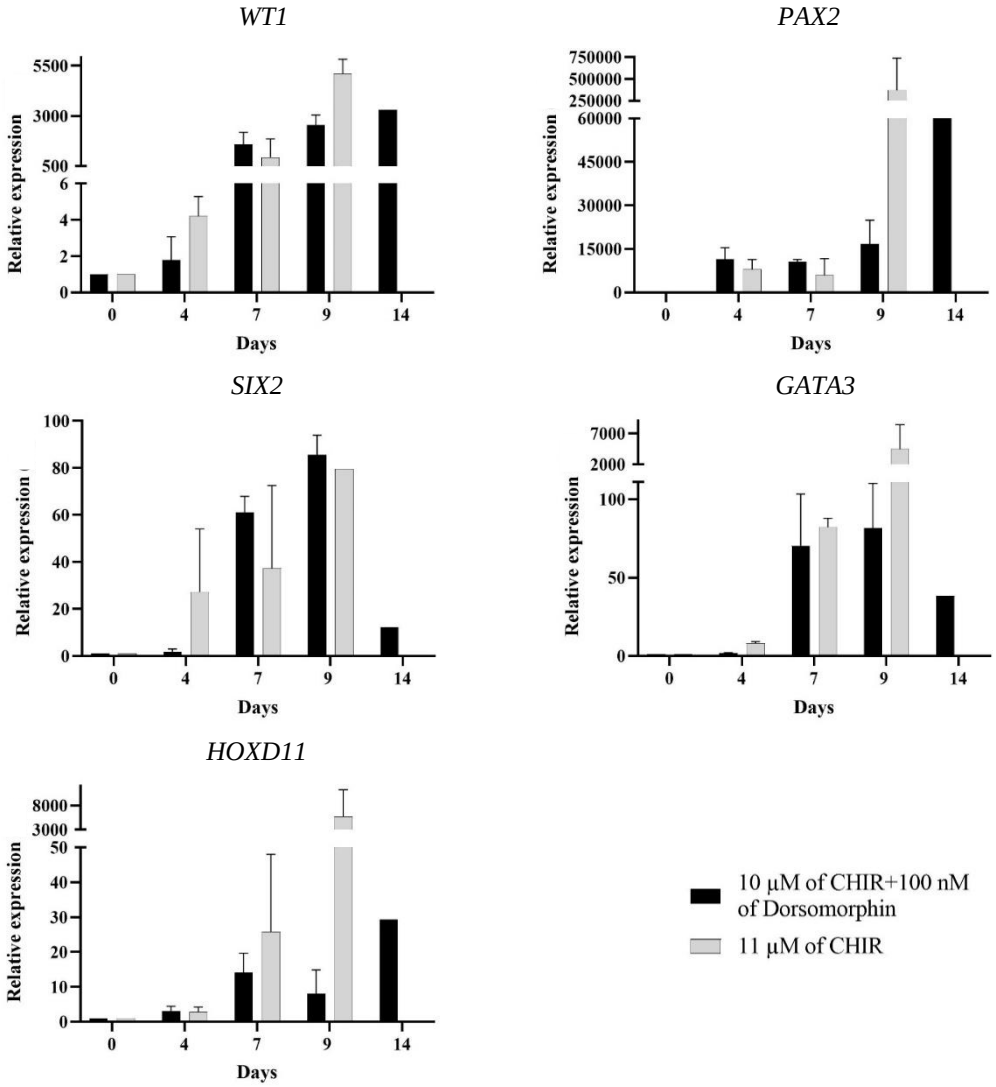

Figure 4.18| Relative expression profiles of mesodermal and renal markers during renal differentiation of hiPSCs upon exposure to WNT signalling for 96 hours. Cells (DF6, P50,51 and 61) were seeded at a density of 3,000 cells/aggregate in AggreWell™ 800 plates in mTeSR Plus™ medium. At day 0 of the differentiation protocol, the medium was changed to Advanced RPMI 1640 medium. Cells were exposed to 10 µM of CHIR and 100 nM of Dorsomorphin or 11 µM of CHIR for 96 hours. Error bars represent SEM. (*n*=2). *WT1*: Wilms' Tumour 1; *PAX2*: Paired box 2; *SIX2*: Sine oculis-related homeobox 2; *GATA3*: GATA binding protein 3; *HOXD11*: Homeobox D11.

The above present graphics do not exhibit any results regarding relative expression of the different genes on day 14 of the differentiation protocol for cellular aggregates exposed to 11 µM of CHIR for 96 hours, as it was not possible to assess these results due to low quantity of RNA.

Moreover, results regarding day 14 of the differentiation protocol for cellular aggregates exposed to 10 µM of CHIR and 100 nM of Dorsomorphin for 96 hours, do not exhibit any error bars as it was not possible to assess relative expression of the referred genes for both of the performed experiments.

As formerly stated (Section I.2.1.3.), *SIX2* expression is characteristic of the self-renewing NPC population present in the condensed CM. Apart from being required to maintain NPCs in a proliferative progenitor state, promoting cell proliferation, *SIX2* is also implicated in the inhibition of differentiation-related genes [65,70]. Results regarding *SIX2* relative expression reveal an increase along time until day 9 of the differentiation protocol for both culture conditions. Day 9 is presented as the time point of the differentiation protocol with the highest *SIX2* relative expression for both culture conditions. This result is concordant with results obtained by Morizane *et al.*, that were able to induce NPCs (*SIX2*$^+$, *SALL1*$^+$, *WT1*$^+$, *PAX2*$^+$) with 90% efficiency on day 9 of the differentiation protocol [91]. After this time point, the obtained results reveal that *SIX2* relative expression sharply decreases for cells exposed to 10 µM of CHIR and 100 nM of Dorsomorphin, which suggests that NPCs lost their progenitor state and differentiated. Downregulation of *SIX2* expression after day 9 of the differentiation protocol was also described by Morizane *et al.* [91].

The obtained results concerning *PAX2* show an increase of relative expression along the differentiation protocol for both culture conditions. Furthermore, results indicate a high relative expression since day 4 of the differentiation protocol. These results seem to be in line with *in vivo* kidney development as *PAX2*, along with *PAX8*, were identified as relevant participants in the specification of the first renal cells in the embryo, being the earliest specific markers of the renal lineage. Afterwards, they remain central players throughout urogenital system development, especially during metanephric kidney induction, branching morphogenesis and nephron differentiation [127]. Also, IM is characterized by *PAX2* expression [128] and this gene is also involved in IM specification along the mediolateral axis [70].

At day 7 of the differentiation protocol, the supposed posterior IM stage, cells of both culture conditions display high levels of *PAX2* expression. According to Morizane *et al.*, posterior IM should co-express *WT1* and *HOXD11*, whereas anterior IM is characterized by co-expression of *PAX2* and *LHX1* markers [91]. Considering the referred results, and despite that *LHX1* expression was not assessed through RT-PCR, it could conceivably be hypothesised that at day 7 of the differentiation protocol both anterior and posterior IM were generated.

Along the differentiation protocol, *PAX2* expression of cells exposed to both culture conditions, does not strongly vary, except for day 9, wherein cells exposed to 11 µM of CHIR display a considerably higher expression of *PAX2*. High *PAX2* relative expression levels on day 9, are also

congruent with NPCs (*SIX2*$^{+}$, S*ALL1*$^{+}$, *WT1*$^{+}$, *PAX2*$^{+}$) generation at this time point of the differentiation protocol. Furthermore, *PAX2* relative expression results are in line with those obtained by Morizane *et al.*, that revealed low *PAX2* relative expression on days 4 and 7, with an increase on day 9 [91].

Also, an increase in *PAX2* expression on day 14 of the differentiation protocol (supposed RV stage), for cells exposed to 10 µM of CHIR and 100 nM of Dorsomorphin, is coherent as *PAX2* participates on MET and it is expressed on early epithelial structures derived from this process [62]. *PAX2* and *PAX8* were found to regulate the transcription factor gene *GATA3*, as these two transcription factors activate *GATA3* expression [127,129]. As a result, early *GATA3* expression in IM requires *PAX2* and *PAX8* expression [130]. *GATA3* plays an important role in nephric duct morphogenesis and guidance along the antero-posterior axis [127,129] and together with *PAX2*, at a later stage, participates in UB establishment [131]. When observing results regarding *PAX2* and *GATA3* expression, it is possible to observe that *GATA3* expression increases with *PAX2* expression until day 9 of the differentiation protocol. However, at day 14 of the differentiation protocol, an increase in *PAX2* expression does not reflect an increase in *GATA3* expression.

Also, *GATA3* is identified by Takasato *et al.* as an anterior IM marker [90]. This aspect might be justified by - apart from participating in nephric duct elongation, as above referred- its important role in regulating *GDNF* receptors expression. Upon GDNF binding to these receptors, PI3K/AKT and/or Ras-Raf-MEK/ERK signalling pathways are activated and participate in cellular proliferation, contributing to UB growth and branching [127,130] (Section I.1.3.4. and Section I.2.1.3.).

The obtained results for *GATA3* expression on day 7 of the differentiation protocol (posterior IM stage) show low levels of this anterior marker when compared to the anterior IM marker, *PAX2*. However, on day 7 of the differentiation protocol, *GATA3* expression is in the same range of values of *HOXD11* expression (posterior IM marker).

Apart from *GATA3*, *PAX2* is also known to regulate *WT1*, which is an essential regulator of early MM [131]. *WT1* is expressed at lower levels in the uninduced mesenchyme and its expression achieves higher levels in the condensed CM, where it promotes differentiation towards the epithelial phenotype [128,62]. Taking into consideration the obtained results regarding *WT1* relative expression, it is possible to say that these results are consistent with the stated information, as *WT1* relative expression increases along time (and consequent condensation) for both culture conditions. Moreover, at day 9 of the differentiation protocol, supposed MM stage with NPCs (*SIX2*$^{+}$, *SALL1*$^{+}$, *WT1*$^{+}$, *PAX2*$^{+}$) generation, high levels of *WT1* expression are exhibited.

MM expresses three *HOX11* paralogs (*HOXA11*, *HOXC11* and *HOXD11*) which are functionally redundant in early kidney development and are necessary to initiate the metanephric development [132,133]. *HOX11* paralogs are required for *SIX2* and *GDNF* expression in the MM as they participate in a molecular complex that directly activates these genes [134,133]. *HOXD11*, in particular, is

expressed in the posterior region of the IM [90,91], and along with *PAX2* and *WT1*, *HOXD11* contributes for epithelial differentiation of the MM [135]. Along the differentiation protocol, *HOXD11* expression of cells exposed to both culture conditions does not strongly vary between them, except for day 9, wherein cells exposed to 11 µM of CHIR display a considerably higher expression of *HOXD11*.

As a matter of fact, a considerably higher gene expression at day 9 for cells exposed to 11 µM of CHIR when compared to cells exposed to 10 µM of CHIR and 100 nM of Dorsomorphin, is true for all the assessed genes with exception of *SIX2* gene.

Another conducted experiment included carrying Morizane protocol until the end of the differentiation protocol (Day 22). In this experiment DF6 cells were seeded in AggreWell™ 800 plates at a density of 3,000 cells/ aggregate and were exposed to 11 µM of CHIR for 96 hours. Cellular aggregates were collected at days 0 and 22 for RT-PCR characterization.

Figure 4.19 depicts relative expression profiles of various genes at the end of renal differentiation.

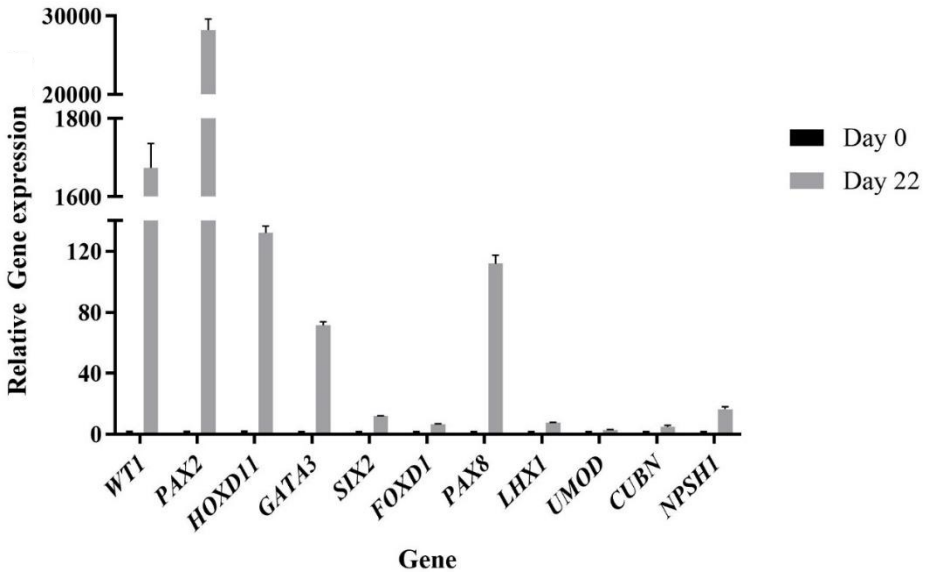

Figure 4.19| Relative expression profiles of renal markers at the end of renal differentiation of hiPSCs. Cells (DF6, P57) were seeded at a density of 3,000 cells/aggregate in AggreWell™ 800 plates in mTeSR Plus™ medium. At day 0 of the differentiation protocol, the medium was changed to Advanced RPMI 1640 medium supplemented with 11 µM of CHIR for 96 hours. Error bars represent SD. (*n*=1). *WT1*: Wilms' Tumour 1; *PAX2*: Paired box 2; *HOXD11*: Homeobox D11; *GATA3*: GATA binding protein 3; *SIX2*: Sine oculis-related homeobox 2; *FOXD1*: Forkhead box D1; *PAX8*: Paired box 8; *LHX1*: LIM homeobox 1; *UMOD*: Uromodulin; *CUBN*: Cubilin; *NPSH1*: NPHS1 adhesion molecule, nephrin.

At the end of the differentiation protocol, and if a successful renal differentiation was obtained, a gradual reduction in mesenchyme and ureteric tip markers followed by the upregulation of genes specific to podocytes, proximal tubule, distal tubule and loop of Henle, would be expectable [90].

As formerly stated, *WT1* is responsible for glomerular cell fate along the proximal-distal axis of the SSB (Section I.2.1.3.). As a result, *WT1* expression is characteristic of the proximal region of

SSB, and later, of differentiated podocytes and glomeruli [70,128]. Results regarding *WT1* expression reveal high expression levels of this marker on day 22, which suggests formation of these renal structures. Also, according to Morizane *et al.*, podocytes are also characterized by *NPHS1* expression [91] however, results reveal low levels of gene expression for this marker.

PAX2 is implicated in MET and it is expressed in early epithelial structures, thenceforward its expression is known to suffer downregulation with tubular epithelia maturation [128,62]. Accordingly, at day 22 of the differentiation protocol, a low value of *PAX2* expression (a mesenchymal marker) would be expectable if mature nephrons were obtained, but that was not verified.

Considering the important role of *PAX2* and *WT1* on condensation, MET and proximal-distal patterning, results concerning *PAX2*, *WT1* and *NPHS1* expression might indicate that at the end of the differentiation protocol, renal structures such as SSB might have been formed but not mature nephrons with podocytes and glomeruli. Concordant with these results, *UMOD* and *CUBN* genes which are characteristic markers of distal tubules/ loops of Henle and proximal tubules, respectively [90,91], also display low levels of expression on day 22 of the differentiation protocol. Moreover, *PAX8* expression is also known to increase with renal tubule maturation [62], and the obtained results reveal low levels of this marker, when compared to *WT1* and *PAX2*.

In addition, results show a reduced *SIX2* relative expression on day 22 of the differentiation protocol, which is indicative of a diminished NPC (*SIX2*$^{+}$) population, and in agreement with cell differentiation.

Overall, although the NPC cell population on day 22 of the differentiation protocol seems diminished, a longer period of culture may be required in order to obtain more differentiated and specialized cell populations.

As previously mentioned, interstitial stromal cells are characterized by *FOXD1* expression. These results show reduced levels of this marker, which can be explained by the high levels of *PAX2* expression, as this gene is known to repress non-nephron lineages [62].

Figure 4.20 depicts the relative expression profiles of *WT1*, *PAX2*, *SIX2*, *GATA3* and *HOXD11* during renal differentiation of cells exposed to WNT signalling for 72 hours.

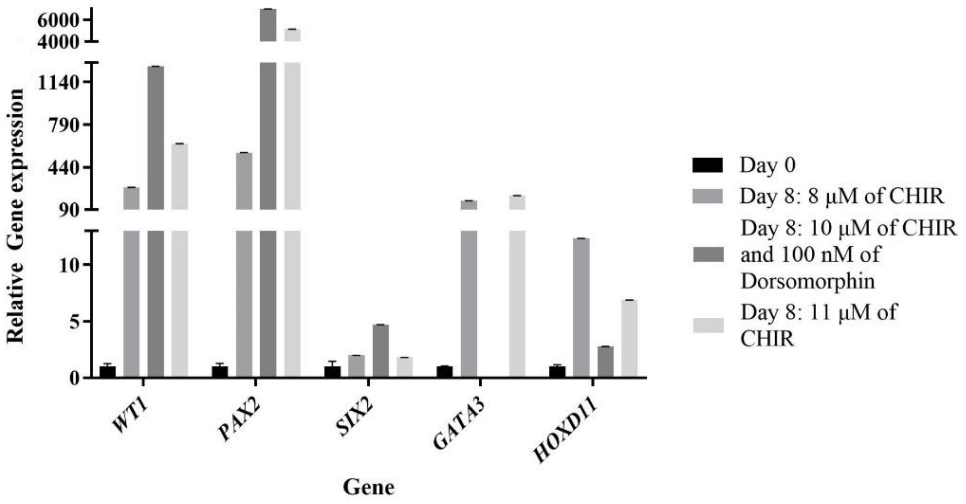

Figure 4.20| Relative expression profiles of mesodermal and renal markers during renal differentiation of hiPSCs exposed to WNT signalling for 72 hours. Cells (DF6, P61) were seeded at a density of 3,000 cells/aggregate in AggreWell™ 800 plates in mTeSR Plus™ medium. At day 0 of the differentiation protocol, the medium was changed to Advanced RPMI 1640 medium supplemented with 8 µM of CHIR, 10 µM of CHIR and 100 nM of Dorsomorphin or 11 µM of CHIR for 72 hours. Error bars represent SD. (*n*=1). *WT1*: Wilms' Tumour 1; *PAX2*: Paired box 2; *SIX2*: Sine oculis-related homeobox 2; *GATA3*: GATA binding protein 3; *HOXD11*: Homeobox D11.

In this experiment cells were exposed to WNT signalling for 72 hours, being followingly exposed to Activin for 72 hours and to FGF9 for more 48 hours. Thus, day 8 of the differentiation protocol is equivalent to day 9 of the differentiation protocol when cells were exposed to WNT signalling for 96 hours.

Relative expression profiles of the assessed genes demonstrate that cells exposed to WNT signalling for 72 hours (Figure 4.20) display, in general, lower levels of expression when compared to cells exposed to WNT signalling for 96 hours (Figure 4.18).

Cells exposed to 8 µM of CHIR display lower levels of *WT1*, *PAX2* and *SIX2* expression than cells exposed to the other two culture conditions.

Gene expression on day 8 of the differentiation protocol strongly varies between cells exposed to 10 µM of CHIR and 100 nM of Dorsomorphin and 11 µM of CHIR, for *WT1*, *GATA3* and *HOXD11*. For these genes, and contrary to cells exposed to WNT signalling for 96 hours, cells exposed to 10 µM of CHIR and 100 nM of Dorsomorphin exhibit higher levels of gene expression than cells exposed to 11 µM of CHIR.

IV.2.1.8.3. Immunofluorescence staining characterisation

Cryosectioned aggregates were characterized through immunofluorescence staining against expression of WT1, SIX2, PAX8, LHX1 and HOXD11 on different days of the differentiation protocol.

Table 4.3 resumes immunofluorescence staining results of cellular aggregates exposed to10 µM of CHIR and 100 nM of Dorsomorphin for 96 hours.

Table 4.3| Immunofluorescence staining of cellular aggregates exposed to 10 µM of CHIR and 100 nM of Dorsomorphin for 96 hours.

Culture Condition	Day of the differentiation protocol	Marker	Expression
10 µM of CHIR and 100 nM of Dorsomorphin for 96 hours	4	OCT4	-
	4	GATA3	-
	7	WT1	+
	7	HOXD11	-
	9	WT1	+
	9	SIX2	+
	14	WT1	+
	14	LHX1	+
	14	PAX8	+
	14	FOXD1	-

OCT4: Octamer-binding transcription factor 4; GATA3: GATA binding protein 3; WT1: Wilm's Tumour 1; HOXD11: Homeobox D11; SIX2: Sine oculis-related homeobox 2; LHX1: LIM Homeobox 1; PAX8: Paired box 8; FOXD1: Forkhead box D1; -: Negative; +: Positive.

Immunofluorescence staining assays reveal that OCT4 expression (a pluripotency marker) was not detected on day 4 of the differentiation protocol. However, this procedure consists of a qualitative analysis and thus, in the interest of accurately confirming the complete absence of pluripotent cells at this time point, flow cytometry analysis would be required.

Figure 4.21 depicts immunofluorescence staining of cellular aggregates exposed to 10 µM of CHIR and 100 nM of Dorsomorphin for 96 hours.

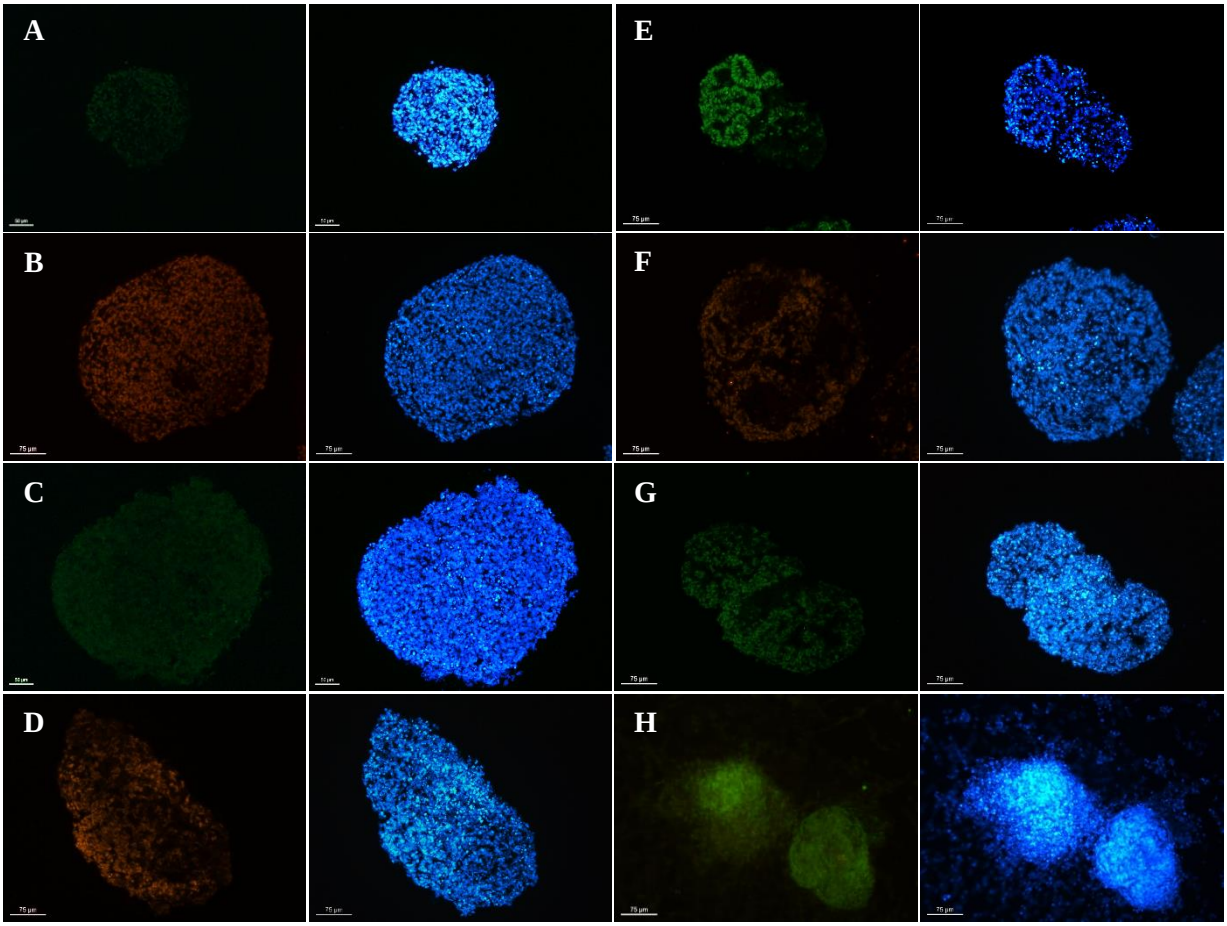

Figure 4.21| Immunofluorescence staining of cellular aggregates exposed to 10 µM of CHIR and 100 nM of Dorsomorphin for 96 hours. Immunofluorescence staining of **A)** WT1 on day 7; **B)** WT1 on day 9; **C)** SIX2 on day 9; **D-E)** LHX1 on day 14; **F-G** WT1 on day 14; **H)** PAX8 on day 14. Nucleus were stained with DAPI (blue). Images were acquired with a fluorescence optical microscope. Images at 200x magnification (scale bars: 75 µm, except for A and C, in which scalebars: 50 µm). WT1: Wilm's Tumour 1; SIX2: Sine oculis-related homeobox 2; LHX1: LIM Homeobox 1; PAX8: Paired box 8; DAPI: 4',6-Diamidino-2-Phenylindole.

The obtained results regarding immunofluorescence staining characterization are coherent with the ones obtained through RT-PCR characterization, insofar as negative expression of GATA3 on day 4 and negative expression of HOXD11 on day 7, coincide with low levels of expression of these genes (Figure 4.18).

According to Morizane and Bonventre, at day 14 of the differentiation protocol, RVs co-expressing PAX8 and LHX1 should be obtained [109]. The above presented results show cellular aggregates with positive expression of LHX1 and PAX8 at day 14. Immunofluorescence staining of LHX1 on day 14 (Figure 4.21, E) discloses round renal structures, which may constitute PTA or RV. Further analysis regarding co-expression of these two markers and LAM assessment would be necessary in order to verify if these structures constitute PTA ($LHX1^+$, $PAX8^+$) or RV ($LHX1^+$, $PAX8^+$, LAM^+) [109].

According to Morizane and Bonventre, renal condensed structures such as PTA and RV should be obtained by days 11 and 14, respectively [109]. Curiously, immunofluorescence staining characterization of cellular aggregates on day 9 of the differentiation protocol (when cells were exposed to 10 µM of CHIR and 100 nM of Dorsomorphin for 96 hours) also revealed the presence of structures similar to the ones observed in Figure 4.21, E. Figure 8.1 (Annexes, Section VIII.) exhibits some examples of the observed structures. These results suggest that when cells are exposed to the above referred culture conditions, the obtained cell stages do not coincide with the ones described by Morizane and Bonventre [109] and cells form condensed renal structures precociously.

Also, cellular aggregates exhibiting round condensed structures on day 9 of the differentiation protocol, were characterized against expression of SIX2, LHX1 and PAX8. Immunofluorescence staining results revealed positive expression of SIX2 and LHX1 and negative expression of PAX8 These results suggest that the condensed renal structures obtained at day 9 do not constitute PTA or RV and are partly constituted by NPCs. These structures may constitute condensed mesenchyme before the PTA and RV stage ($PAX2^+$ and $PAX8^-$) [136], but further characterization would be necessary to ascertain this.

Table 4.4 resumes immunofluorescence staining results of cellular aggregates exposed to11 µM of CHIR for 96 hours.

Table 4.4| Immunofluorescence staining of cellular aggregates exposed to 11 µM of CHIR for 96 hours.

Culture Condition	Day of the differentiation protocol	Marker	Expression
11 µM of CHIR for 96 hours	4	OCT4	-
	4	WT1	+
	7	WT1	+
	7	HOXD11	+
	9	WT1	-
	9	SIX2	+
	14	PAX8	+

OCT4: Octamer-binding transcription factor 4; WT1: Wilm's Tumour 1; HOXD11: Homeobox D11; SIX2: Sine oculis-related homeobox 2; PAX8: Paired box 8; +: Positive; -: Negative.

Figure 4.22 depicts immunofluorescence staining of cellular aggregates exposed to 11 µM of CHIR for 96 hours.

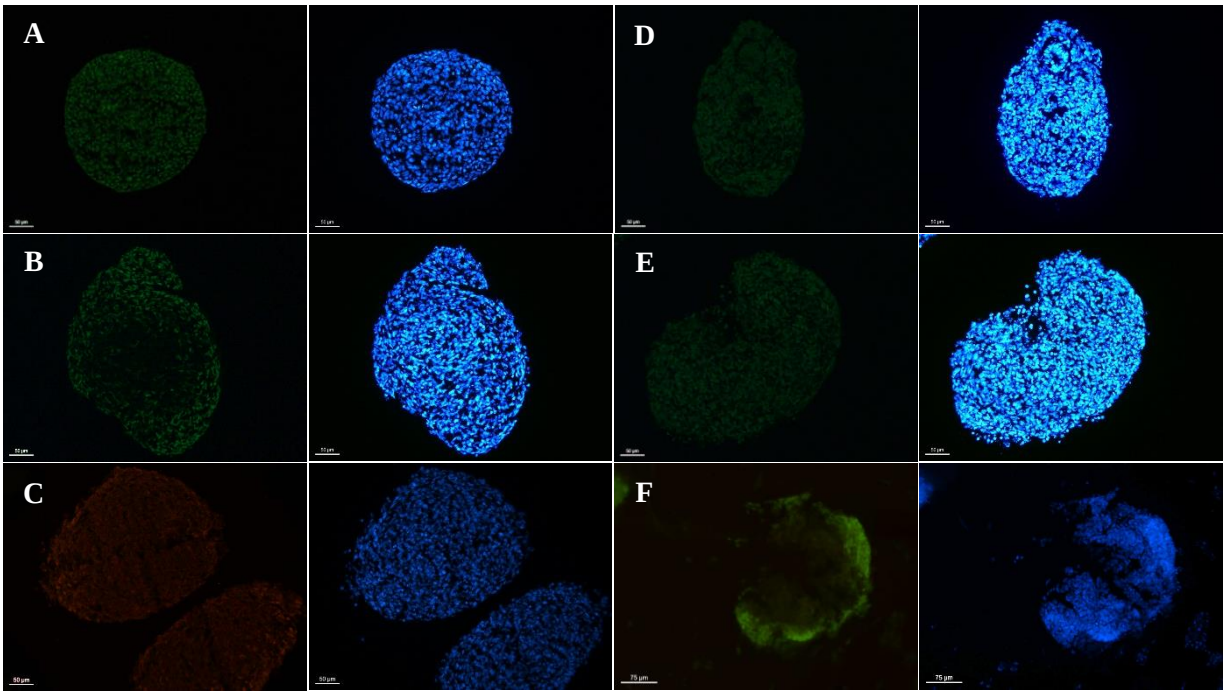

Figure 4.22| Immunofluorescence staining of cellular aggregates exposed to 11 µM of CHIR for 96 hours. Immunofluorescence staining of **A)** WT1 on day 4; **B)** WT1 on day 7; **C)** HOXD11 on day 7; **D-E)** SIX2 on day 9; **F)** PAX8 on day 14. Nucleus were stained with DAPI (blue). Images were acquired with a fluorescence optical microscope. Images at 200x magnification (scale bars: 50 µm, except for E, in which scalebars: 75 µm). WT1: Wilm's Tumour 1; HOXD11: Homeobox D11; SIX2: Sine oculis-related homeobox 2; PAX8: Paired box 8; DAPI: 4',6-Diamidino-2-Phenylindole.

As presented in Table 4.4, cells exposed to 11 µM of CHIR for 96 hours show negative expression of WT1 on day 9 of the differentiation protocol, however, RT-PCR results (Figure 4.18) show high levels of WT1 relative expression on this day. Furthermore, day 9 exhibits superior levels of WT1 expression than day 7 (Figure 4.18), wherein cells presented WT1 positive expression on immunofluorescence assays (Figure 4.22).

When characterizing cellular aggregates exposed to 11 µM of CHIR for 96 hours, through immunofluorescence staining against SIX2 expression on day 9, it was possible to observe a condensed renal structure. Once more, this result suggests that when cells are exposed to 11 µM of CHIR for 96 hours, also form condensed renal structures precociously. Nevertheless, only two cellular aggregates with renal structures were observed in the performed immunofluorescence assays for this culture condition, whereas, various condensed structures were observed in immunofluorescence assays of cells exposed to 10 µM of CHIR and 100 nM of Dorsomorphin for 96 hours (Annexes, Section VIII., Figure 8.1).

Once more, OCT4 expression was not detected on day 4 of the differentiation protocol.

IV.2.1.9. Takasato protocol: 3D Culture #7

DF6 cells were seeded in AggreWell™ 800 plates at a density of 3,000 cells/ aggregate. The differentiation protocol was initiated 24 hours after seeding and, thenceforward, cells were cultured on STEMdiff™ APEL™ 2 supplemented with 10 µM of CHIR and 100 nM of Dorsomorphin for 96 hours.

Cellular aggregates were collected at days 0, 4, 7, 9 and 14 for RT-PCR characterization and for immunofluorescence staining characterization.

IV.2.1.9.1. Aggregate size evaluation

During this experiment, several brightfield images were acquired in order to assess aggregates size fluctuation along time.

Table 4.5 summarizes aggregates diameter 24 hours after cell seeding which corresponded to day 0 of Takasato differentiation protocol.

Table 4.5| Aggregate size (number of cells per aggregate/microwell) and correspondent aggregate diameter mean value 24 hours after cell seeding/day 0 of the differentiation protocol. (*n*=1).

Culture condition	Diameter mean value (µm)	Standard Deviation (SD)
3,000 Cells per aggregate	254	4

The aggregates diameter distribution along time is depicted in Figure 4.23.

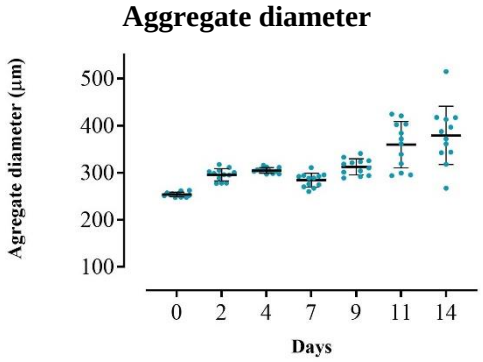

Figure 4.23| Aggregates diameter distribution along time. Cells (DF6, P51) were seeded at a density of 3,000 cells/aggregate in AggreWell™ 800 plates in mTeSR Plus™ medium. At day 0 of the differentiation protocol, the culture medium was changed to STEMdiff™ APEL™ 2 supplemented with 10 µM of CHIR and 100 nM of Dorsomorphin for 96 hours. The black bars represent diameters mean values and error bars represent SD. (*n*=1).

As it can be observed, aggregate diameter tends to increase along time when conducting Takasato differentiation protocol. Day 0 is presented as the time point with the lowest aggregate diameters, with a mean value of 254 µm (Table 4.5), and day 14 is presented as the time point with the highest aggregate diameters, with a mean value of 379 µm.

IV.2.1.9.2. Quantitative real-time polymerase chain reaction characterisation

Expression of *WT1*, *PAX2*, *SIX2*, *GATA3* and *HOXD11* genes were assayed through RT-PCR along the differentiation protocol, and normalised against expression at day 0 and expression of the endogenous control gene, *GAPDH*.

Figure 4.24 depicts the relative expression profiles of these genes during renal differentiation of cells according to Takasato protocol.

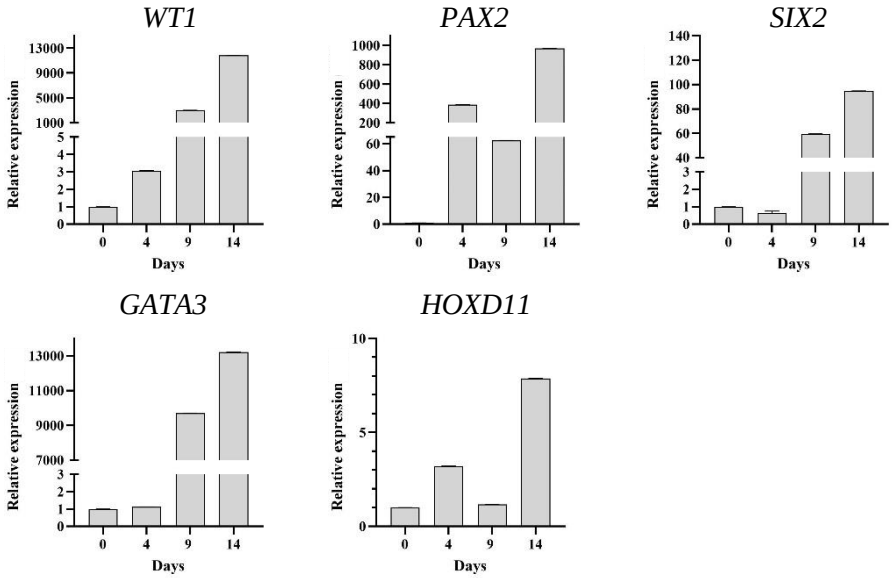

Figure 4.24| Relative expression profiles of mesodermal and renal markers during renal differentiation of hiPSCs exposed to WNT signalling for 96 hours. Cells (DF6, P51) were seeded at a density of 3,000 cells/aggregate in AggreWell™ 800 plates in mTeSR Plus™ medium. At day 0 of the differentiation protocol, the medium was changed to STEMdiff™ APEL™ 2 medium. Cells were exposed to 10 µM of CHIR and 100 nM of Dorsomorphin for 96 hours. Error bars represent SD. (*n*=1). *WT1*: Wilms' Tumour 1; *PAX2*: Paired box 2; *SIX2*: Sine oculis-related homeobox 2; *GATA3*: GATA binding protein 3; *HOXD11*: Homeobox D11.

When comparing the obtained results for RT-PCR characterization of cells cultured under Morizane protocol and exposed to 10 µM and 100 nM of Dorsomorphin (Figure 4.18) with RT-PCR characterization of cells cultured under Takasato protocol (Figure 4.24), it is possible to verify that relative gene expression levels considerably fluctuate between the two protocols, in particular for *WT1*, *PAX2* and *GATA3* genes.

This aspect is particularly evident when considering *WT1* relative expression on day 14 of the differentiation protocol, which presents levels of *WT1* expression three times higher than *WT1* expression of cells cultured under Morizane protocol on this day. *WT1* relative expression increases along the differentiation protocol.

Regarding *GATA3* expression, apart from considerable superior levels of gene expression, the decrease in *GATA3* expression on day 14 of the differentiation protocol observed on Morizane

protocol, did not occur on Takasato protocol. These accentuated differences in *GATA3* expression (anterior IM marker) may be explained, in part, by the fact that Morizane protocol intends to only generate posterior IM in order to efficiently generate NPCs [91,109], while Takasato protocol was found to be able to simultaneously induce both anterior and posterior IM [90]. Although cells on day 7 of Takasato differentiation protocol (supposed IM stage) were not characterized, it can be hypothesized that high levels of *GATA3* relative expression on days 9 and 14 may be attributed to anterior IM induction. However, when considering *HOXD11* (posterior IM marker) relative expression, the same time points present low levels of expression of this gene, which suggests low induction of posterior IM.

Contrastingly, *PAX2* relative expression of cells cultured under Takasato protocol along the differentiation protocol, is considerably inferior than *PAX2* relative expression of cells cultured under Morizane protocol.

IV.2.1.9.3. Immunofluorescence staining characterisation

Cryosectioned aggregates were characterized through immunofluorescence staining against expression of WT1, SIX2, PAX8, LHX1 and HOXD11 on different days of the differentiation protocol.

Table 4.6 resumes immunofluorescence staining results of cellular aggregates exposed to 10 µM of CHIR and 100 nM of Dorsomorphin according to Takasato protocol.

Table 4.6| Immunofluorescence staining of cellular aggregates exposed to 10 µM of CHIR and 100 nM of Dorsomorphin for 96 hours.

Culture Condition	Day of the differentiation protocol	Marker	Expression
10 µM of CHIR and 100 nM of Dorsomorphin	4	OCT4	-
	4	HOXD11	-
	9	WT1	+
	9	SIX2	-
	14	WT1	+
	14	PAX8	-
	14	LHX1	+
	14	HOXD11	-

OCT4: Octamer-binding transcription factor 4; HOXD11: Homeobox D11; WT1: Wilm's Tumour 1; SIX2: Sine oculis-related homeobox 2; PAX8: Paired box 8; LHX1: LIM homeobox 1; -: Negative; +: Positive.

Figure 4.25 depicts immunofluorescence staining of cellular aggregates exposed to 10 µM of CHIR and 100 nM of Dorsomorphin for 96 hours according to Takasato protocol.

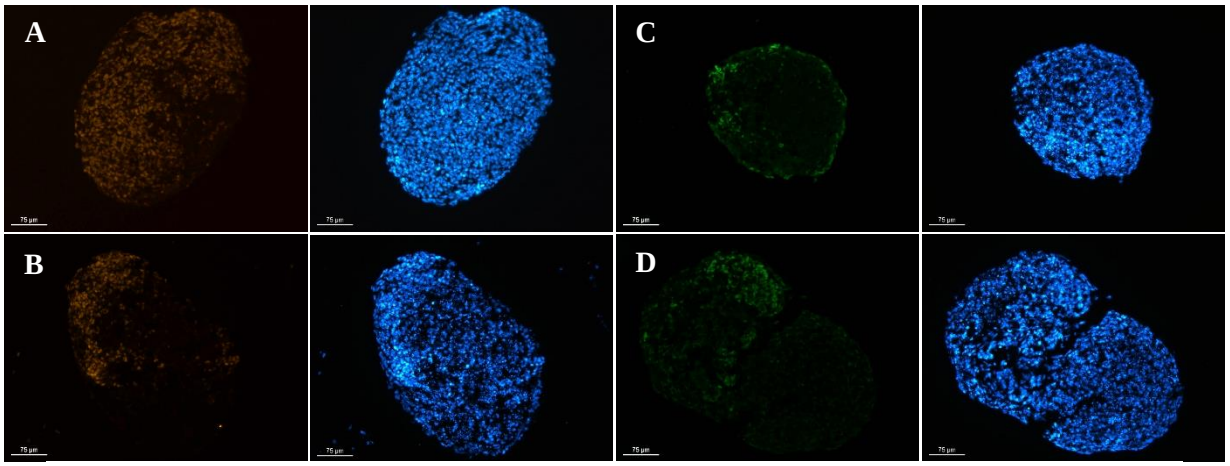

Figure 4.25| Immunofluorescence staining of cellular aggregates exposed to 10 µM of CHIR and 100 nM of Dorsomorphin for 96 hours. Immunofluorescence staining of **A)** WT1 on day 9; **B)** WT1 on day 14; **C-D)** LHX1 on day 14. Nucleus were stained with DAPI (blue). Images were acquired with a fluorescence optical microscope. Images at 200x magnification (scale bars: 75 µm). WT1: Wilm's Tumour 1; LHX1: LIM homeobox 1; DAPI: 4',6-Diamidino-2-Phenylindole.

Immunofluorescence staining results are coherent with the obtained results through RT-PCR characterization, insofar as negative expression of HOXD11 on days 4 and 14, and negative expression of SIX2 on day 9, coincide with low levels of expression of these genes (Figure 4.24). Immunofluorescence staining assays also allowed to identify a condensed renal structure by day 14 of the differentiation protocol (Annexes, Section VIII., Figure 8.2). Once more, OCT4 expression was not detected on day 4 of the differentiation protocol.

V. CONCLUSION

The main objective in this work was to generate kidney organoids from hiPSCs under 3D conditions, which comprised the conduction and adaptation of both differentiation protocols to this cell culture configuration, in particular, in AggreWell™ system. The obtained results throughout this project indicate that full optimization of the differentiation protocols under 3D conditions was not achieved yet. Besides, optimization of the differentiation protocols for the three tested cell lines was not possible.

Although the obtained results are partially consistent with a successful renal differentiation induction, these results also support the fact that the obtained cellular aggregates do not display the expected renal structures by the time point of day 14 of the differentiation protocol. In addition, results regarding day 22 of the differentiation protocol depict generation of immature kidney organoids. Overall, it is apparent that when conducting the differentiation protocols under 3D culture and employing the tested culture conditions, the obtained cellular stages do not temporally correspond to cellular stages described by Morizane *et al* [91], and the differentiation protocol using this methodology should be carried out for a longer period of time.

Previously presented results state the formation of renal condensed structures on day 9 of the differentiation protocol. In order to accurately assess the achieved stages along the differentiation protocol, and to confirm temporal correspondence or discrepancy, it would have been important to evaluate different renal markers on the supposed time points.

Morizane *et al.* characterized the obtained kidney organoids for different time points of the differentiation protocol, regarding cellular types and their ratios [91]. On the contrary, throughout experiments under 3D culture during this project, cellular types and ratios of cells in cellular aggregates for the different time points, were not assessed through flow cytometry analysis. For this reason, it is not possible to accurately compare the obtained results and comment on their similarity/ dissimilarity.

Withal, on the initially performed experiments, only WT1 (mesodermal marker) expression was evaluated, while characteristic markers of the previous cell stage, primitive streak, were not assessed. Thence, it was not possible to assess if primitive streak induction was occurring in a successful way and in a concordant temporal sequence, and consequently it is not possible to determine if this aspect limited renal differentiation. Furthermore, the initially performed experiments could have been evaluated regarding anterior and posterior markers.

Both of the referred protocols combine monolayer and 3D culture. Takasato *et al.* defend that the initial monolayer culture enables them to more precisely control anteroposterior cell fate on the primitive streak cell stage than in embryoid bodies culture [110]. Having this in mind, one could hypothesize that conducting the whole protocol under 3D conditions may conditionate the correct

definition of the primitive streak, and consequently implicate on the following differentiation stages.

This project set out with the aim of generating kidney organoids under 3D conditions with simultaneous induction of both ureteric epithelium and MM. For that purpose, the period of exposure to WNT signalling was optimized. Morizane and Bonventre defend a period of exposure to WNT signalling of 96 hours (4 days) [109], whereas Takasato advises an adjustment of this period between 2-5 days [110]. Bearing this in mind, periods of exposure to WNT signalling of 72 and 96 hours were applied.

Morizane *et al.* state that by day 21 of the differentiation protocol, elongated epithelial nephron structures were observable, whereas outgrowths of collecting duct structures ($CDH1^+$, DBA^+) (UB derived) were not present, confirming the specificity of the developed protocol for NPCs efficient induction [91]. In opposition, Takasato *et al.* were able to induce both ureteric epithelium ($GATA3^+$, $PAX2^+$, $ECAD^+$) and MM ($PAX2^+$, $ECAD^-$) by day 18 of the differentiation protocol [90].

Although both anterior and posterior mesodermal markers were evaluated throughout this work during renal differentiation, it was not possible to understand if these two cell populations were simultaneously formed. Thus, in order to assess if this initial objective was accomplished, experiments under the tested culture conditions should be carried until days 22 and 18 and assessment of CDH1/DBA and GATA3/PAX2/ECAD presence, respectively, would be necessary.

Also, the obtained results demonstrated that the most suitable period of exposure to WNT signalling differs between monolayer culture and 3D culture, as does the concentration of CHIR required to perform an efficient differentiation. When conducting experiments under adherent conditions, a period of exposure to WNT signalling for 72 hours was successful in inducing a 'loosely dense' cell morphology (Figure 4.7). On the other hand, a period of exposure to WNT signalling for 96 hours seems to be the most suitable for a successful renal differentiation on 3D conditions (Figure 4.18 and Figure 4.20).

The evaluation of the effect of the initial aggregate size towards the efficiency of hiPSCs derivation into IM was defined as an initial goal in this project. The obtained data on the performed experiments along this work do not allow to get to a conclusion regarding this objective. The efficiency of IM specification, through WT1 expression assessment, was not evaluated for every performed experiment. As a consequence, it was not possible to establish a relation between aggregate size and efficiency of IM specification. However, initial aggregate diameters similar to those used for other mesodermal differentiation protocol, such as cardiac

differentiation, were successfully applied. On top of that, more suitable mesodermal markers for flow cytometry analysis would be required in order to answer this question.

As previously commented, the achieved level of maturity is a common organoid generation limitation. The two referred protocols are not able to generate kidney organoids reaching an adult stage of maturation. More precisely, kidney organoids generated through Takasato protocol on 3D conditions were found to be transcriptionally similar to the human first-trimester kidney [90]. Throughout this work, only Morizane differentiation protocol was carried to the end (day 22), once. Although the obtained organoids were not characterized regarding their complete transcriptional profile, RT-PCR results disclosed low levels of expression of genes expressed in the different nephron segments (Figure 4.19), providing evidence of immature organoids. The immaturity of the generated organoids is particularly important when considering kidney organoids as systems to model kidney disease, in view of the fact that most of the aforementioned inherited kidney diseases (Section I.3.1.) develop after birth [110].

A worthy attention detail concerns the used differentiation media on the conducted protocols. STEMdiff™ APEL™ 2 is a commercially available medium which was specifically designed for hESCs and hiPSCs differentiation, containing all the requirements for that process, whereas, Advanced RPMI 1640 medium is a quite simple basal medium that requires supplementation, and thus, less robust. With this in mind, it is likely that this aspect may have influenced the obtained results.

It is plausible that a number of limitations may have influenced the obtained results throughout this work. The limitations of the present study naturally include the low number or absence of replicates in the performed experiments. Although results regarding experiments conducted under Morizane and Takasato protocols were compared in previous sections, an accurate comparison would require a higher number of replicates for each experiment.

The absence of flow cytometry analysis of the different mesodermal and renal markers along the differentiation protocols, also constitutes a limitation of the present study. However, the lack of this analysis is justified by the fact that the available antibodies are not suitable for this type of procedure, and were overcomed by RT-PCR analysis.

On a final note, this work contributed to start the adaptation of two renal differentiation protocols to 3D conditions. Therefore, further work will be needed to achieve a complete optimization of these protocols and efficiently generate kidney organoids under 3D conditions for various purposes.

VI. FUTURE WORK

In order to improve the renal differentiation process under 3D conditions there are some strategies which may be applied in future work.

As previously stated, when driving renal differentiation on AggreWell™ plates, cells tended to disaggregate after some days of culture. A possible strategy to prevent this situation would imply the transference of cellular aggregates from AggreWell™ plates to 96-well, round-bottom, ultra-low attachment plates previous to their disaggregation. Aggregates transference would be beneficial as ultra-low attachment plates force cell aggregation. Furthermore, ultra-low attachment plates would overcome the fact that cellular aggregates tend to adhere to Polydimethylsiloxane (PDMS), which constitutes AggreWell™ 800 plates.

As previously mentioned, each hiPSC line has its own propensity to undergo towards a certain cell fate depending on its cell type of origin (Section I.1.3.3.). Having this in mind, using renal cells, such as urine-derived cells, as a source for cell reprogramming, could favour kidney organoids generation under 3D conditions [82].

Another possible strategy would include organoid encapsulation with Matrigel®, as this substrate would grant structural support and promote organoid maturation, as perceived in cerebral organoids development [137].

Future work could also include combination of different 3D culture strategies such as AggreWell™ 800 plates and porous membranes, or even, the conduction of the differentiation protocols exclusively on porous membranes, as this strategy seems to be effective for organoids maturation.

To conclude, another alternative to generate cellular aggregates containing both anterior and posterior IM would imply using two different protocols to specifically derive each cell population. After this initial step, cells from anterior and posterior IM would be singularized and mixed prior to seeding in microwells to proceed with the differentiation protocol.

VII. REFERENCES

1. Rippon, H. J. & Bishop, A. E. Embryonic stem cells. *Cell Prolif.* **37**, 23–34 (2004).
2. Fernandes, T., Diogo, M. & Cabral, J. M. S. *Stem cell bioprocessing for cellular therapy, diagnostics and drug development*. (Woodhead Publishing, 2013).
3. Services., D. of H. and H. *Stem Cells: Scientific Progress and Future Research Directions*. (2001).
4. Alberts, B. *et al. Molecular Biology of the cell*. (Garland Science, 2015).
5. Solter, D. From teratocarcinomas to embryonic stem cells and beyond: A history of embryonic stem cell research. *Nat. Rev. Genet.* **7**, 319–327 (2006).
6. Brignier, A. C. & Gewirtz, A. M. Embryonic and adult stem cell therapy. *J. Allergy Clin. Immunol.* **125**, 336–344 (2010).
7. De Los Angeles, A. *et al.* Hallmarks of pluripotency. *Nature* **525**, 469–478 (2015).
8. Odorico, J. S., Kaufman, D. S. & Thomson, J. A. Multilineage Differentiation from Human Embryonic Stem Cell Lines. *Stem Cells* **19**, 193–204 (2009).
9. Donovan, P. J. & Gearhart, J. The end of the beginning for pluripotent stem cells. *Nature* **414**, 92–96 (2001).
10. Bongso, A. & Hin Lee, E. Stem Cells: Their Definition, Classification and Sources. in *Stem Cells: From Bench to Bedside* 1–13 (World Scientific Publishing Co. Pte. Ltd., 2005).
11. Biswas, A. & Hutchins, R. Embryonic Stem Cells. *Stem Cells Dev.* **16**, 213–222 (2007).
12. Panski, B. *Review of medical embryology*. (Embryome Sciences, Alameda, CA., 1982).
13. Andrews, P. W. *et al.* Embryonic stem (ES) cells and embryonal carcinoma (EC) cells: opposite sides of the same coin. *Biochem. Soc. Trans.* **33**, 1526–1530 (2005).
14. Evans, M. J. & Kaufman, M. H. Establishment in culture of pluripotential cells from mouse embryos. *Nature* **292**, 154–156 (1981).
15. Martin, G. R. Isolation of a pluripotent cell line from early mouse embryos cultured in medium conditioned by teratocarcinoma stem cells. *Proc. Natl. Acad. Sci. U. S. A.* **78**, 7634–7638 (1981).
16. Thomson, J. A. Embryonic stem cell lines derived from human blastocysts. *Science (80-.).* **282**, 1145–1147 (1998).
17. Niwa, H. How is pluripotency determined and maintained? *Development* **134**, 635–646 (2007).
18. Yeo, J. C. & Ng, H. H. The transcriptional regulation of pluripotency. *Cell Res.* **23**, 20–32 (2013).
19. Bishop, A. E., Buttery, L. D. K. & Polak, J. M. Embryonic stem cells. *J. Pathol.* **197**, 424–429 (2002).
20. Gilbert, D. M. The future of human embryonic stem cell research: Addressing ethical conflict with responsible scientific research. *Med. Sci. Monit.* **10**, 99–103 (2004).
21. Dakhore, S., Nayer, B. & Hasegawa, K. Human pluripotent stem cell culture: Current status, challenges, and advancement. *Stem Cells Int.* **2018**, (2018).
22. Takahashi, K. & Yamanaka, S. Induction of Pluripotent Stem Cells from Mouse Embryonic and Adult Fibroblast Cultures by Defined Factors. *Cell* **126**, 663–676 (2006).
23. Takahashi, K. *et al.* Induction of Pluripotent Stem Cells from Adult Human Fibroblasts by Defined Factors. *Cell* **131**, 861–872 (2007).
24. Yu, J. *et al.* Induced pluripotent stem cell lines derived from human somatic cells. *Science (80-.).* **318**, 1917–1920 (2007).
25. González, F., Boué, S. & Belmonte, J. C. I. Methods for making induced pluripotent stem cells: Reprogramming à la carte. *Nat. Rev. Genet.* **12**, 231–242 (2011).
26. Haridhasapavalan, K. K. *et al.* An insight into non-integrative gene delivery approaches to generate transgene-free induced pluripotent stem cells. *Gene* **686**, 146–159 (2019).
27. Kang, X. *et al.* Effects of integrating and non-integrating reprogramming methods on copy number variation and genomic stability of human induced pluripotent stem cells. *PLoS One* **10**, e0131128 (2015).

28. Schlaeger, T. M. Nonintegrating human somatic cell reprogramming methods. in *Advances in Biochemical Engineering/Biotechnology* vol. 163 1–21 (Springer Science and Business Media Deutschland GmbH, 2018).
29. Rao, M. S. & Malik, N. Assessing iPSC reprogramming methods for their suitability in translational medicine. *J. Cell. Biochem.* **113**, 3061–3068 (2012).
30. Cherkashova, E. A. *et al.* Methods of Generation of Induced Pluripotent Stem Cells and Their Application for the Therapy of Central Nervous System Diseases. *Bull. Exp. Biol. Med.* **168**, 566–573 (2020).
31. Hu, C. & Li, L. Current reprogramming systems in regenerative medicine: From somatic cells to induced pluripotent stem cells. *Regen. Med.* **11**, 91–105 (2016).
32. Takahashi, K. & Yamanaka, S. A decade of transcription factor-mediated reprogramming to pluripotency. *Nat. Rev. Mol. Cell Biol.* **17**, 183–193 (2016).
33. Zacharias, D. G., Nelson, T. J., Mueller, P. S. & Hook, C. C. The science and ethics of induced pluripotency: What will become of embryonic stem cells? *Mayo Clin. Proc.* **86**, 634–640 (2011).
34. Yamanaka, S. Induced pluripotent stem cells: Past, present, and future. *Cell Stem Cell* **10**, 678–684 (2012).
35. Kim, K. *et al.* Donor cell type can influence the epigenome and differentiation potential of human induced pluripotent stem cells. *Nat. Biotechnol.* **29**, 1117–1119 (2011).
36. Kim, K. *et al.* Epigenetic memory in induced pluripotent stem cells. *Nature* **467**, 285–290 (2010).
37. Pera, M. F. & Tam, P. P. L. Extrinsic regulation of pluripotent stem cells. *Nature* **465**, 713–720 (2010).
38. Chng, Z., Vallier, L. & Pedersen, R. Activin/Nodal Signaling and Pluripotency. in *Vitamins and Hormones* vol. 85 39–58 (Academic Press, 2011).
39. Xu, R. H. *et al.* Basic FGF and suppression of BMP signaling sustain undifferentiated proliferation of human ES cells. *Nat. Methods* **2**, 185–190 (2005).
40. Ding, V. M. Y. *et al.* FGF-2 modulates Wnt signaling in undifferentiated hESC and iPS cells through activated PI3-K/GSK3β signaling. *J. Cell. Physiol.* **225**, 417–428 (2010).
41. Fathi, A., Eisa-Beygi, S. & Baharvand, H. Signaling molecules governing pluripotency and early lineage commitments in human pluripotent stem cells. *Cell J.* **19**, 194–203 (2017).
42. Manning, B. D. & Cantley, L. C. AKT/PKB Signaling: Navigating Downstream. *Cell* **129**, 1261–1274 (2007).
43. Yu, J. S. L. & Cui, W. Proliferation, survival and metabolism: The role of PI3K/AKT/mTOR signalling in pluripotency and cell fate determination. *Dev.* **143**, 3050–3060 (2016).
44. Chang, F. *et al.* Signal transduction mediated by the Ras/Raf/MEK/ERK pathway from cytokine receptors to transcription factors: Potential targeting for therapeutic intervention. *Leukemia* **17**, 1263–1293 (2003).
45. Sokol, S. Y. Maintaining embryonic stem cell pluripotency with Wnt signaling. *Development* **138**, 4341–4350 (2011).
46. Xu, Z. *et al.* Wnt/β-catenin signaling promotes self-renewal and inhibits the primed state transition in naïve human embryonic stem cells. *Proc. Natl. Acad. Sci.* **113**, E6382–E6390 (2016).
47. Gan, Q., Yoshida, T., McDonald, O. G. & Owens, G. K. Concise Review: Epigenetic Mechanisms Contribute to Pluripotency and Cell Lineage Determination of Embryonic Stem Cells. *Stem Cells* **25**, 2–9 (2007).
48. Ng, H. H. & Surani, M. A. The transcriptional and signalling networks of pluripotency. *Nat. Cell Biol.* **13**, 490–496 (2011).
49. Wiegand, C. & Banerjee, I. Recent advances in the applications of iPSC technology. *Curr. Opin. Biotechnol.* **60**, 250–258 (2019).
50. Engle, S. J. & Vincent, F. Small molecule screening in human induced pluripotent stem cell-derived terminal cell types. *J. Biol. Chem.* **289**, 4562–4570 (2014).
51. Diecke, S. *et al.* Recent technological updates and clinical applications of induced

pluripotent stem cells. *Korean J. Intern. Med.* **29**, 547–557 (2014).
52. Liu, G., David, B. T., Trawczynski, M. & Fessler, R. G. Advances in Pluripotent Stem Cells: History, Mechanisms, Technologies, and Applications. *Stem Cell Rev. Reports 2019 161* **16**, 3–32 (2019).
53. Angelos, M. G. & Kaufman, D. S. Pluripotent stem cell applications for regenerative medicine. *Curr. Opin. Organ Transplant.* **20**, 663–670 (2015).
54. Miranda, C. C., Fernandes, T. G., Diogo, M. M. & Cabral, J. M. S. Human Pluripotent Stem Cells: Applications and Challenges for Regenerative Medicine and Disease Modeling. in *Advances in Biochemical Engineering/Biotechnology* vol. 171 189–224 (Springer, Cham, 2019).
55. Yamanaka, S. Pluripotent Stem Cell-Based Cell Therapy—Promise and Challenges. *Cell Stem Cell* **27**, 523–531 (2020).
56. Junqueira, L. & Carneiro, J. Urinary System. in *Junqueira's Basic Histology: Text & Atlas* 371–388 (McGraw-Hill/Appleton & Lange, 2002).
57. VanPutte, C. *et al.* Urinary System. in *Seeley's anatomy & physiology* 958–981 (McGraw-Hill Education, 2017).
58. Treuting, P. M. & Kowalewska, J. Urinary System. in *Comparative Anatomy and Histology* (eds. Treuting, P. M. & Dintzis, S. M.) 229-251,959-973 (Elsevier Inc., 2012).
59. Gilbert, S. F. & Barresi, M. J. F. *Developmental Biology*. (Sinauer Associates, Inc., 2016).
60. Little, M. H. Kidney Development in the Mammal. in *Kidney Transplantation, Bioengineering, and Regeneration: Kidney Transplantation in the Regenerative Medicine Era* 787–799 (Academic Press, 2017). doi:10.1016/B978-0-12-801734-0.00056-4.
61. Moritz, K. M., Wintour-Coghlan, M., Black, M. J., Bertram, J. F. & Caruana, G. Morphological development of the mammalian kidney. in *Factors Influencing Mammalian Kidney Development: Implications for Health in Adult Life. Advances in Anatomy Embryology and Cell Biology* vol. 196 1–9 (Springer, Berlin, Heidelberg, 2008).
62. Faa, G. *et al.* Morphogenesis and molecular mechanisms involved in human kidney development. *J. Cell. Physiol.* **227**, 1257–1268 (2012).
63. Seely, J. C. A brief review of kidney development, maturation, developmental abnormalities, and drug toxicity: juvenile animal relevancy. *J. Toxicol. Pathol.* **30**, 125–133 (2017).
64. Dressler, G. R. The Cellular Basis of Kidney Development. *Annu. Rev. Cell Dev. Biol.* **22**, 509–529 (2006).
65. McMahon, A. P. Development of the Mammalian Kidney. in *Current Topics in Developmental Biology* (ed. Wassarman, P. M.) vol. 117 31–64 (Academic Press Inc., 2016).
66. Little, M. H., Kumar, S. V. & Forbes, T. Recapitulating kidney development: Progress and challenges. *Semin. Cell Dev. Biol.* **91**, 153–168 (2019).
67. Taguchi, A. *et al.* Redefining the in vivo origin of metanephric nephron progenitors enables generation of complex kidney structures from pluripotent stem cells. *Cell Stem Cell* **14**, 53–67 (2014).
68. Rosenblum, N. D. Developmental biology of the human kidney. *Semin. Fetal Neonatal Med.* **13**, 125–132 (2008).
69. Khoshdel Rad, N., Aghdami, N. & Moghadasali, R. Cellular and Molecular Mechanisms of Kidney Development: From the Embryo to the Kidney Organoid. *Front. Cell Dev. Biol.* **8**, 183–199 (2020).
70. Dressler, G. R. Advances in early kidney specification, development and patterning. *Development* **136**, 3863–3874 (2009).
71. Rowan, C. J., Deloui, S. S. & Rosenblum, N. D. Origin and function of the renal stroma in health and disease. in *Results and Problems in Cell Differentiation* vol. 60 205–229 (Springer Verlag, 2017).
72. Magella, B. *et al.* Cross-platform single cell analysis of kidney development shows

stromal cells express Gdnf. *Dev. Biol.* **434**, 36–47 (2018).
73. Morizane, R., Miyoshi, T. & Bonventre, J. V. Concise Review: Kidney Generation with Human Pluripotent Stem Cells. *Stem Cells* **35**, 2209–2217 (2017).
74. Lancaster, M. A. & Knoblich, J. A. Organogenesis in a dish: Modeling development and disease using organoid technologies. *Science (80-.).* **345**, 1247125–1247125 (2014).
75. Fatehullah, A., Tan, S. H. & Barker, N. Organoids as an in vitro model of human development and disease. *Nat. Cell Biol.* **18**, 246–254 (2016).
76. Kim, J., Koo, B. K. & Knoblich, J. A. Human organoids: model systems for human biology and medicine. *Nat. Rev. Mol. Cell Biol.* **21**, 571–584 (2020).
77. Clevers, H. Modeling Development and Disease with Organoids. *Cell* **165**, 1586–1597 (2016).
78. Drost, J. & Clevers, H. Translational applications of adult stem cell-derived organoids. *Dev.* **144**, 968–975 (2017).
79. Lehmann, R. *et al.* Human organoids: A new dimension in cell biology. *Mol. Biol. Cell* **30**, 1129–1137 (2019).
80. Little, M. H. Organoids: A special issue. *Dev.* **144**, 935–937 (2017).
81. Munsie, M., Hyun, I. & Sugarman, J. Ethical issues in human organoid and gastruloid research. *Dev.* **144**, 942–945 (2017).
82. Yengej, F. A. Y., Jansen, J., Rookmaaker, M. B., Verhaar, M. C. & Clevers, H. Kidney Organoids and Tubuloids. *Cells 2020, Vol. 9, Page 1326* **9**, 1326–1346 (2020).
83. Romagnani, P. *et al.* Chronic kidney disease. *Nat. Rev. Dis. Prim. 2017 31* **3**, 1–24 (2017).
84. Little, M. H. & Combes, A. N. Kidney organoids: accurate models or fortunate accidents. *Genes Dev.* **33**, 1319–1345 (2019).
85. Narayanan, K. *et al.* Human embryonic stem cells differentiate into functional renal proximal tubular–like cells. *Kidney Int.* **83**, 593–603 (2013).
86. Kang, M. & Han, Y.-M. Differentiation of Human Pluripotent Stem Cells into Nephron Progenitor Cells in a Serum and Feeder Free System. *PLoS One* **9**, e94888 (2014).
87. Lam, A. Q. *et al.* Rapid and Efficient Differentiation of Human Pluripotent Stem Cells into Intermediate Mesoderm That Forms Tubules Expressing Kidney Proximal Tubular Markers. *J. Am. Soc. Nephrol.* **25**, 1211–1225 (2014).
88. Takasato, M. *et al.* Directing human embryonic stem cell differentiation towards a renal lineage generates a self-organizing kidney. *Nat. Cell Biol. 2013 161* **16**, 118–126 (2013).
89. Xia, Y. *et al.* The generation of kidney organoids by differentiation of human pluripotent cells to ureteric bud progenitor–like cells. *Nat. Protoc. 2014 911* **9**, 2693–2704 (2014).
90. Takasato, M. *et al.* Kidney organoids from human iPS cells contain multiple lineages and model human nephrogenesis. *Nat. 2015 5267574* **526**, 564–568 (2015).
91. Morizane, R. *et al.* Nephron organoids derived from human pluripotent stem cells model kidney development and injury. *Nat. Biotechnol. 2015 3311* **33**, 1193–1200 (2015).
92. Ciampi, O. *et al.* Generation of functional podocytes from human induced pluripotent stem cells. *Stem Cell Res.* **17**, 130–139 (2016).
93. Lund, A. W., Yener, B., Stegemann, J. P. & Plopper, G. E. The Natural and Engineered 3D Microenvironment as a Regulatory Cue During Stem Cell Fate Determination. *Tissue Eng. Part B Rev.* **15**, 371–380 (2009).
94. Johnson, B. V., Shindo, N., Rathjen, P. D., Rathjen, J. & Keough, R. A. Understanding pluripotency--how embryonic stem cells keep their options open. *Mol. Hum. Reprod.* **14**, 513–520 (2008).
95. Grossmann, J. Molecular mechanisms of "detachment-induced apoptosis—Anoikis". *Apoptosis 2002 73* **7**, 247–260 (2002).
96. Riento, K. & Ridley, A. J. Rocks: Multifunctional kinases in cell behaviour. *Nat. Rev. Mol. Cell Biol.* **4**, 446–456 (2003).
97. Ohgushi, M. *et al.* Molecular pathway and cell state responsible for dissociation-induced apoptosis in human pluripotent stem cells. *Cell Stem Cell* **7**, 225–239 (2010).
98. Watanabe, K. *et al.* A ROCK inhibitor permits survival of dissociated human embryonic stem cells. *Nat. Biotechnol.* **25**, 681–686 (2007).

99. Ishizaki, T. *et al.* Pharmacological Properties of Y-27632, a Specific Inhibitor of Rho-Associated Kinases. *Mol. Pharmacol.* **57**, 976–983 (2000).
100. Edmondson, R., Broglie, J. J., Adcock, A. F. & Yang, L. Three-dimensional cell culture systems and their applications in drug discovery and cell-based biosensors. *Assay Drug Dev. Technol.* **12**, 207–218 (2014).
101. Celiz, A. D. *et al.* Materials for stem cell factories of the future. *Nat. Mater.* **13**, 570–579 (2014).
102. Amelian, A., Wasilewska, K., Megias, D. & Winnicka, K. Application of standard cell cultures and 3D in vitro tissue models as an effective tool in drug design and development. *Pharmacol. Reports* **69**, 861–870 (2017).
103. Antoni, D., Burckel, H., Josset, E. & Noel, G. Three-Dimensional Cell Culture: A Breakthrough in Vivo. *Int. J. Mol. Sci.* **16**, 5517–5527 (2015).
104. Fang, Y. & Eglen, R. M. Three-Dimensional Cell Cultures in Drug Discovery and Development: *SLAS Discov. Adv. Life Sci. R&D* **22**, 456–472 (2017).
105. Langhans, S. A. Three-dimensional in vitro cell culture models in drug discovery and drug repositioning. *Front. Pharmacol.* **9**, 6 (2018).
106. Simian, M. & Bissell, M. J. Organoids: A historical perspective of thinking in three dimensions. *J. Cell Biol.* **216**, 31–40 (2017).
107. Breslin, S. & O'Driscoll, L. Three-dimensional cell culture: the missing link in drug discovery. *Drug Discov. Today* **18**, 240–249 (2013).
108. Ravi, M., Paramesh, V., Kaviya, S. R., Anuradha, E. & Solomon, F. D. P. 3D Cell Culture Systems: Advantages and Applications. *J. Cell. Physiol.* **230**, 16–26 (2015).
109. Morizane, R. & Bonventre, J. V. Generation of nephron progenitor cells and kidney organoids from human pluripotent stem cells. *Nat. Protoc. 2016 121* **12**, 195–207 (2016).
110. Takasato, M., Er, P. X., Chiu, H. S. & Little, M. H. Generation of kidney organoids from human pluripotent stem cells. *Nat. Protoc.* **11**, 1681–1692 (2016).
111. Watt, F. M. & Driskell, R. R. The therapeutic potential of stem cells. *Philos. Trans. R. Soc. B Biol. Sci.* **365**, 155–163 (2010).
112. Ungrin, M. D., Joshi, C., Nica, A., Bauwens, C. & Zandstra, P. W. Reproducible, Ultra High-Throughput Formation of Multicellular Organization from Single Cell Suspension-Derived Human Embryonic Stem Cell Aggregates. *PLoS One* **3**, e1565 (2008).
113. Nath, S. C., Horie, M., Nagamori, E. & Kino-oka, M. Size- and time-dependent growth properties of human induced pluripotent stem cells in the culture of single aggregate. *J. Biosci. Bioeng.* **124**, 469–475 (2017).
114. Miranda, C. C., Fernandes, T. G., Diogo, M. M. & Cabral, J. M. S. Towards Multi-Organoid Systems for Drug Screening Applications. *Bioeng. 2018, Vol. 5, Page 49* **5**, 49 (2018).
115. Kleinman, H. K. *et al.* Isolation and Characterization of Type IV Procollagen, Laminin, and Heparan Sulfate Proteoglycan from the EHS Sarcoma. *Biochemistry* **21**, 6188–6193 (1982).
116. Kleinman, H. K. & Martin, G. R. Reconstituted basement membrane complex with biological activity. vol. 50 1–15 (1989).
117. Beers, J. *et al.* Passaging and colony expansion of human pluripotent stem cells by enzyme-free dissociation in chemically defined culture conditions. *Nat. Protoc. 2012 711* **7**, 2029–2040 (2012).
118. Jang, T. H. *et al.* Cryopreservation and its clinical applications. *Integr. Med. Res.* **6**, 12–18 (2017).
119. Hunt, C. J. Cryopreservation: Vitrification and Controlled Rate Cooling. *Methods Mol. Biol.* **1590**, 41–77 (2017).
120. Freshney, R. I. *Culture of Animal Cells: A Manual of Basic technique and Specialized Applications*. (John Wiley & Sons, Inc., 2010). doi:10.1002/9780470649367.
121. Silva, T. P. *et al.* Design principles for pluripotent stem cell-derived organoid engineering. *Stem Cells Int.* **2019**, (2019).
122. Kubista, M., Akerman, B. & Norden, B. Characterization of Interaction between DNA

and 4',6-Diamidino-2-phenylindole by Optical Spectroscopy. *Biochemistry* **26**, 4545–4553 (1987).
123. Chen, K. G., Mallon, B. S., McKay, R. D. G. & Robey, P. G. Human Pluripotent Stem Cell Culture: Considerations for Maintenance, Expansion, and Therapeutics. *Cell Stem Cell* **14**, 13–26 (2014).
124. Bosnakovski, D. *et al.* Maintenance of Human iPS Cells in a Feeder-free Culture System. 1–8 (2012).
125. Branco, M. A. *et al.* 3D Microwell Platform for Cardiomyocyte Differentiation of Human Pluripotent Stem Cells. 1–17 (2020) doi:10.1007/7651_2020_336.
126. Bauwens, C. L. *et al.* Control of Human Embryonic Stem Cell Colony and Aggregate Size Heterogeneity Influences Differentiation Trajectories. *Stem Cells* **26**, 2300–2310 (2008).
127. Sharma, R., Sanchez-Ferras, O. & Bouchard, M. Pax genes in renal development, disease and regeneration. *Semin. Cell Dev. Biol.* **44**, 97–106 (2015).
128. Yokoo, T., Fukui, A., Matsumoto, K. & Okabe, M. Stem cells and kidney organogenesis. *Front. Biosci.* **13**, 2814–2832 (2008).
129. Grote, D., Souabni, A., Busslinger, M. & Bouchard, M. Pax2/8-regulated Gata3 expression is necessary for morphogenesis and guidance of the nephric duct in the developing kidney. *Development* **133**, 53–61 (2006).
130. Marcotte, M., Sharma, R. & Bouchard, M. Gene regulatory network of renal primordium development. *Pediatr. Nephrol. 2013 294* **29**, 637–644 (2013).
131. Little, M. H. & McMahon, A. P. Mammalian kidney development: Principles, progress, and projections. *Cold Spring Harb. Perspect. Biol.* **4**, 3 (2012).
132. Wellik, D. M., Hawkes, P. J. & Capecchi, M. R. Hox11 paralogous genes are essential for metanephric kidney induction. *Genes Dev.* **16**, 1423–1432 (2002).
133. Reidy, K. J. & Rosenblum, N. D. Cell and Molecular Biology of Kidney Development. *Semin. Nephrol.* **29**, 321–337 (2009).
134. Marcotte, M., Sharma, R. & Bouchard, M. Gene regulatory network of renal primordium development. *Pediatr. Nephrol. 2013 294* **29**, 637–644 (2013).
135. Burrow, C. R. Regulatory molecules in kidney development. *Pediatr. Nephrol. 2000 143* **14**, 240–253 (2000).
136. Narlis, M., Grote, D., Gaitan, Y., Boualia, S. K. & Bouchard, M. Pax2 and Pax8 Regulate Branching Morphogenesis and Nephron Differentiation in the Developing Kidney. *J. Am. Soc. Nephrol.* **18**, 1121–1129 (2007).
137. Lancaster, M. A. *et al.* Cerebral organoids model human brain development and microcephaly. *Nat. 2013 5017467* **501**, 373–379 (2013).

VIII. ANNEXES

Table 8.1| Complete formulation of RPMI 1640 medium.

Constituent	Concentration (mg/L)	Constituent	Concentration (mg/L)
Amino Acids			
Glycine	10.0	L-Lysine Hydrochloride	40.0
L-Arginine	200.0	L-Methionine	15.0
L-Asparagine	50.0	L-Phenylalanine	15.0
L-Aspartic acid	20.0	L-Proline	20.0
L-Cystine 2HCl	65.0	L-Serine	30.0
L-Glutamic Acid	20.0	L-Threonine	20.0
L-Histidine	15.0	L-Tryptophan	5.0
L-Hydroxyproline	20.0	L-Tyrosine Disodium Salt	29.0
L-Isoleucine	50.0	L-Valine	20.0
L-Leucine	50.0		
Vitamins			
Biotin	0.2	Pyridoxine Hydrochloride	1.0
Choline Chloride	3.0	Riboflavin	0.2
D-Calcium Pantothenate	0.25	Thiamine Hydrochloride	1.0
Folic Acid	1.0	Vitamin B12	0.005
Niacinamide	1.0	I-Inositol	35.0
Para-Aminobenzoic Acid	1.0		
Inorganic Salts			
Calcium Nitrate (Tetrahydrate)	100.0	Sodium Bicarbonate	2,000.0
Magnesium Sulfate (Heptahydrate)	100.0	Sodium Chloride	6,000.0
Potassium Chloride	400.0	Sodium Phosphate Dibasic (Heptahydrate)	1512.0
Other Components			
D-Glucose (Dextrose)	2,000.0	Phenol Red	5.0
Glutathione (Reduced)	1.0		

Table 8.2| Complete formulation of Advanced RPMI 1640 medium.

Constituent	Concentration (mg/L)	Constituent	Concentration (mg/L)
Amino Acids			
Glycine	10.0	L-Leucine	50.0
L-Alanine	8.9	L-Lysine Hydrochloride	40.0
L-Arginine	200.0	L-Methionine	15.0
L-Asparagine	50.0	L-Phenylalanine	15.0
L-Aspartic acid	20.0	L-Proline	20.0
L-Cystine 2HCl	65.0	L-Serine	30.0
L-Glutamic Acid	20.0	L-Threonine	20.0
L-Histidine	15.0	L-Tryptophan	5.0
L-Hydroxyproline	20.0	L-Tyrosine Disodium Salt	29.0
L-Isoleucine	50.0	L-Valine	20.0
Vitamins			
Ascorbic Acid Phosphate	2.5	Para-Aminobenzoic Acid	1.0
Biotin	0.2	Pyridoxine Hydrochloride	1.0
Choline Chloride	3.0	Riboflavin	0.2
D-Calcium Pantothenate	0.25	Thiamine Hydrochloride	1.0
Folic Acid	1.0	Vitamin B12	0.005
Niacinamide	1.0	I-Inositol	35.0
Inorganic Salts			
Calcium Nitrate (Tetrahydrate)	100.0	Sodium Chloride	6,000.0
Magnesium Sulfate (Anhydrous)	48.84	Sodium Phosphate Dibasic (Anhydrous)	800.0
Potassium Chloride	400.0	Zinc Sulfate (Heptahydrate)	0.874
Sodium Bicarbonate	2,000.0		
Proteins			
AlbuMAX® II	400.0	Insulin Recombinant Full Chain	10.0
Human Transferrin (Holo)	7.5		
Trace Elements			
Ammonium Metavanadate	3.0E-4	Manganous Chloride	5.0E-5
Cupric Sulfate	0.00125	Sodium Selenite	0.005
Other Components			
D-Glucose (Dextrose)	2,000.0	Phenol Red	5.0
Ethanolamine	1.9	Sodium Pyruvate	110.0
Glutathione (Reduced)	1.0		

Table 8.3| Sequences of the used primers in quantitative real-time polymerase chain reactions.

Gene		Sequence
GAPDH	Forward	GAGTCAACGGATTTGGTCGT
	Reverse	TTGATTTTGGAGGGATCTCG
WT1	Forward	CCAGCCCGCTATTCGCAATC
	Reverse	CGAGTACTGCTGCTCACCCA
PAX2	Forward	GACTATGTTCGCCTGGGAGATTC
	Reverse	AAGGCTGCTGAACTTTGGTCCG
SIX2	Forward	CACACAGGTCAGCAACTGGTTC
	Reverse	TCATCCTCCGAGCTGCCTAACA
GATA3	Forward	ACCACAACCACACTCTGGAGGA
	Reverse	TCGGTTTCTGGTCTGGATGCCT
HOXD11	Forward	CAGTCCCTGCACCAAGGCGAC
	Reverse	GGTATAGGGACAGCGCTTTTTCC

Table 8.4| Resume of the tested conditions in experiment 3D Culture #1.

Condition	Nº of cells/aggregate	CHIR concentration (µM)	Dorsomorphin concentration (nM)
1	3,000	5	-
2			250
3			500
4	4,000	8	-
5			250
6			500
7	5,000	5	-
8			250
9			500
10	3,000	8	-
11			250
12			500
13	4,000	5	-
14			250
15			500
16	5,000	8	-
17			250
18			500

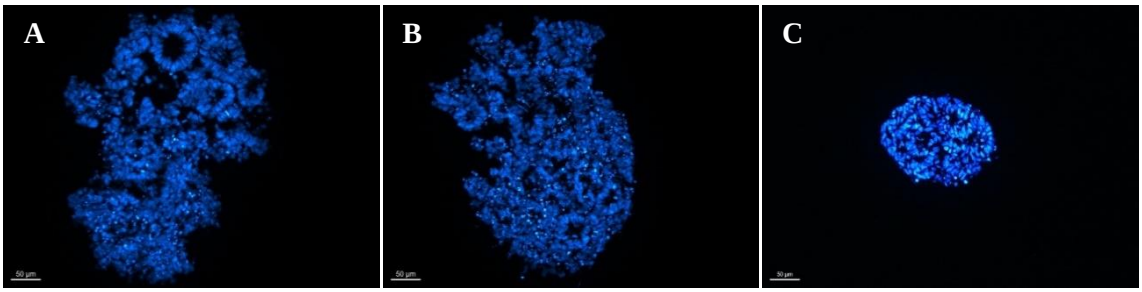

Figure 8.2| Nuclear staining of cellular aggregates exposed to 10 µM of CHIR and 100 nM of Dorsomorphin and 11 µM of CHIR for 96 hours under Morizane protocol. A-B) Cellular aggregates upon exposure to 10 µM of CHIR and 100 nM of Dorsomorphin, on day 9 of the differentiation protocol; **C)** Cellular aggregate upon exposure to 11 µM of CHIR, on day 7 of the differentiation protocol. Cellular aggregates display renal structures. Images were acquired with a fluorescence optical microscope. Images at 200x magnification (scale bars: 50 µm).

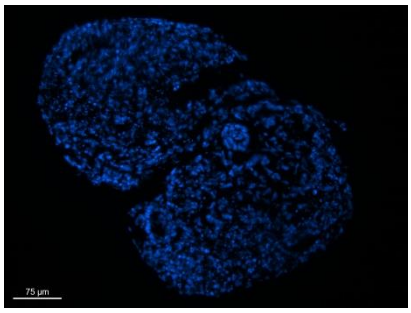

Figure 8.2| Nuclear staining of a cellular aggregate exposed to 10 µM of CHIR and 100 nM of Dorsomorphin for 96 hours under Takasato protocol. Cellular aggregate upon exposure to 10 µM of CHIR and 100 nM of Dorsomorphin, on day 14 of the differentiation protocol. The cellular aggregate displays a renal structure. Images were acquired with a fluorescence optical microscope. Image at 200x magnification (scale bar: 75 µm).

2021

MARIANA ISABEL BARATA MOÇO

DERIVATION OF KIDNEY ORGANOIDS FROM HUMAN INDUCED PLURIPOTENT STEM CELLS UNDER 3D CONDITIONS

NOVA SCHOOL OF SCIENCE & TECHNOLOGY